UNIVERSIDADE DE LISBOA

Faculdade de Ciências

Departamento de Física

Analysis of the use of dosimetrically equivalent linear accelerators for Intensity Modulated Radiotherapy treatments

Rafaela Cristina Sepúlveda da Silva

Orientadores

Drª Miriam Zarza Moreno, Serviço de Radioterapia do Instituto Português de Oncologia de Lisboa

Prof. Dr. Nuno Matela, Instituto de Biofísica e Engenharia Biomédica, Departamento de Física da Faculdade de Ciências da Universidade de Lisboa

Mestrado Integrado em Engenharia Biomédica e Biofísica
Perfil em Sinais e Imagens Médicas

Dissertação

2015

Acknowledgments

I would like to express my gratitude to Instituto Português de Oncologia de Lisboa Francisco Gentil (IPOLFG) and Dr. Margarida Roldão, director of the Radiotherapy Service, for giving me the opportunity of doing my Master Internship and perform this study in the service.

To Dr. Miriam Moreno, who have orientated this work, a very special thanks for receiving me with so much generosity since the first day and for always being available to patiently answer to my questions, despite being always busy with her work. Her dedication and ideas had a major role in this work, and I have no words to thank all I have learnt from her and all the encouragement she gave me during the Internship. I hope to return all the effort she put into this work by following her example of professionalism, dynamism and persistence, always offering a smile and a nice word, in my future professional career. I will always remember her great contribution to my academic achievements and to make me grow as a person, by reminding me of the importance of transforming insecurities into motivation and disciplined work.

To Prof. Nuno Matela, my supervisor, I would like to thank for always being available and for clarifying all my doubts related to the Faculty required procedures, as well as for his encouragement words and his suggestions for this thesis, in spite of the subject being not directly related to his field of work.

I would also like to express a special thanks to all the Physics staff for the support and availability to clarify my doubts when Dr. Miriam was not present. To them and to the other professionals of the Radiotherapy Service who pass their cards to open the door in order to let me in and out of the Physics office every day, I want to thank for the patience.

I also want to thank to all the professionals from Brachytherapy, CT and treatment units for the support and explanations during the first months of my Internship.

I would also like to express my special gratitude to Prof. Eduardo Ducla Soares for encouraging me to choose Radiotherapy as subject of my Master Internship, despite of my initial insecurity due to the unawareness of the subject from my previous academic experience. I sincerely thank for the motivation, since, although I had difficulties in the beginning, they were surpassed and currently Radiotherapy is a subject that I truly appreciate and that is in accordance with my initial expectations when I choose Biomedical Engineering as academic route.

I would like to thank very much to my family, especially to my parents, for providing me the opportunity to invest in my academic formation, contributing to make this work possible, and also for always giving me freedom to make my academic decisions and for, since I was a child,

letting me take the responsibility of my duties by my own. Without that freedom and all the support they gave me through all these years, I would not have achieved the success that I have experienced in my academic life and would not like so much to learn as well. I hope my love and dedication would be enough to return the great education I have received and also hope that, one day, I would be capable of providing that support and that freedom to my children.

A special thanks also to my friends for their support through all these years, especially in my worst moments of demotivation and frustration, when they encouraged me to continue my studies in Biomedical Engineering in another Faculty, leading me to make the decision of doing the Master in Biomedical and Biophysics in FCUL, which was one of the most positive decisions I made in my life. Thanks to them also for, in the last months, listening to me talking about my thesis with so much patience.

A final special thanks to all the teachers I had for all I have learnt from them, for creating in me the desire of always try to do my best and to achieve great things and for guiding me until this point in my life.

Resumo

O uso de radiações para terapia iniciou-se pouco tempo após a descoberta dos raios-X por Wilhelm Röntgen em 1895, tendo ocorrido uma grande evolução ao nível da tecnologia geradora de raios-X até ao presente. Essa evolução tornou possível que sejam produzidos feixes de fotões e electrões de altas energias.

Os aceleradores lineares são actualmente os principais produtores de raios X de alta energia utilizados em Radioterapia. Devido à evolução tecnológica das últimas décadas e ao elevado nível de reprodutibilidade e precisão dos feixes produzidos por estes equipamentos, tem-se verificado um esforço progressivo, por parte dos fabricantes, para uniformizar o desenho e a tecnologia dos aceleradores lineares. Esta uniformização permite que aceleradores lineares idênticos possam ser instalados com ajuste dosimétrico (*beam-matching*) e considerados dosimetricamente equivalentes.

A instalação com *beam-matching* permite um aumento da flexibilidade e eficiência dos aceleradores lineares, pois reduz a necessidade de interrupção ou replaneamento dos tratamentos em caso de paragem de um dos equipamentos, devido à possibilidade da utilização indistinta dos mesmos. A utilização indistinta dos aceleradores lineares assume um papel bastante importante nas unidades de tratamento, pois as interrupções do funcionamento normal dos equipamentos são relativamente frequentes, devido a intervenções de manutenção preventiva periódica, bem como a avarias. Por este motivo, tem-se tornado comum nos serviços de radioterapia a instalação de aceleradores lineares com *beam-matching* em relação a equipamentos similares instalados previamente, fazendo com que os aceleradores lineares existentes no serviço sejam dosimetricamente equivalentes e permitindo a sua utilização indistinta.

Apesar dos ajustes dosimétricos, podem ocorrer pequenas variações nas características dos aceleradores lineares, que podem resultar de diversos factores, como desgaste dos equipamentos ou condições de utilização. Têm sido realizados estudos [1-4] com a finalidade de avaliar a equivalência dosimétrica de aceleradores lineares instalados com *beam-matching* dentro de uma unidade de tratamento. Os resultados obtidos nestes estudos confirmam a equivalência dosimétrica entre os equipamentos, sugerindo que o processo de *beam-matching* é suficiente para garantir a utilização indistinta dos aceleradores lineres.

No entanto, resultando as possíveis variações nas características dos equipamentos de diversos factores, é necessário avaliar individualmente a equivalência dosimétrica dos aceleradores lineares para diferentes unidades, bem como verificar se esta equivalência é mantida a longo-prazo ou se, por outro lado, surgem diferenças significativas ao nível das características dosimétricas que justifiquem a adaptação do sistema de planeamento aos novos parâmetros. Esta necessidade assume especial relevância para técnicas avançadas, como a Radioterapia de Intensidade Modulada (IMRT), na qual se verificam elevados gradientes de dose e são utilizados colimadores multi-lâminas (MLC), bem como campos de reduzidas dimensões, que podem conduzir a um maior impacto das variações ao nível dos planeamentos dosimétricos.

Deste modo, no âmbito do Estágio realizado no Instituto Português de Oncologia de Lisboa Francisco Gentil (IPOLFG), foi realizado um estudo que consistiu, por um lado, na avaliação da estabilidade a longo prazo das características dos feixes de fotões de 6 MV e, por outro, na comparação dosimétrica para a técnica de Radioterapia de Intensidade Modulada (IMRT).

Para a realização do presente estudo, foram utilizados três aceleradores lineares do modelo 2100C/D da Varian Medical Systems, Inc., que produzem fotões com energias de 6 MV e com um valor de energia mais elevado, 10 MV ou 15 MV, bem como electrões com diversas energias. Um dos aceleradores lineares, denominado DHX01, foi instalado em Março de 2012, enquanto os dois restantes, DHX02 e DHX03, foram instalados em Novembro e Dezembro de 2012, respectivamente. Os aceleradores lineares DHX02 e DHX03 foram instalados com *beam-matching*, sendo dosimetricamente equivalentes no sistema de planeamento e usados indistintamente em caso de interrupção do funcionamento de um dos equipamentos. Os três aceleradores lineares são usados para tratamentos de Radioterapia de Intensidade Modulada (IMRT), contendo, para o efeito, um colimador multilâminas (MLC) Millenium^{TM} MLC com 120 lâminas, divididas por dois bancos com 60 lâminas. Estão também equipados com um dispositivo electrónico de imagem portal (EPID), usado para verificação de planos de IMRT.

A avaliação da estabilidade a longo-prazo das características dosimétricas dos aceleradores lineares consistiu na análise de dados adquiridos nas verificações realizadas no âmbito dos controlos de qualidade diário e trimestral durante o ano de 2014 para fotões de 6 MV (energia utilizada para tratamentos de IMRT). Na análise foram também incluídos os resultados de medições realizadas para controlo de qualidade do MLC. Os resultados obtidos com os três aceleradores lineares foram analisados usando o *software* SPSS Statistics Package, sendo realizada uma comparação entre os três equipamentos para verificar se, de modo geral, os resultados obtidos nos controlos de qualidade compromete a equivalência dosimétrica em estudo.

A comparação dosimétrica dos três aceleradores lineares para tratamentos de IMRT foi realizada através de verificação de planos de tratamento para patologia de cabeça e pescoço (H&N) e próstata, criados com o sistema de planeamento Eclipse^{TM} da Varian Medical Systems, Inc. Foram selecionadas amostras contendo doentes tratados em cada um dos aceleradores lineares usando a técnica de IMRT, para cada uma das duas patologias, num total de seis amostras. Para além das verificações originais realizadas antes do início dos tratamentos, usando o equipamento em que o doente foi tratado, novas verificações foram realizadas com os restantes dois aceleradores lineares, sem troca de unidade de tratamento no sistema de planeamento, i.e., mantendo os parâmetros originais do plano de tratamento, sem recálculo para equipamento diferente. As verificações foram realizadas através de Análise Gamma de imagens portais adquiridas através de EPID. A comparação entre os três equipamentos consistiu na comparação das percentagens de pontos em conformidade com os critérios estabelecidos para a Análise Gamma com critérios 3.0%, 3.0 mm obtidas nas três verificações efectuadas para cada amostra e análise das diferenças obtidas com realização da verificação com um equipamento diferente. Foi ainda realizada uma análise de doses no sistema de planeamento, que consistiu na troca de unidade de tratamento no sistema de planeamento para todos os

doentes de cada uma das amostras, com posterior recálculo de dose, e determinação da das diferenças obtidas devido à troca de equipamento ao nível da dose e unidades monitor (UM) calculadas pelo TPS. Esta última análise teve a finalidade de determinar se possíveis desvios obtidos nos resultados da Análise Gamma para as verificações com EPID são resultantes de diferenças nas características dosimétricas dos aceleradores lineares ou se, por outro lado, resultam de diferenças acentuadas entre as unidades de tratamento no sistema de planeamento, comprometendo o ajustamento experimental a um equipamento diferente.

Ambas as avaliações foram realizadas com a finalidade de estudar dois aspectos principais. Um deles consistiu na verificação da equivalência dosimétrica a longo-prazo dos aceleradores lineares DHX02 e DHX03, instalados com *beam-matching*, bem como a verificação desta equivalência no caso de tratamentos de IMRT. O outro aspecto em estudo consistiu na possibilidade de utilizar indistintamente o terceiro acelerador linear, DHX01, instalado sem *beam-matching*, como dosimetricamente equivalente aos outros dois equipamentos para tratamentos de IMRT.

Os resultados obtidos estão de acordo com os valores de tolerância recomendados e confirmam a equivalência dosimétrica entre os aceleradores lineares. No entanto, sugerem precaução na utilização indistinta do equipamento DHX01, pois, embora os resultados estejam dentro dos limites estabelecidos (acordos da Análise Gamma superiores a 90.00%), diferem dos obtidos para os restantes aceleradores lineares, com desvios máximos de 8.00%. Apesar de as diferenças obtidas não serem, em geral, significativas (desvios médios são de aproximadamente 4.00%) não comprometerem totalmente a utilização indistinta do equipamento DHX01, é recomendada a actualização das características dos aceleradores lineares no sistema de planeamento.

Palavras-chave: Aceleradores Lineares, *Beam-matching*, Radioterapia de Intensidade Modulada (IMRT), Dispositivos Electrónicos de Imagem Portal (EPID), Análise Gamma

Abstract

Linear accelerators are currently the mostly used high energy X-rays generators for Radiotherapy. Due to the evolution occurred in the last decades, as well as to the high reproducibility and precision of the beams generated by these machines, a progressive standardization of their design and technology has occurred. This standardization allows similar linear accelerators to be installed with dosimetric adjustments (*beam-matching)* and considered dosimetrically equivalent in the treatment planning system, reducing the need of treatment interruption or replanning if a linear accelerator is not functioning.

In spite of the dosimetric adjustments, small variation in outputs may occur due to several factors, as equipment wear or use conditions. Several studies [1-4] that supported the dosimetric equivalence between *beam-matched* linear accelerators have been performed. However, as the possible variations result from diverse factors, it is recommended to evaluate the dosimetric equivalence of linear accelerators individually for each treatment facility, especially for advanced treatment techniques, as Intensity Modulated Radiotherapy (IMRT), in which dose gradients are high and multileaf collimators (MLC) and small fields are used, possibly increasing the impact of the variations for dosimetric plans.

For this reason, in the context of the Internship in Instituto Português de Oncologia de Lisboa Francisco Gentil (IPOLFG), a long term stability evaluation has been performed for the characteristics of 6 MV photons from three linear accelerators installed in the Radiotherapy Service (two of them are beam-matched), acquired during daily and trimestral quality assurance procedures. It was also performed a dosimetric comparison between the three machines for Intensity Modulated Radiotherapy (IMRT), using portal imaging and Gamma Analysis, in order to verify the differences resultant from the indistinct use of the linear accelerators.

The obtained results supported the dosimetric equivalence of the linear accelerators, but suggesting caution when using indistinctly the linear accelerator installed without beam-matching, especially for Head and Neck treatments, since, although the results are in accordance the recommended tolerance of 90.00% for the agreement of the Gamma Analysis, higher deviations were obtained for this equipment, with approximate average values of 4.00% and maximum value of 8.00%.

Key-words: Linear Accelerators, Beam-matching, Intensity Modulated Radiotherapy (IMRT), Electronic Portal Imaging Devices (EPID), Gamma Analysis.

Table of Contents

List of Tables

List of Figures

List of Abbreviations

3DCRT – Three-dimensional Conformal Radiation Therapy

AAA – Anisotropic Analytical Algorithm

AMFPI – Active matrix, flat panel imager

a-Si – Amorphous Silicon

BQF – Beam Quality Factor

CAX – Dose in Central Axis

CT – Computed Tomography

DDR – Digitally Reconstructed Radiograph

DLS – Dosimetric Leaf Separation

DMLC – Dynamic Multileaf Collimator

DTA – Distance-to-Agreement

DVH – Dose-Volume Histogram

EBRT – External Beam Radiotherapy

EPID – Electronic Portal Imaging Device

IMAT – Intensity-Modulated Arc Therapy

IMRT – Intensity Modulated Radiation Therapy

Linac – Linear Accelerator

MC – Monte Carlo

MLC – Multileaf Collimator

MRI – Magnetic Resonance Imaging

PDP – Portal Dose Prediction

PET – Positron Emission Tomography

QA – Quality Assurance

RF – Radiofrequency

SMLC – Segmented Multileaf Collimator

SAD – Source-Axis Distance

SDD – Source- Detector Distance

SSD – Source-Surface Distance

TFT – Thin-Film Transistor

TPS – Treatment Planning System

VMAT – Volumetric-Modulated Arc Therapy

Chapter 1

Motivation

The use of radiations for therapy began soon after the discovery of X-rays in 1895, experiencing a great evolution in X-rays generating technology and allowing to obtain high energy photon and electron beams. Currently, linear accelerators are the most used high energy X-ray generators in Radiotherapy, due to its versatility [5].

Linear accelerators technology has significantly improved in last decades, allowing the generation of more accurate and reproducible beams, leading to an increasing effort from the manufactures to standardize the design and technology of linear accelerators [6]. This standardization represents an increase in treatment flexibility and efficiency, since, if the linear accelerators of an unit are dosimetrically equivalent, it is possible to indistinctly interchange patients between the machines, without replanning, in case of interruption of the functioning of one of the linear accelerators, continuing the treatment in other equipment.

The possibility of indistinct use of the linear accelerators is of major importance for a treatment unit, since the interruptions of the normal functioning of the linear accelerators are frequent, due either to preventive maintenance interventions or equipment damage.

For this reason, it has become common, in Radiotherapy facilities, the installation of linear accelerators with beam-matching in relation to a previously installed equipment, creating a dosimetric equivalence that allows the indistinct use of the linear accelerators.

However, several factors can cause variations in the functional characteristics of the linear accelerators, as conditions of use or component wear, which creates the need of verifying if the dosimetric equivalence is maintained in the long-term or significant differences in the dosimetric characteristics start to occur, justifying the adaptation of the treatment planning system to the new parameters.

Several studies have been already performed in this subject [1-4], but an identical evaluation was considered necessary for the particular case of the Radiotherapy Service of IPOLFG, since, as already mentioned, several factors can influence the stability of the dosimetric characteristics of the linear accelerators and, for this reason, it is not viable to adapt the results obtained in other studies for the Service.

Consequently, a verification of beam characteristics of 6 MV photons of the three similar linear accelerators installed in the service was performed, by means of the analysis of daily and trimestral quality assurance procedures, in order to verify the stability of the parameters and if significant differences between the three linear accelerators were obtained.

Moreover, the main purpose of present work was to perform an intercomparision for Intensity Modulated Radiotherapy (IMRT) treatments, since the use of multileaf collimators (MLC) and small fields can lead to an increased influence of small variations in beam characteristics, justifying the need of analyzing the dosimetric equivalence of linear accelerators in particular for this technique [6]. Therefore, comparisons were performed between dose distributions from treatment plans obtained for the three linear accelerators with experimental dose distributions obtained both with the original plan equipment and with the other two linear accelerators, without replanning before the change to a different unit. The experimental dose was obtained using Electronic Portal Imaging Device (EPID) and ionization chamber, which allow the comparison of the experimental and expected dose fluences and values, respectively.

At the IPOLFG, only two of the three accelerators considered in the study were installed as beam-matched. For this reason, two different aspects were analyzed in the present study. The first was the verification, at the long-term, of the dosimetric equivalence of the beam-matched linear accelerators and if this equivalence is also verified for IMRT treatments. The other aspect in study was the possibility of using indistinctly a third linear accelerator, previously installed in the service without beam-matching, as dosimetric equivalent to the other two linear accelerators for IMRT treatments.

Chapter 2

Introduction to External Radiotherapy: the IMRT concept

2.1. Brief Introduction

Radiotherapy is a branch of medicine that uses ionizing radiation in the treatment of malignant disease [5]. This treatment modality has become widely used in the treatment of cancer due to its efficacy in tumor cells eradication, caused by the ionization of matter, process by which one or more electrons are liberated in collisions of the particles with atoms or molecules, and its simultaneous ability to spare normal tissues [7, 8]. Radiotherapy is divided in two branches: external beam radiotherapy (EBRT), in which the radiation source is external in relation to the patients, and brachytherapy (BT), in which the radiation source is placed inside or in contact with the target region [9].

The beginning of radiotherapy was impelled by discovery of X-rays by Wilhelm Röntgen in 1895. Further investigation on this new type of radiation lead to a fast understanding of its radiographic and therapeutic potential, with several applications in oncologic pathologies during the year of 1896 [5].

The evolution of radiotherapy during 20^{th} century was also marked by the discovery of natural radioactivity by Becquerel in 1896, the isolation of a new radioactive chemical element, radium, used in external beam radiotherapy in the following years, by Marie and Pierre Curie in 1898, the production of artificial radioactive elements by Irène Curie and Fréderic Joliot in 1934, which lead to the adoption of cobalt 60 (^{60}Co) as an alternative source of high energy radiation, and a progressively more profound understanding of atomic and nuclear structures [8, 9].

In the beginning, external beam radiotherapy treatments were performed with X-ray tubes, similar to the Crookes tube used by Röntgen in the experiments that led to the discover of X-rays [9]. In 1913, William Coolidge developed the “hot-cathode tube” that did not need gas for the production of X-rays. This tube contained a cathode, which was a tungsten filament heated by a low-voltage circuit and a target that functioned as an anode. Electrons were originated in

the cathode due to the thermionic effect caused by the heating. These electrons were accelerated in the vacuum towards the target by a constant potential electrostatic field [5, 10, 11].

In parallel, high energy photon treatments were performed with radium, which was the only source of γ-rays during almost two decades, using radium needles and tubes placed a few centimeters away from the patient [10].

The ^{60}Co unit was invented by H.E. Johns in the early 1950s and allowed higher photon energies, placing the cobalt unit at the forefront of radiotherapy for decades. The ^{60}Co radioisotope is produced from the irradiation of ^{59}Co (natural element) with neutrons, in a nuclear reactor, and is then stored in a sealed source. The ^{60}Co isotope decays emitting γ-rays with energies of 1.17 and 1.33 MeV [5, 9].

In 1950s, a new device was developed by several investigators, including Varian brothers and Henry Kaplan. This new device, called linear accelerator (linac), generates high energy X-rays and electrons, which had been reported since the 1930s as advantageous for cancer therapy [10, 12]. This equipment became soon after the most used radiation source in modern radiotherapy, due to its versatility and wide range of energies [5].

2.2. The technological evolution: from 2D to IMRT

In the last decades, the ability of identifying cancer cells and target them with radiation has greatly improved, as a result of technological progresses. These advances lead to an evolution from two-dimensional (2D) radiotherapy, which consisted of a single beam, usually with opposed lateral fields or four-field “boxes” and was based on two-dimensional X-ray images and hand calculations, to three-dimensional (3D) radiotherapy [13].

The increasing use of computed tomography (CT), which allowed three-dimensional treatment planning, making non-coplanar beams possible to plan and deliver, had a great influence in the evolution from 2D to 3D radiotherapy techniques. Additionally, linear accelerators became equipped with electronic MV portal (EPID) and kilovoltage imaging systems for verification of patient positioning, improving the conformity between the planned and delivered absorbed doses. Digitally reconstructed radiographs (DRRs) were constructed from CT scans by digitally simulating the passage of X-rays through the patient’s CT representation in the same geometry as the treatment and could be compared with X-ray images acquired at the time of treatment to verify the patient treatment position. These innovations allowed the implementation of three-dimensional conformal radiation therapy (3D-CRT), which uses 3D planning techniques and special delivery systems to shape the field, in order to obtain a more accurate treatment delivery to tumors. In relation to conventional approaches, 3D-CRT tends to use more treatment fields and reduces the absorbed dose to normal tissues surrounding the target volume, while potentially allowing higher tumor absorbed doses, as well as increasing the conformity between the delivered and planned doses [14].

Another important advancement in external beam radiation therapy was the introduction of multileaf collimators (MLC) in linacs (Figure 1), designed to replace the molded heavy metal blocks used in conventional radiotherapy used to deliver coplanar beams, usually of relatively uniform intensity across the field. The MLC consists in individual leaves (80-120) of high atomic material moving independently. MLCs allowed the use of multiple complex-shaped fields, even in the same treatment session [14].

Multileaf collimators improved greatly 3D-CRT technique due to its ability to replace the use of wedges or compensators to account for a curved or sloping patient entering surface. This replacement simplifies the attempts to make the beam shape conform to the tumor shape and to achieve absorbed-dose distributions with improved homogeneity [14].

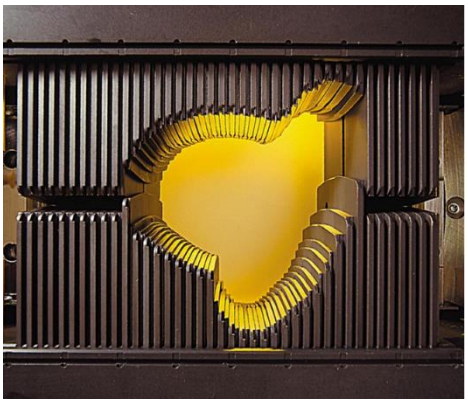

Figure 1 - Varian's 120-leaf Millenium MLC
[http://newsroom.varian.com/index.php?s=31899&mode=gallery&cat=2473]

Multileaf collimators also allowed to modulate the intensity of radiation fields, leading to the development of Intensity-Modulated Radiotherapy (IMRT). This technique derived from the prediction that the optimal radiation pattern from any single direction was typically non-uniform and that a set of intensity modulated beams from multiple directions could be designed to produce dose homogeneity within the tumor similar to that from conventional radiotherapy but with superior conformity, especially for complex-shaped volumes, thereby sparing adjacent normal tissues. IMRT also allows the production of non-uniform absorbed-dose distributions if required for treatment of a volume within another volume (concomitant boost or simultaneous integrated boost techniques). IMRT attempts to achieve more optimal absorbed-dose distributions by varying the beam intensity (or fluence, which can be defined as the quotient between the number of particles incident on a given sphere and the cross-sectional area of that sphere [7]) within each incident beam, usually by subdividing the beam into smaller segments and modulated each to achieve a selected fluence contribution [14].

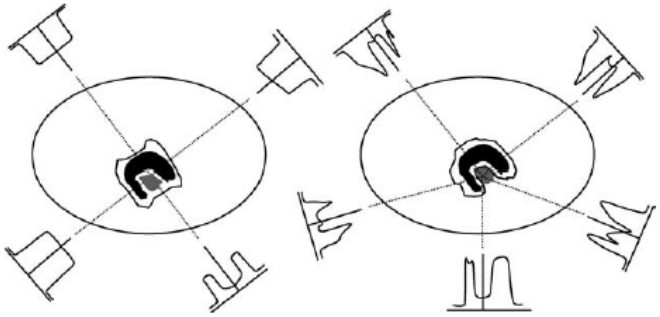

Figure 2 - Comparison of 3D-CRT (left) and IMRT (right), with target volume represented by the black region and volume at risk represented by gray region. IMRT beams can have highly non-uniform beam intensities and are capable of producing more concave-shaped absorbed-dose distribution, better avoiding the volume at risk, as indicated by the line around the target volume, which is a typical isodose contour [14].

The calculation of the fluence required from each beam segment has only recently became viable with the development of computational algorithms taking an iterative approach to dose calculation and referred to as "inverse treatment planning", which means that the treatment planning starts at the desired result and is performed backwards to establish the best way to achieve that result [14].

There are two main ways of delivering IMRT, both using multileaf collimators [5]:

- *segmented MLC (SMLC)*, often referred to as "step-and-shoot" mode, which is a static technique, since there is no MLC motion while the beam is turned on, with the intensity modulated fields delivered with a sequence of small segments or subfields, each subfield with a uniform intensity. The beam is only turned on when the MLC leaves are stationary in each of the prescribed subfield positions.
- *dynamic MLC (DMLC*), also referred to as "sliding-window" mode, which is a dynamic technique, with the intensity modulated fields delivered in a dynamic way with the leaves of the MLC moving during the irradiation of the patient. For a fixed gantry position the opening formed by each pair of opposing MLC leaves is swept across the target volume under computer control with the radiation beam turned on to produce the desired fluence map.

The advantages of IMRT are significant in concave target volumes where organs at risk are surrounding the volume, such as for head and neck or prostate treatments. In the case of head and neck pathologies, an increased therapeutic gain is achievable with IMRT in tumors close to the base of the skull, for which a higher rate of local control and a lower incidence of complications have been reported in comparison with conventional techniques. A substantial reduction in late radiation-induced toxicity have been reported, without any reduction in local tumor control. A decrease of rectal complications was also observed in prostate treatments with IMRT in relation to conventional techniques [14].

Over the past decades, there have been significant advances in the delivery of IMRT radiotherapy technique. IMRT can be delivered with rotational techniques, as intensity-modulated arc therapy (IMAT) and tomotherapy [14].

IMAT uses conventional linear accelerators and MLCs, as well as a dynamic MLC approach, while the gantry rotates around the patient [5, 14]. To deliver intensity-modulated fields, IMAT can require several rotational arcs each with different patterns of irradiation, since a single rotation yields only a step-wise intensity pattern, either open or blocked, from each arc segment through which the arc passes, while multiple arcs allow more intensity levels. However, it has been shown that controlled variation of absorbed-dose rate during the gantry rotation can achieve some intensity modulation of the beam even if a single rotation is delivered [14]. This observation lead to the implementation of volumetric-modulated arc therapy (VMAT), a single-arc form of IMAT that delivers apertures of varying weights with a single-arc rotation and dose-rate variation [15].

Tomotherapy is also an intensity-modulated rotational therapy, but uses a narrow CT-like fan beam modulated by a binary collimator. The binary collimator has multiple leaves, specifically designed for rotating fan beams. It is called a binary collimator due to the rapid leaf movements from the closed position to the open position through the fan beam to expose the source. The amount of time a leaf remains in the open position determines the intensity delivered by the sub-beam or "beamlet". The fan-beam width is collimated by a pair of jaws above the binary MLC. In the first form of tomotherapy, serial tomotherapy, a fan beam is rotated around the patient with the couch fixed. In helical tomotherapy, mostly used currently, the fan beam rotation and the couch move simultaneously so that the radiation source describes a helical pattern in relation to the patient [14].

Both modalities achieve superior target dose quality in a range of tumor sites when compared to static IMRT and require lower radiation doses, with shorter treatment times than static IMRT [16]. However, there are some differences between both techniques: IMAT must account for restrictions on MLC movements as the gantry moves from one beam angle to the next, while in tomotherapy these restrictions do not exist due to the use of a binary MLC. On the other hand, IMAT uses a conventional linac, thus can be delivered with the same treatment unit than other treatments [15].

2.3. Fundamentals of radiotherapy physics and dosimetry

2.3.1. Interaction of ionizing radiation with matter

Radiation can be classified into two main categories, non-ionizing radiation and ionizing radiation, depending on its ability to ionize matter [5]. Unlike non-ionizing radiation, ionizing radiation have the ability to excite and ionize atoms of matter with which they interact [17]. Ionization is the process in which an atom or molecule gains or loses an electron, acquiring positive or negative charge. For this reason, ionizing radiation are used in radiotherapy, due to its ability to cause ionization of malignant cells. The ionization of matter due to the action of ionizing radiation can occur directly or indirectly [5, 17]:

- Directly ionizing radiation deposits energy in the medium through direct interactions between charged particles and orbital electrons of atoms in the medium;
- Indirectly ionizing radiation consists of neutral particles (photons or neutrons), which deposit energy in the medium through a two-step process. In the first step, energy is transferred from the radiation to charged particles in the medium. In the second step, these charged particles deposit their energy to the medium through interactions with orbital electrons of the atoms.

Both directly and indirectly radiations are used in radiotherapy. Directly ionizing radiations (as electrons and protons) are mainly used for superficial lesions, due to its lower penetration in the tissues, while indirectly ionizing radiations (as X- and γ- rays) are widely used in radiotherapy, due to its higher power of penetration in the tissues, which results from the lower probability of this radiation of interacting with matter.

2.3.1.1. Photon interactions in matter

Depending on their origin, the indirectly ionizing radiation can be classified into three main categories [5]:

- Characteristic or discrete X-rays, which are emitted in transitions of orbital electrons from one allowed orbit to a vacancy in another allowed orbit. In some cases, instead of a characteristic X-ray, an orbital electron, or Auger electron, can be ejected, as a result of this interaction;

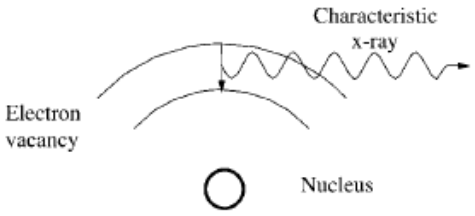

Figure 3 - Emission of a characteristic X-ray [18].

- *Bremsstrahlung* or continuous X-rays, which are emitted through interactions between an incident electron and a nucleus. During the interaction, the incident electron is decelerated and lose some of its kinetic energy in the form of *bremsstrahlung*.

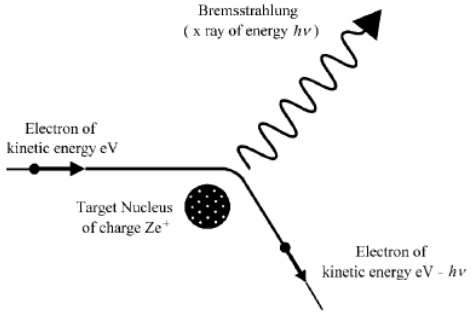

Figure 4 - Production of bremsstrahlung X-rays [18].

- γ-rays, emitted due to nuclear transitions in γ decay, in which an excited nucleus attains the ground state.

There are five major types of interactions with matter by X- and γ- rays, consisting of indirectly ionization processes [17]:

- Photoelectric effect;
- Compton effect;
- Pair production;
- Rayleigh (coherent scattering);
- Photonuclear interactions.

Photoelectric effect

In the photoelectric effect, an incident photon with energy $h\nu$ interacts with a tightly bound orbital electron and disappears, while the electron is ejected from the atom as a photoelectron with a kinetic energy E_K given as:

$$E_K = h\nu - E_B \tag{2.1}$$

where $h\nu$ is the incident photon energy and E_B is the binding energy of the electron [5].

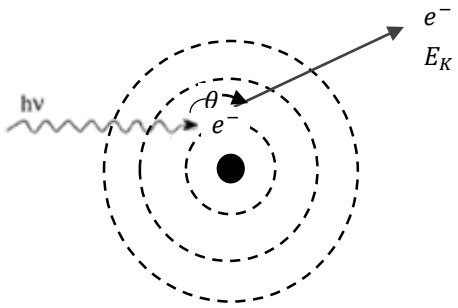

Figure 5 - Schematic representation of the photoelectric effect (adapted from [18]).

The electron is ejected with an angle θ in relation to the photon's direction of incidence, carrying a momentum p. The atom from which the electron was removed suffers a very slight deviation in the direction taken for momentum conservation [17].

The photoelectric effect occurs mostly for electron in the inner shells of atoms with high atomic number, which present higher binding energies. The occurrence of the photoelectric effect is also more likely to occur for photons with low $h\nu$, as long as $h\nu > E_B$, since, when both energies are similar, the photon is totally absorbed in the interaction, ceasing to exist [17].

Compton effect

The Compton effect represents an interaction between a photon and an essentially free and stationary orbital electron from the outer shells of an atom. The incident photon energy $h\nu$ is much larger than the binding energy of the electron. During the collision, the photon loses part of its energy to the electron, which is ejected with an angle ϕ in relation to the incident photon,

with a kinetic energy E_K. The photon is scattered through an angle θ and with an energy $h\nu' < h\nu$ [5].

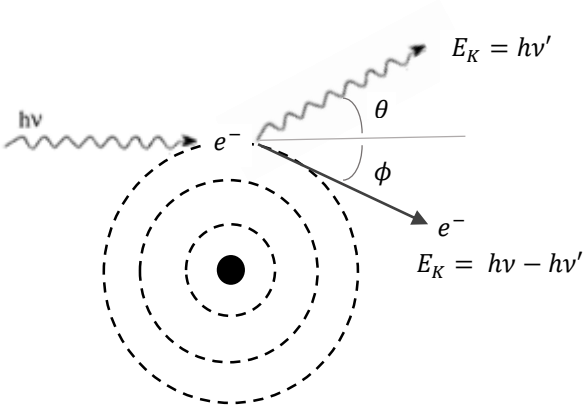

Figure 6 - Schematic representation of the Compton effect (adapted from [18]).

Pair production

Pair production is an absorption process in which a photon disappears, producing an electron and a positron [17]. Usually, it occurs near an atomic nucleus and has an energy threshold equal to the sum of the kinetic energies of the produced particles at rest, since that is the energy required to produce the mass of the electron-positron pair. The probability of occurrence of the pair production process increases rapidly with photon energy above the threshold. Although with lower probability, this effect can also take place in the field of an atomic electron, in a process usually called triplet production, since three particles share the available energy (an electron-positron pair and the orbital electron) [5, 17].

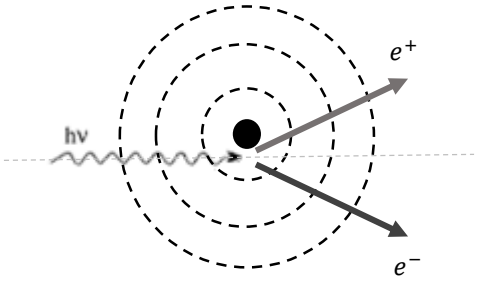

Figure 7 - Schematic representation of pair production (adapted from [17]).

Coherent (Rayleigh) scattering

In coeherent (Rayleigh) scattering the photon interacts with a bounded orbital electron, with a combined action of the whole atom. It is an elastic event, since the photons loses essentially none of its energy and is scattered through a small angle [5]. Coherent scattering has more practical importance at lower energies, since for low energy values the scattering angle is greater. However, the importance of this effect in tissue and tissue equivalent materials is small in comparison with other photon interactions [5].

Photonuclear interactions

In a photonuclear interaction an energetic electron enters and excites a nucleus, which then emits a proton or a neutron [17]. This type of interaction has a much smaller probability of occurrence than the other photon interactions and, for this reason, does not play an important role in radiation in clinical applications. However, photonuclear interactions are of concern for radiation protection in the case of high energy radiotherapy treatments because of the neutron production and of the radioactivity that is induced in the treatment room air and in machine components [5].

2.3.1.2. Electron interactions in matter

An energetic electron interacts with matter through Coulomb interactions with atomic orbital electrons and atomic nuclei, in which the electron may lose its kinetic energy (collision and radiative losses) or change its direction of travel (scattering) [5]

The collision between an incident electron and an orbital electron or nucleus of an atom may be elastic or inelastic. In the case of elastic collision, the electron is deflected from the original path, but it does not lose energy, while in an inelastic collision the electron is deflected from its original path and loses some of its energy. The lost energy is transferred to an orbital electron or emitted in the form of *bremsstrahlung*. Energetic electrons experiences a series of collisions as they traverse a medium. The type of interaction that an electron undergo with an atom of atomic radius a depends on the impact parameter b of the interaction, defined as the perpendicular distance between the electron direction before the interaction and the atomic nucleus [5], as can be observed in Figure 8:

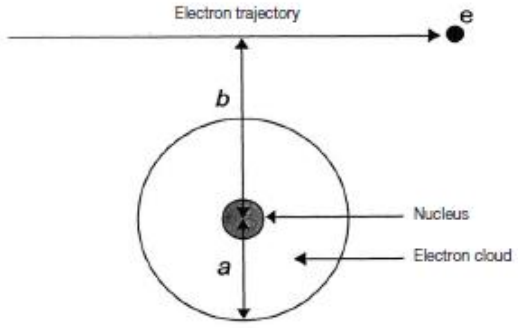

Figure 8 - Schematic representation of an interaction of an electron with an atom, where a is the atomic radius and b is the impact parameter [5].

- For $b \gg a$ the electron will undergo a soft collision with the whole atom. Only a small amount of energy will be transferred from the incident electron to orbital electrons;
- For $b \approx a$ the electron will undergo a hard collision with an orbital electron and an appreciable fraction of the electron's kinetic energy will be transferred to the orbital electron;
- For $b \ll a$ the incident electron undergoes a radiative interaction (collision) with the atomic nucleus. The electron will emit a photon (*bremsstrahlung*) with energy

between zero and the incident electron kinetic energy. The energy of the emitted *bremsstrahlung* photon is inversely proportional to the magnitude of the impact parameter b.

2.3.2. Basic clinical radiation dosimetry

Radiation dosimetry deals with methods for a quantitative determination of energy deposited in a given medium by ionizing radiation. A number of quantities and units have been defined for describing radiation beams [5], and the most relevant are described below:

Fluence and Energy Fluence

The fluence,Φ, is the quotient of dN by da, where dN is the number of particles incident on a sphere of cross-sectional area da [7]:

$$\Phi = \frac{dN}{da}. \tag{2.2}$$

The energy fluence, Ψ, is the quotient of dR by da, where dR is the radiant energy, which is the energy of the particles that are emitted, transferred or received (excluding rest energy), incident on a sphere of cross sectional area da [7]:

$$\Psi = \frac{dR}{da}. \tag{2.3}$$

The unit of fluence is m^{-2} and the unit of energy fluence is $J.m^{-2}$. The use of a sphere of cross-sectional area da expresses in the simplest manner the fact that one considers an area da perpendicular to the direction of each particle [7].

Kerma

The kerma, K, for ionizing uncharged particles, is the quotient of dE_{tr} by dm, where dE_{tr} is the mean sum of the initial kinetic energies of all the charged particles liberated in a mass dm of a material by the uncharged particles incident on dm [7]:

$$K = \frac{dE_{tr}}{dm}. \tag{2.4}$$

K quantifies the average amount of energy transferred from indirectly ionizing radiation to directly ionizing radiation [5].

Absorbed dose

The absorbed dose, D, is the quotient of $d\bar{\varepsilon}$ by dm, where $d\bar{\varepsilon}$ is the mean energy imparted by ionizing radiation to matter of mass dm [7]:

$$D = \frac{d\bar{\varepsilon}}{dm}. \tag{2.5}$$

Geometric parameters: SSD, SAD, Beam Central Axis and Field Size

The geometric parameters are of major importance for positioning the patient in relation to the radiation source and for a correct dose delivery.

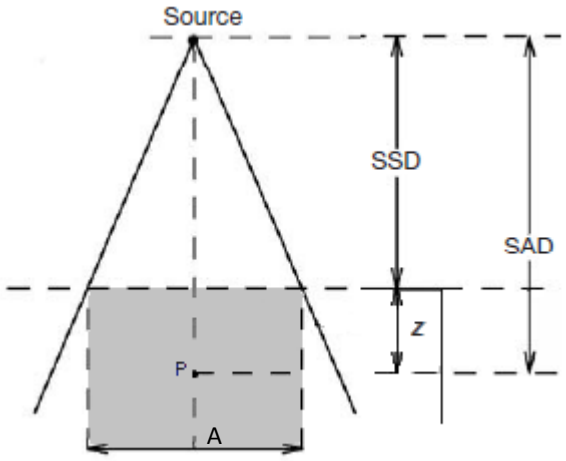

Figure 9 – Schematic representation of geometrical beam parameters - SSD, SAD and field size A (adapted from [5]).

Figure 9 shows the most relevant geometric beam parameters: SSD, SAD and field size A.

SSD, or source-surface distance, is the distance between the source and the surface of the phantom or patient skin. SAD, or source-axis distance, is the distance between the source and a point P located in the center of the target volume. SAD corresponds to the sum of the SSD and the depth z at which the target point is located [19].

The field size A is the cross section of the beam, commonly at the surface of the phantom or patient, but it can also be specified for a depth z [19].

The beam central axis corresponds to the vertical dashed line represented in Figure 9 and consists in the geometric center of the beam [19].

Percentage Depth Dose

A direct measurement of the dose distribution inside the patient is essentially impossible, yet it is necessary to know precisely and accurately the dose distribution in the irradiated volume for a successful outcome of treatments. This is usually achieved through the use of several functions that link the dose at any arbitrary point inside the patient to the known dose at the beam calibration (or reference) point in a phantom.

A typical dose distribution on the central axis (absorbed dose variation with depth) of a megavoltage photon beam striking a patient is represented in Figure 10. The beam enters the patient on the surface, where it delivers a certain surface dose D_s. Beneath the surface the dose

first rises rapidly, reaches a maximum value at depth z_{max} and then decreases almost exponentially until it reaches a value D_{ex} at the patient's exit point [5].

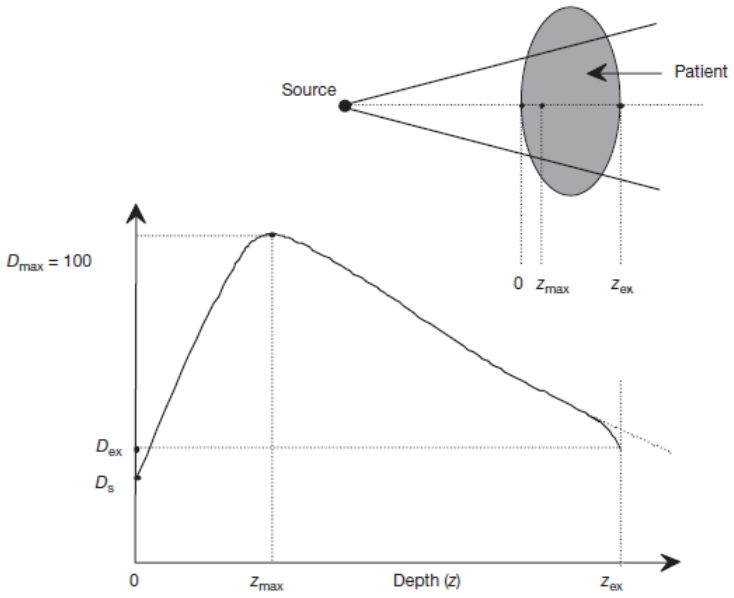

Figure 10 - Dose deposition from a megavoltage photon beam in a patient. D_s is the surface dose at the beam entrance surface, D_{ex} is the surface dose at the beam exit site and D_{max} is the dose maximum often normalized to 100, resulting in a curve of absorbed dose variation with depth, percentage depth dose (PDD) distribution [5]

Central axis dose distributions inside a patient or phantom are usually normalized to D_{max} = 100% at the depth of dose maximum z_{max} and referred to as percentage depth dose (PDD) distributions [5].

Off-axis beam profiles

In addition to dose distributions along the central axis, off-axis dose profiles can be obtained. Beam profiles are graphical representations of absorbed dose distribution in function of the distance to the beam central axis, measured perpendicularly to the axis at a given depth. An example is shown in Figure 11.

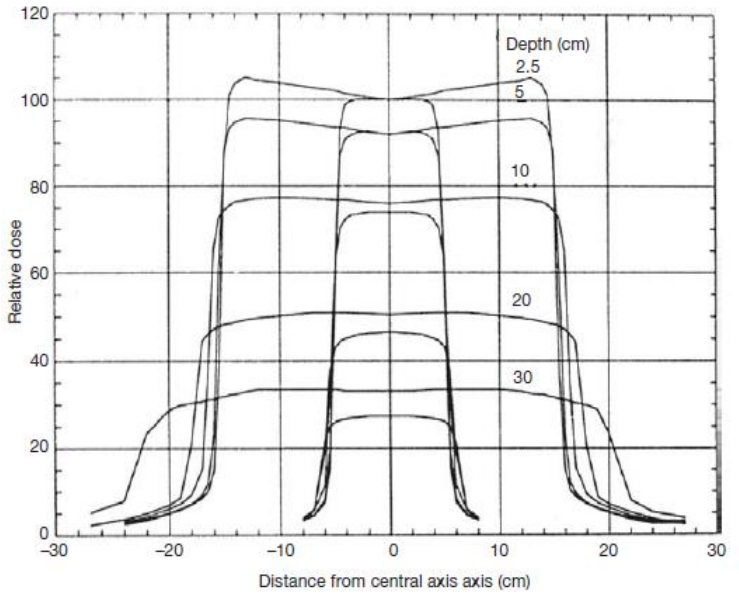

Figure 11 - Example of beam profiles for two field sizes (10 x 10 cm² and 30 x 30 cm²) and 10 MV X-ray beam at various depths in water [5].

Off-axis beam profiles can be obtained for x and y axis, with the denomination of crossline and inline profiles, respectively.

2.4. Medical Linear Accelerators

2.4.1. General Concepts

A linear accelerator is an isocentrically mounted machine that uses high-frequency electromagnetic waves to accelerate electrons to energies in the range of 4-25 MeV, using linear acceleration structures. These electron beams can be directly used for superficial lesions or transformed in high-energy X-rays, after collision with a target [9].

Figure 12 - Linear accelerator [https://www.varian.com/oncology/products/treatment-delivery/clinac-ix]

Modern linacs are usually capable of emitting two X-ray energies, 6 MV and another in the range 10-23 MV, as well as a wide range of electron energies. It is divided in five major sections, as it can be seen on Figure 13: gantry, gantry stand or support, modulator cabinet, patient support assembly (treatment table) and control console [5].

For the beam generation, the main components of modern medical linacs involved are [5]:

- Injection system, or electron gun;
- RF power generation system;
- Accelerating waveguide;
- Auxiliary system (vacuum pump, cooling system, among others);
- Beam transport system;
- Beam collimation and beam monitoring system.

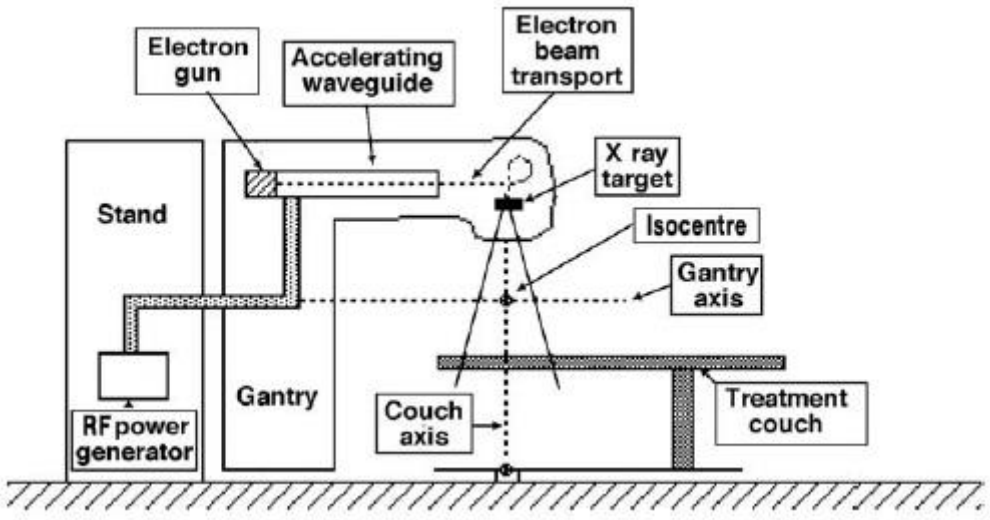

Figure 13 – Schematic representation of a linear accelerator [5].

The injection system, also called electron gun, is the source of electrons, containing a heated filament cathode and a perforated anode. Electrons are emitted thermionically from the heated cathode, focused into a pencil beam by a curved focusing electrode and accelerated towards the anode, through which they pass to the accelerator waveguide, due to the action of electrostatic fields [5, 20].

In the accelerating waveguide, microwave radiation is used to accelerate the electrons produced in the electron gun to the desired kinetic energy. For the production of the microwave radiation, a RF power generation system is used, consisting of a pulsed modulator and an RF power source [5]. The pulsed modulator applies synchronized high frequency, high current and short duration pulses to the electron gun and the RF power source [5, 20]. The RF power source can be a magnetron or a klystron. The functioning of both consists in accelerate and decelerate electrons in vacuum in order to produce high power RF. However, a magnetron produces high power RF, while a klystron is a power amplifier that amplifies RF generated by a low power oscillator (RF driver) [5].

The microwaves are carried to the accelerating waveguide by reflection in the walls of rectangular waveguides. To increase efficiency of RF conduction, the waveguides are pressurized with a dielectric gas, usually sulphur hexafluoride (SF_6) to twice the atmospheric pressure [5].

The simplest kind of accelerating waveguide is divided into a series of cylindrical cavities, resultant from the addition of a series of discs with circular holes at the center, placed at equal distances along the tube. These cavities were evacuated to allow free propagation of electrons and have two main purposes: couple and distribute the microwave energy between adjacent cavities and provide an adequate electrical field pattern for the acceleration of the electrons [5].

The electrons leave the accelerator waveguide in the form of pencil, or narrow, beams to the beam transport system in order to produce photon or electron beams in the linear accelerator treatment head, according to the selected treatment mode [20].

The accelerating waveguide is usually mounted parallel to the gantry rotation axis for linear accelerators operating at energies above 6 MeV. For this reason, bending magnets are used to bend the electron beam in order to make it strike the X-ray target or be able to exit the beam exit window. Three systems for electron bending have been developed: 90^o degrees bending, 270^o bending (achromatic) and 112.5^o bending. Steering coils and focusing coils are also components of the beam transport system, used for steering and focusing of accelerated electron beam [5].

The main components of a typical linac treatment head are [5]:

- Retractable X-ray targets;
- Flattening filters and electron scattering foils (also called scattering filters);
- Primary and adjustable secondary collimators;
- Dual transmission ionization chambers;
- A field defining light and a range finder or optical distance indicator;
- Optional MLC;
- Optional retractable wedges.

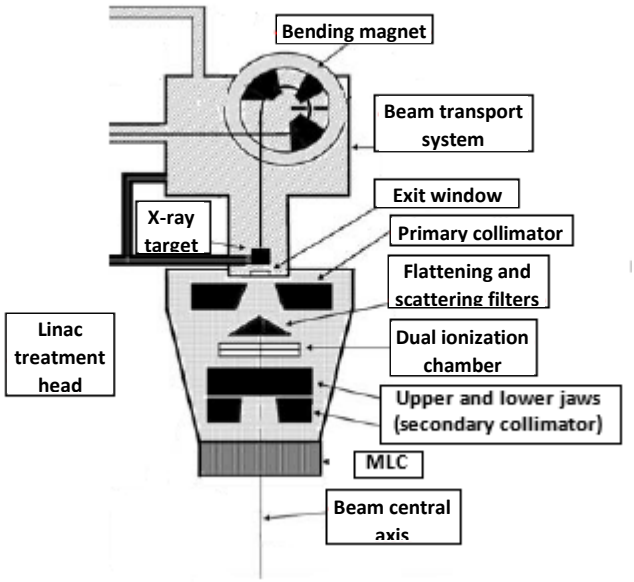

Figure 14 - Schematic representation of a linac treatment head (adapted from [5]).

Clinical photon beams are produced with a combination of target-flattening filters, while clinical electron beams are produced by retracting the target and flattening filter from the electron beam and either scattering the pencil beam with scattering foils or deflecting and scanning the pencil beam magnetically to cover the field size required for electron treatment.

The electron beam currents that produces clinical electron beams also differs, being two or three orders of magnitude lower than the electron currents used for the production of clinical photon beams in the linear accelerator X-ray target [5].

The primary and secondary collimators define the field dimensions: a maximum circular field is defined by the primary collimator, while the secondary collimator, which consists of four adjustable blocks, two forming the upper and two forming the lower jaws of the collimator, can provide rectangular or square fields at the linear accelerator isocenter, with maximum dimensions of 40 x 40 cm^2 [5].

Besides the primary and adjustable secondary collimators, a multileaf collimator (MLC) can also be used for photon beam collimation. MLCs contain several leaves, usually 120 (60 pairs in two banks), with an individual computer controlled motor for each leaf, and are used for intensity modulated fields supply, either in step and shot mode or in a continuous dynamic mode [5]. Special cones, or applicators, are used for the collimation of clinical electron beams.

Dual transmission ionization chamber are used for monitoring continuously photon and electron beam output during patient treatment. The ionization chambers are sealed, in order to make their response independent of ambient temperature and pressure [5].

The field defining light and the range finder (or optical distance indicator) are used as visual methods for correctly positioning the patient according to reference marks that are drawn in the patient body (or in immobilization devices) in the planning CT. These reference marks have the finality of guarantying that the position of the patient during the treatment sessions is the same than in the acquisition of the CT images used for the treatment planning. The range finder is used to place the patient at the correct treatment distance by projecting in the patient's skin a centimeter scale that indicates the vertical distance from the linear accelerator isocenter [5].

Linear accelerators include also an auxiliary system that consists of several services that are not directly involved with electron acceleration, yet make the acceleration possible and the linear accelerator viable for clinical operation [5]. This auxiliary system includes [5, 20]:

- A vacuum pumping system with an ionic pump that produces vaccum in the electron gun, RF generator, accelerating guide and electron beam transport system;
- A water cooling system used for cooling the accelerator guide, target, circulator and RF generator ;
- A pressure system with SF_6 to the waveguides that conducts the microwaves to the accelerating guide;
- An automatic frequency control system to maintain the optimal operation frequency in the accelerating guide;
- Shielding system against leakage radiation.

2.4.2. Quality Assurance

The selection, installation and clinical use of modern radiation equipment involves several procedures: development of the specifications of the radiation equipment, design and construction of the facilities to accommodate the selected radiation equipment, including radiation shielding, installation of the selected radiation equipment, acceptance testing of the installed equipment, commissioning of the accelerator for active clinical use, training of the staff for the use of the accelerator and development and application of a comprehensive quality assurance (QA) program [21].

Acceptance tests assure that the specifications contained in the purchase order are fulfilled and that the environment is free of radiation and electrical hazards to staff and patients. The tests can be divided into three groups: safety checks, mechanical checks and dosimetry measurements. Upon satisfactory completion of the acceptance tests, a document certifying that the conditions are met is signed and the unit is transferred to the institution [5].

After the transference of the unit to the institution, a commissioning process is required, including tasks as acquisition of all radiation beam data, including beam output, required for the treatment, organization of these data into a dosimetry data book, entering these data into a computerized treatment planning system (TPS), development of all dosimetry, treatment planning and treatment procedures, verification of the accuracy of these procedures, establishment of quality control tests and procedures and training of all personnel [5].

In addition, it is necessary to assure that the machine characteristics do not deviate significantly from their baseline values acquired in acceptance and commissioning procedures during its functioning life, by implementing quality assurance procedures. These procedures reduce uncertainties and errors, improving dosimetric and geometric accuracy and the precision of dose delivery and, consequently, treatment outcomes, raising tumor control rates as well as reducing complication and recurrence rates. Quality assurance increases also the probability of recognizing and rectifying sooner possible errors and accidents, reducing their consequences for patient treatment. For linear accelerators, quality assurance is recommended daily, weekly, trimestral and annually [22]. In the context of present work, further details about the daily and trimestral quality controls are presented in the next sections.

2.4.2.1. Daily Quality Assurance

Daily quality assurance includes mechanical, safety and dosimetric procedures, as well as verification of room conditions, such as temperature and pressure [22]:

- The mechanical tests include verification of laser localization, optical distance indicator and field size indicators.
- The Safety tests include verification of interlocks (treatment console beam off button and switch, emergency beam off switches, collision interlocks, door interlock, for instance), beam on indicators, door closing safety and audiovisual monitor.

- Output constancy verifications for all photon and electron energies are performed as daily quality assurance dosimetric tests, which are studied with more detail above.

A summary of daily quality assurance procedures and recommended tolerances can be observed in Table 1, obtained from [22].

Procedure	IMRT tolerance
Dosimetry	
X-ray output constancy (all energies) Electron output constancy (weekly, except for machines with unique e-monitoring requiring daily)	3%
Mechanical	
Laser localization	1.5 mm
Distance indicator (ODI) @ iso	2 mm
Collimator size indicator	2 mm
Safety	
Door interlock (beam off)	Functional
Door closing safety	Functional
Audiovisual monitor(s)	Functional
Stereotactic interlocks (lockout)	NA
Radiation area monitor (if used)	Functional
Beam on indicator	Functional

Table 1 - Daily quality assurance recommended procedures and tolerances for IMRT (adapted from [22]).

Dosimetric verifications, the most important for the present study, consist mainly on the verification of the stability of dose in central axis (CAX), flatness, symmetry in X (left-right) and Y (gun-target) axis and beam quality factor (BQF), using constancy check devices.

Dose is determined in the central axis of the linac in relation to a reference value and a percentage CAX dose is obtained, allowing to verify its stability over time.

Beam flatness is obtained by finding the maximum D_{max} and minimum D_{min} dose point values on the beam profile (dose in function of distance to the central axis) within the central 80% of the beam width and then using the relationship [5]:

$$F = 100 \times \frac{D_{max} - D_{min}}{D_{max} + D_{min}}. \tag{2.6}$$

Beam symmetry can be defined as the dose difference between any two dose points on a beam profile, equidistant from the central axis point [22]. In the daily quality assurance, the symmetry is determined for the X-axis (from left to right) and for the Y-axis (from gun to target). An alternative, although equivalent, is to describe the symmetry (S) as the deviation between the doses on both sides (left and right) of the central axis [5]:

$$S = 100 \times \frac{area_{left} - area_{right}}{area_{left} + area_{right}}. \tag{2.7}$$

Beam quality is related with the fact that a beam contains a large spread of energies, which determine the penetration of a beam in a material. However, the direct measure of the beam

spectra is difficult and, for this reason, the beam quality is approximated by the potential that generates the radiation and the half value layer, HVL, which represents the thickness of an attenuator that decreases the measured air kerma rate in air to half of its original value [5, 23].

Although the recommended tolerance for daily quality assurance is of 3.00% [22] in the service a 2.00% tolerance was established as indicator for stability monitoring.

2.4.2.2. Trimestral and Annual Quality Assurance

Although mensal QA procedures are recommended, a different QA program was established in IPOLFG Radiotherapy Service, in which trimestral verifications are performed after periodic preventive maintenance.

The tests performed in trimestral QA are similar to the summarized in Table 2, consisting mainly in verifications of X-ray and electron output constancy, dose monitoring as a function of dose rate, photon and electron beam profile constancy, as well as verification of light/radiation field coincidence and mechanical indicators position [22]. The tests are performed using a water phantom and ionization chambers.

Procedure	IMRT tolerance
Dosimetry	
X-ray output constancy Electron output constancy Backup monitor chamber constancy	2%
Typical dose rate[a] output constancy	2% (@ IMRT dose rate)
Photon beam profile constancy	1%
Electron beam profile constancy	1%
Electron beam energy constancy	2%/2 mm
Mechanical	
Light/radiation field coincidence[b]	2 mm or 1% on a side
Light/radiation field coincidence[b] (asymmetric)	1 mm or 1% on a side
Distance check device for lasers compared with front pointer	1mm
Gantry/collimator angle indicators (@ cardinal angles) (digital only)	1.0°
Accessory trays (i.e., port film graticle tray)	2 mm
Jaw position indicators (symmetric)[c]	2 mm
Jaw position indicators (asymmetric)[d]	1 mm
Cross-hair centering (walkout)	1 mm
Treatment couch position indicators[e]	2 mm/1°
Wedge placement accuracy	2 mm
Compensator placement accuracy[f]	1 mm
Latching of wedges, blocking tray[g]	Functional
Localizing lasers	±1 mm
Safety	
Laser guard-interlock test	Functional

Table 2 – Monthly quality assurance recommended procedures and tolerances for IMRT (adapted from [22]).

Annually, in one of the trimestral verifications, more detailed tests are performed, according to annual QA recommendations. The verifications are similar to the performed in the trimestral

QA, although with absolute measurements. The recommended annual QA procedures are summarized in Table 3.

Procedure	IMRT tolerance
Dosimetry	
X-ray flatness change from baseline	1%
X-ray symmetry change from baseline	±1%
Electron flatness change from baseline	1%
Electron symmetry change from baseline	±1%
SRS arc rotation mode (range: 0.5–10 MU/deg)	NA
X-ray/electron output calibration (TG-51)	±1% (absolute)
Spot check of field size dependent output factors for x ray (two or more FSs)	2% for field size $<4\times4$ cm^2, 1% $\geq4\times4$ cm^2
Output factors for electron applicators (spot check of one applicator/energy)	±2% from baseline
X-ray beam quality (PDD_{10} or TMR_{10}^{20})	±1% from baseline
Electron beam quality (R_{50})	±1 mm
Physical wedge transmission factor constancy	±2%
X-ray monitor unit linearity (output constancy)	±5% (2–4 MU), ±2% ≥5 MU
Electron monitor unit linearity (output constancy)	±2% ≥5 MU
X-ray output constancy vs dose rate	±2% from baseline
X-ray output constancy vs gantry angle	±1% from baseline
Electron output constancy vs gantry angle	±1% from baseline
Electron and x-ray off-axis factor constancy vs gantry angle	±1% from baseline
Arc mode (expected MU, degrees)	±1% from baseline
TBI/TSET mode	Functional
PDD or TMR and OAF constancy	1% (TBI) or 1 mm PDD shift (TSET) from baseline
TBI/TSET output calibration	2% from baseline
TBI/TSET accessories	2% from baseline
Mechanical	
Collimator rotation isocenter	±1 mm from baseline
Gantry rotation isocenter	±1 mm from baseline
Couch rotation isocenter	±1 mm from baseline
Electron applicator interlocks	Functional
Coincidence of radiation and mechanical isocenter	±2 mm from baseline
Table top sag	2 mm from baseline
Table angle	1°
Table travel maximum range movement in all directions	±2 mm
Stereotactic accessories, lockouts, etc.	NA
Safety	
Follow manufacturer's test procedures	Functional
Respiratory gating	
Beam energy constancy	2%
Temporal accuracy of phase/amplitude gate on	100 ms of expected
Calibration of surrogate for respiratory phase/amplitude	100 ms of expected
Interlock testing	Functional

Table 3 - Annual quality assurance recommended procedures and tolerances for IMRT [22].

For linacs equipped with multileaf collimators, weekly and trimestral QA procedures for verification of MLC parameters are also performed, including determination of MLC transmission, leaf position accuracy and travel speed, for instance [22].

MLC transmission factor, or leaf transmission factor, can be defined as the ratio between the dose measured with an open field and the dose measured with a field of the same dimension with the leaves closed, describing the average transmission through the leaves [24].

Besides MLC transmission factor, it is important to determine the separation between the leaves, resultant from the rounded shape of lead ends, which improves the dosimetric characteristics of the MLC, but allows the transmission of radiation through the leaves even when they are completely closed. As leaf ends are defined as square in the TPS, it is necessary to perform an adjustment to take into account the separation between the leaves, resultant from their rounded end shape. This adjustment is performed by means of the dosimetric leaf separation (DLS) [24]. It is also important to verify DLS stability, since the separation between the leaves is susceptible to external factors, such the presence of dust between the leaves.

In the present study only dosimetric and MLC constancy tests are analyzed, using dose calibration factor, symmetry in X (left-right) and Y (gun-target) axis, MLC transmission and dosimetric leaf separation (DLS).

Other frequent constancy tests are performed with EPID imaging, such as garden fence and chair tests, used to evaluate the stability of MLC leaves movements and differentiate the impact of the MLC transmission factor and dosimetric leaf separation, respectively [22, 25].

For IMRT treatments, individual verification for each treatment is performed using EPID dosimetry.

Dose calibration factor consists in a factor that relates the number of monitor units (MU) with which the phantom is irradiated and the dose value measured with the ionization chambers. Monitor units (MU) refer to a numeric value defined in the treatment machine for treatment delivery in accordance with the planned doses. However, it is necessary to calibrate the treatment machines to make the number of monitor units delivered coincident with the planned doses. The calibration is performed by the calculation of the previously mentioned factor, output factor or dose calibration factor for medical linear accelerators. In the case of medical linacs, the dose calibration factor is expressed in cGy/MU [5].

Beam symmetry can be defined as the dose difference between two points equidistant to the central axis, as described for daily quality assurance [22].

2.4.3. Beam-Matching

Many radiation therapy centers are equipped with more than one linear accelerator of the same vendor, model and MLC. In these cases, treatment efficiency can be increased if immediate interchange of patients between the accelerators, without needing to replan, is possible, in the case of interruption of the functioning of one of the machines, due to improperly functioning or periodic preventive maintenance. To make this possible, a high similarity level between the dosimetric characteristics of the linear accelerators is required, which is achieved by tuning the

treatment beams of a unit being installed in such a way that the dosimetric characteristics meet reference values within a specified interval. If all the linacs in an institution have been tuned to these reference values, they are also tuned to each other [1, 26].

This tuning procedure is called “beam-matching”. As mentioned previously for commissioning process, during a conventional installation of a linac an extensive set of dosimetric data has to be gathered for a proper commission of the equipment, as well as to obtain all beam data need for beam modeling in the TPS. However, dosimetric workload during the commissioning can be significantly reduced with beam-matching, since, instead of measuring the full set of dosimetric data, only a set of cross-check measurements is needed to verify the agreement of subsequently installed units with the reference beams data, gathered during the commissioning of a reference unit [1]. Matched linear accelerators are then represented by a common set of data in the TPS [26].

Manufacturers beam-matching acceptance criteria are usually based on depth dose curves, as well as dose profiles, measured at a predefined geometry, using only some points of the curves to evaluate the quality of beam-matching, instead of the entire curves [1]. For these reasons, some doubts have arisen in relation to the viability of using indistinctly beam-matched linacs, representing them by the same set of data in the TPS and further tests have been suggested to verify the dosimetric equivalence for more parameters and for advanced techniques as IMRT, in which small photon fields are used, as well as movement of the MLC, increasing the susceptibility to small variations in output factors or MLC speed or leaf separation, for instance [2, 6].

2.5. Treatment Planning System

2.5.1. General Fundamentals

Computerized treatment planning systems (TPSs) are used in external beam radiotherapy to generate beam shapes, configuration and dose distributions in order to reach the goal of all radiotherapy treatment: maximize the dose to target volume and minimize normal tissue irradiation [5].

Until the 1970s dose computation equipment was available and was used to develop isodose distribution atlases. During 1970s and 1980s, treatment planning computers became more specialized, with more sophisticated dose calculation algorithms and image display capabilities. Currently, computerized TPSs are widely used in radiotherapy centers. Many of these systems have both complex three dimensional image manipulation and dose calculation capabilities [27].

The radiation treatment planning is a complex process involving several steps. The first step consists in the derivation of patient anatomical information from CT scans or other image modalities, such as magnetic resonance imaging (MRI) or positron emission tomography (PET). This anatomical information is then used to determine the location of the tumor and surrounding critical normal tissues that can be affected by the radiation treatment and a TPS is

used to determine the dose distribution that will result in the body from incident beams. The optimum beam arrangement to provide adequate coverage of the malignant tissues while minimizing the dose to critical normal tissues is selected and the radiation dose is then calculated throughout the volume of interest by the TPS. Further addition of beams or modification of beam direction, weighting or shaping may be required to improve the treatment plan, if the dose distribution is not adequate [27].

For conventional radiotherapy techniques, as well as for 3DCRT, the treatment planning is performed by defining a set of beams and then adjusting the beams to obtain a desired distribution, which is called direct planning. However, for modulated advanced techniques, as IMRT, the treatment planning is performed using an inverse planning technique. In inverse planning, a desired distribution is defined and then the characteristics of the beams to obtain that distribution are determined by the algorithm. This is done by describing a series of descriptors characterizing the desired absorbed-dose distribution within the tumor and additional descriptors designed to spare normal tissues. The inverse planning process works iteratively to determine beam shapes and fluence patterns to achieve an optimal, or acceptable, absorbed-dose distribution. These descriptors are incorporated into a mathematical objective function that attempts to specify the function's merit (also called goodness of the plan) with a single number. The optimization procedure consists in an iterative search for the solution that maximizes the goodness, guided by the objective function. The values of the descriptors are adjusted throughout the process, in order to achieve a compromise among the different goals. Due to the iterative nature of the process and the need to change the values of the treatment descriptors, this treatment planning procedure is also called "optimized planning" [14].

2.5.1.1. Definition of Volumes

To determine the dose distribution that will result from incident beams in target volumes and surrounding healthy tissues, in order to obtain a treatment plan, it is necessary to previously define several volumes. Delineation of these volumes is an obligatory step in the planning process, since absorbed dose cannot be prescribed, recorded and reported without specification of the target volumes and volumes of normal tissues at risk. The main volumes are [14]:

- The gross tumor volume (GTV) is the gross demonstrable extent and location of the tumor. Typically, The GTV may consist of a primary tumor, metastatic regional nodes or distant metastasis;
- The clinical target volume (CTV) is a volume of tissue that contains the GTV and/or subclinical malignant disease with a certain probability of occurrence;
- The internal target volume (ITV) can be defined as the CTV plus a margin taking into account uncertainties in size, shape and position of the CTV within the patient. It is considered an optional tool in helping to delineate the PTV;
- The planning target volume (PTV) is a geometrical concept introduced for treatment planning and evaluation, recommended to ensure that the prescribed absorbed dose will actually be delivered to all parts of the CTV with a clinically acceptable

probability, despite geometrical uncertainties such as organ motion and setup variations. It is also used for absorbed dose prescription and reporting, since it surrounds the representation of the CTV with a margin such that the planned absorbed dose is delivered to the CTV. This margin takes into account both the internal and the setup uncertainties. The latter consists in uncertainties in patient positioning and alignment of the therapeutic beams during the treatment planning and through all treatment sessions.

The organ at risks (OARs), or critical structures, are tissues that, if irradiated, could suffer significant morbidity and thus might influence the treatment planning and/or the absorbed dose prescription. In principle, all non-target tissues could be OARs, but usually normal tissues are considered as OARs depending on the location of the CTV and/or the prescribed absorbed dose [14].

Finally, planning organ at risk volume (PRV) is analog to PTV, consisting in margins that are added to OARs to compensate for uncertainties and possible variations in the positions of the OAR during treatment [14].

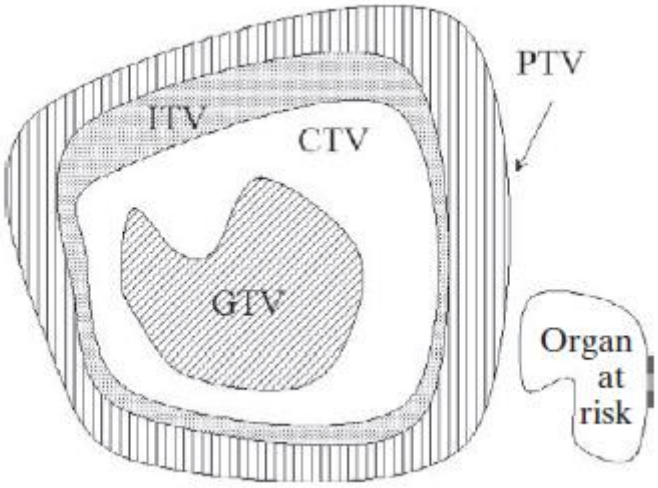

Figure 15 - Graphical representation of the volumes of interest [5].

2.5.2. Dose Calculation: The Analytical Anistropic Algorithm

The functionality and quality of a TPS depends on the type and accuracy of the algorithms used in the planning process. An algorithm can be defined as a sequence of instructions that operates on a set of output results that are of interest to the user [27].

Accuracy has always been a concern for the definition of TPS algorithms, especially when it is used for IMRT treatments planning, in the presence of heterogeneities, since predictions of correction-based dose calculation algorithms may deviate greatly from the measurement in or near heterogeneous regions. In these algorithms, dose distributions are typically calculated by density scale to correct for dose changes in the presence of heterogeneities, with density values obtained by CT images [28, 29].

Monte Carlo simulation consists in the successive sampling of random variables until a result of acceptable precision is obtained for the proposed problem, which, in the case of radiotherapy, is the description of radiation and matter interaction processes [30]. The large calculation uncertainty in the presence of heterogeneities results from the invariance of the dose kernel, or energy spread obtained from the simulation, which in correction-based algorithms, does not account for spectral changes depending on the distance from the interaction point to the energy absorption point [5, 28].

Over the last years, it is believed that precise dose calculation need MC methods to take correctly into account the electron transport governing the dose deposition process. However, MC methods are too time consuming to be used in clinical situations [29]. Due to the previous limitations, improvements in the algorithms had to be made, with a preference for convolution/superposition algorithms for use in TPSs. In these convolution/superposition algorithms, dose calculations are performed in heterogeneous media by transforming the dose kernel using the density scaling derived from the electron density distributions obtained from CT images [28].

The anisotropic analytical algorithm (AAA) is a convolution/superposition algorithm implemented in Eclipse™ treatment planning system of Varian Medical Systems, Inc. The total dose deposition is calculated as the superposition of the dose deposited by two photon sub-sources (primary photons and secondary or scattered extra-focal photons) and by an electron contamination sub-source (scattered electrons). The AAA algorithm accounts for heterogeneities by calculating the photon dose as a three-dimensional convolution of MC precalculated scatter kernels, scaled according to the changes in electron density in the neighborhood of an interaction point [28, 29]. The clinical beam is divided into small beamlets and the patient body volume is divided into a matrix of 3D calculation voxels along these beamlets. The calculation voxels are associated with a mean electron density that is computed from the patient CT images according to a user-defined calibration curve [29]. Convolution is performed on one beamlet for each of the three sub-sources and then the final dose distribution is obtained by superposition of the dose contributions of all the individual beamlets [28]. An optimization algorithm determines the parameters characterizing the multiple source model by optimizing the agreement between the calculated and measured depth dose curves and profiles for the beam data [29].

2.5.3. Dose evaluation tools: isodose and Dose Volume Histogram

After the calculation of dose distributions, which can be obtained for a few significant points within the target volume, a grid of points over a two-dimensional contour or image, or a three-dimensional array of points that covers the patient's anatomy, evaluation of the plan has to be performed [5].

The treatment plan evaluation consists of verifying the treatment simulation in the 3D geometry, in order to ensure that the desired PTV is targeted adequately. Other evaluation tools are also verified to ensure that target coverage is adequate and that critical structures

surrounding the PTV are spared as necessary, including isodose curves, orthogonal planes and isodose surfaces, dose distribution statistics, differential and cumulative dose-volume histograms (DVHs) [5].

Isodose curves are used to evaluate treatment plans along a single plan or several plans in the patients. The isodose covering the periphery of the target is compared with the isodose at the isocenter and, if the ratio is within a desired range, close to 100%, and critical organ doses are not exceeded, the plan may be accepted [5].

However, if a larger number of transverse planes are used for calculation, such as with CT scans, isodose distributions can be generated on orthogonal CT planes, reconstructed from the original axial data. Sagittal and coronal, coronal and transversal plane isodose distributions are commonly available in 3D TPSs, and displays on arbitrary oblique planes are also available in some TPSs. It is also possible to map the isodoses in three dimensions and overlay the resulting isosurface on a 3D surface of the target and/or surrounding organs [5].

Dose statistics can also be used for plan evaluation, which, in spite of not showing the spatial distribution of dose superimposed on CT slices or on anatomy that has been outlined based on CT slices, provide quantitative information on the volumes of the target or critical structures and on the dose received by that volume. The mostly used dose statistics for plan evaluation are [5, 31]:

- The minimum dose (D_{min}), which is the lowest dose in a defined volume;
- The maximum dose (D_{max}), which is the highest dose in a defined volume;
- The mean dose (D_{mean}), which is the average of the dose values of a large number of discrete points uniformly distributed in the volume in question;
- The volume irradiated to at least 95% of the prescribed dose, $V_{95\%}$.

DVHs are another important tool for the evaluation of treatment plans. In the simplest form, a DVH represent a frequency distribution of dose values within a given volume. However, DVHs are usually presented in the form of per cent volume as a function of dose for a volume of interest. Two types of DVH can be used: direct (or differential) DVH and cumulative (or integral) DVH, represented in Figures 16 and 17. The direct DVH results from the sum of voxels with an average dose within a given range and plots the result percentage volume as a function of dose. The ideal direct DVH for a target volume would be a single column indicating that the prescribed dose is received by 100% of the target volume. However, since not only the dose received by 100% of the volume is important for the evaluation of a treatment plan, cumulative DVHs are more used. The cumulative DVH is displayed by the planning system by means of calculation of the volume of the target or critical structure that received at least the given dose and plot this volume (or percentage volume) versus dose, starting with 100% of the volume for 0 Gy (all the volume receives at least no dose) [5].

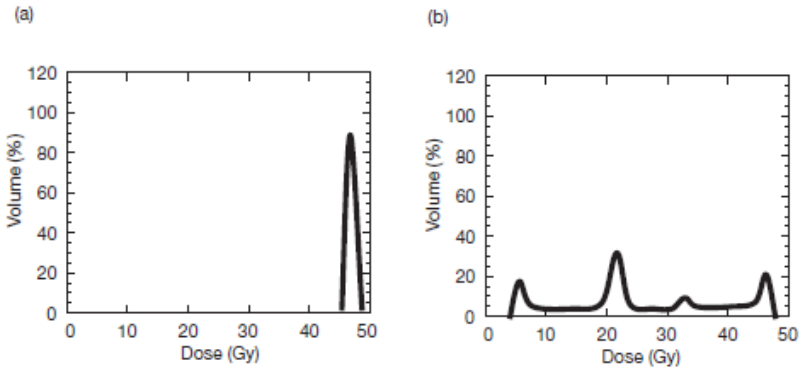

Figure 16 - Differential DVHs for a prostate treatment plan for a) the target volume and b) a critical structure [5].

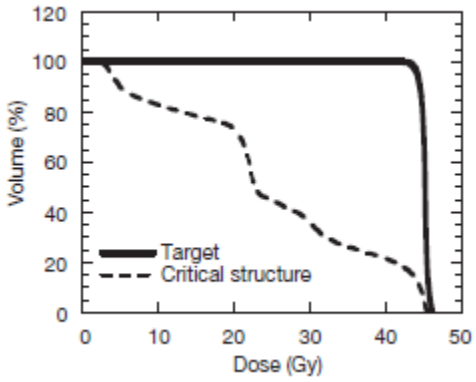

Figure 17- Cumulative DVHs for the target volume and critical structures of the same prostate treatment plan of Figure 7 [5].

2.6. IMRT Verification

As mentioned previously, IMRT is a powerful technique to achieve a better dose conformity to the tumor volume and an increased sparing of normal tissues for many tumor sites, However, this is only achieved if the planned fluence is delivered accurately at the treatment unit, requiring careful verification, since IMRT is more susceptible to the occurrence of errors, due to the use of small size fields and the strong role of MLC leaf movements in this technique. In some cases, the calculated leaf sequence does not accurately result in the fluence pattern used by the TPS for dose calculation, justifying the implementation of pre-treatment verification in order to ensure the accuracy of IMRT treatments [32].

Pre-treatment verification is included in patient-specific QA and can be performed using phantom (water phantom, solid water phantom or polystyrene rectangular phantom), which are irradiated with the planned beams. The absorbed dose distributions can be obtained as the sum of all the beams contributions, using ionization chambers or films, and the measured absorbed dose value is compared with TPS calculated absorbed dose, either through point doses, line profiles or two dimensional dose matrices [14, 33].

It is also possible to measure the intensity of individual beams by directing the beam normally onto a phantom with a flat surface and measuring the absorbed dose received, using dosimeter

detectors placed at convenient locations. The dosimeter system is then irradiated using the planned beams all delivered from a single gantry angle (0°, for instance) and the incident irradiation pattern from each beam is generated by the TPS and compared with the measurements. The comparison is usually performed individually for each field delivered and, if all the intensity patterns are acceptable, it is assumed that the absorbed dose in the patient will be correct. Although film-based dosimetry can also be used to determine beam intensity, multipoint planar dosimeters, as diode arrays and electron portal imaging devices (EPID) are the most used systems [14].

A complementary pre-treatment verification method consists in independent absorbed-dose calculations for the patient-specific beam intensity pattern, using a different algorithm, for instance, which are then compared with TPS calculated absorbed dose values [14].

In vivo dosimetry can also be performed as part of patient-specific QA, using thermoluminescent dosimeters (TLDs), diodes and MOSFETs to determine the dose absorbed by the patient during the treatment. However, this method is not used in all radiotherapy centers, due to its limitations, which consists in the determination of the absorbed dose at only one or few points that could not be the typical absorbed dose in the entire target volume. In IMRT, this limitation is increased by the possibility of the existence of significant gradients at the measure point that can lead to reading uncertainties [14].

2.6.1. Dosimetry Equipment

2.6.1.1. Electronic Portal Imaging: EPID

Electronic portal imaging devices (EPID) provides a more efficient and effective method for verifying IMRT delivery due to their digital nature, which provides quantitative tools for population-based or individual patient systematic and random error analysis and replaces the multiple manual steps involved in portal film imaging with computer-controlled image acquisition, processing and display. EPID also allows to capture multiple images during each treatment without the need to re-enter the room to position the device [34, 35].

The development of electronic portal imagers began in the 1950s, becoming commercially available in the late 1980s as a system consisting of a metal plate-phosphor screen used to convert photon beam intensities into light images, as well as to block low energy scattered photons. The light in the screen was viewed by a camera using a mirror set at a 45° angle, generating a video signal in the camera. This video signal was digitized and viewed on a monitor [5, 36, 37].

These camera-based EPIDs present major limitations related to light collection efficiency of the optical chain. Since the light is highly scattered within the phosphor screen, it is emitted from the rear of the screen in all directions with equal probability and only the light photons that are emitted within a small cone subtended by the lens of the camera can generate a video signal in the camera. However, the use of large aperture lenses leads to a decrease in spatial resolution and depth of field, generating also distortions in the images [37].

Although the limitations of camera-based EPIDs has been partially surpassed by adjustments in the system, alternative EPID systems have been developed. One of these systems, matrix ion chamber device, consists of a matrix of 256 x 256 ionization cells, formed by two sets of electrodes, with 256 wires each, oriented perpendicularly to each other and separated by a 0.80 mm gap, which is filled with a fluid (2,2,4-trimethylpentane) that is ionized when the device is irradiated. One set of electrodes is connected to 256 electrometers and the other set is connected to a high-voltage supply. The device contains also a plastoferrite plate in order to convert primary X-rays into high energy electrons, as well as to block low energy scattered radiation. The matrix ion chamber array is read out by successively applying a high voltage to each of the electrodes and measuring the signal generated in each of the 256 signal electrodes [36, 37].

Important advantages of the matrix ion chamber include its compact size, which makes the device a good replacement for film cassettes, and the lack of geometric distortions in the image. However, the total dose required to generate an image is larger than for other EPID systems to compensate the fact that only a single electrode is switched on at a time [36].

Besides these two EPID methods, a more recent method, AMFPIs (active matrix, flat-panel imagers) became commercially available and is widely used in radiotherapy clinics. Active matrix, flat panel imagers consist usually of a large area, pixelated array, an overlying X-ray converter, an electronic acquisition system that controls the operation of the array and extracts and processes analog signals from the array pixels and, finally, a host computer and information system, which sends commands to the acquisition system, receives and processes digital pixel data and displays and archives the resulting digital images [36].

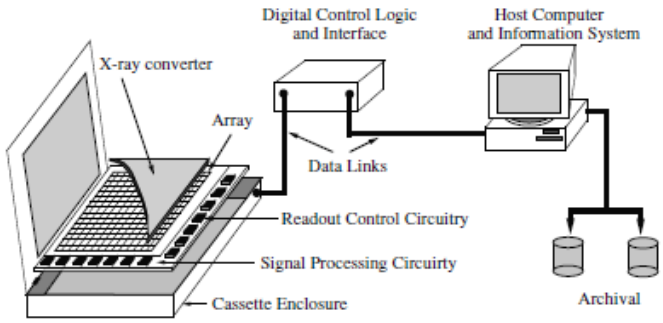

Figure 18 – Schematic illustration of the elements of an active matrix, flat-panel imager [34].

The AMFPI array consists of a glass substrate of approximately 1 mm thick, on which thin-film electronic circuits are placed. Each pixel in an active matrix array incorporates a thin-film switch connected to a capacitive element. The pixels are organized in a two-dimensional grid and the conductivity of the pixel switches is controlled through variation of the voltage of control lines with each control line connected to all of the pixels in a single row. When the imager is operating, the pixel switches are generally kept non-conducting so that charge generated directly or indirectly by incident radiation interacting in an overlying X-ray converting material is integrated in the capacitive element of each pixel. Typically, one row of pixels is read out at a

time for maximum spatial resolution. When the pixel switches are conducting, imaging signals stored in the pixels are sampled by external peripheral electronics by means of data lines, with each data line connected to all the pixel switches in a given column and the pixels are then reinitialized [36].

The conversion of incident X-rays into charge stored in the capacitive element of each pixel can be accomplished using two different approaches. One of these approaches is indirect detection, which usually uses a phosphor to convert incident X-rays into visible light that is then converted in electron-hole pairs by a photodiode matrix. The other approach, direct detection, uses a photoconductor, as amorphous selenium (a-Se) to directly convert X-rays into electron-hole pairs. The charges are collected in the capacitive elements of the active matrix during the irradiation and are then read [20, 36].

The indirect detection is the most used approach, containing a phosphor screen, or a scintillator structure, in contact with the active matrix. Each pixel of the active matrix consists of a photosensitive element, usually an amorphous silicon (a-Si) photodiode, connected to a thin film transistor (TFT), that generates an electrical charge with a magnitude proportional to the light flux emitted by the phosphor in the neighborhood of the pixel. The charge is collected in the pixel until the active matrix is read [20].

EPIDs are typically mounted on the gantry on the opposite side of the isocenter in relation to the radiation source (Figure 19) to guarantee that the imager will always be appropriately positioned during imaging. To minimize the degree to which the imager attached to the gantry restricts treatment positions, it is desirable that EPIDs capable of being retracted towards the gantry or removed when not in use [36].

Figure 19 - a-Si EPID panel mounted on a linac gantry [https://www.varian.com/oncology/products/treatment-delivery/trilogy-system].

2.6.1.2. Ionization Chambers

Although pre-treatment verification performed with EPID presents many advantages over point, as with ionization chamber, it is recommended to perform the verification using a different method, due to the uncertainties related with the choice of gamma analysis criteria and acceptance tolerance limits, as well as to detect possible inaccuracies in gamma analysis that can result from an incorrect EPID panel functioning, for instance. One of the methods used for this purpose is IMRT verification with ionization chambers.

Ionization chambers are used to determine radiation dose. An ionization chamber consists essentially of a gas filled cavity surrounded by a conductive outer wall and having a central electrode. The wall and the central electrode are separated with a high quality insulator to reduce the leakage current when a polarizing voltage is applied to the chamber. A guard electrode is usually also provided in the chamber to intercept the leakage current and allow it to flow to ground, bypassing the collecting electrode. Although several shapes and sizes of ionization chambers, cylindrical ionization chambers are the recommended for high energy photons verifications [5, 23].

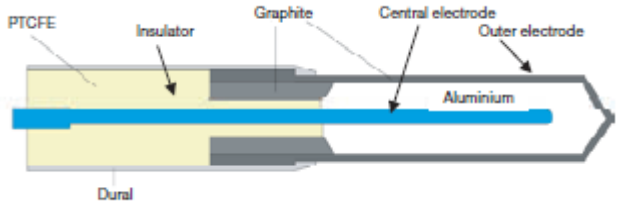

Figure 20 - Basic design of a cylindrical Farmer type ionization chamber [5].

The most used cylindrical ionization chambers are the Farmer type, also called thimble ionization chambers, due to its resemblance to a thimble. The chamber cavity should have a volume between 0.1 and 1.0 cm^3, in order to have a good compromise between the need for sufficient sensitivity and the ability to measure dose at a point [5, 23].

The construction of a chamber should be as homogeneous as possible, although, for technical reasons, the central electrode is likely to be of a different material from that of the walls. It is also necessary that the air cavity is not sealed, in order to allow a rapid equilibrium with the ambient temperature and air pressure [23].

To perform dose measurements, cylindrical ionization chambers are placed inside phantoms. Although water phantoms are recommended as a reference for absorbed dose measurements, solid phantoms in slab form of materials as polystyrene, PMMA and certain water equivalent plastics can also be used. Ideally, the phantom material should be water equivalent, which means that have the same absorption and scatter properties as water [23].

Electrometers are also used in the verifications with ionization chambers to measure the charge collected by the ionization chamber, functioning also as a power supply for polarizing the ionization chamber. The dose values are then obtained from the charge readings, using calibration factors that depend on the measuring conditions [23].

2.6.2. Gamma Analysis

IMRT QA with EPID can be performed by calculating a portal dose prediction (PDP) by superimposing the patients' treatment fields onto the geometry of the portal imager using the TPS. A separate PDP is calculated for each field using the planned gantry angle, collimator rotation, field size, dynamic multileaf collimator sequence (in case of dMLC treatments), dose rate and number of MU that will be used in patients' treatment. QA fields are delivered and the measured EPID response is compared with the PDP using portal dosimetry system to perform a gamma analysis [38].

Gamma analysis is an accurate method to compare measured and calculated dose distribution. The comparison can also be performed using qualitative evaluation methods as superimposition of isodose distributions, which can highlight the presence of significant disagreement areas. However, these method is time consuming and are a more quantitative assessment may be needed for approval [39, 40].

Quantitative evaluation methods directly compare measured and calculated dose distribution values. A first attempt to define a quantitative evaluation method consisted in the use of the dose difference as acceptance criterion. However, it was perceived that dose distribution comparisons should be subdivided into high and low dose gradient regions, each with a different acceptance criterion. In low gradient regions, the doses are compared directly, with an acceptance tolerance placed on the difference between the measured and calculated doses. On the other hand, in high dose gradient regions, a small spatial error, either in the calculation or the measurement, can result in a large dose difference between measurement and calculation [39, 41]. For these reason, distance-to-agreement (DTA) started to be used to evaluate high dose gradient regions. DTA is the distance between a measured point and the nearest point in the calculated dose distribution that exhibits the same dose [39]

A composite analysis with superimposed isodose plots, dose-difference and DTA distributions was developed, using a pass-fail criteria of both the dose-difference and DTA. Each measured point is evaluated to determine if both the criteria exceed the selected tolerances (3.0%, 3.0mm, for instance) [40, 42]. The logical union of locations that fail both acceptance criteria is calculated and displayed [42]. However, as the composite analysis consists in a binary distribution, it does not lend itself to a convenient display and, by convention the quantity displayed is the dose difference, which can accentuate the impression of failure in high dose gradient regions [39]. Besides, this method does not provide a quantitative measure of the magnitude of disagreement [40].

A generalization of the composite distribution that addresses its limitations was developed and termed γ distribution. This method uses a comparison between two distributions: an evaluated and a reference distribution, which are commonly the measured and the calculated distributions, respectively. In general, the evaluated distribution will have at least as high a dimensionality as the reference distribution [39, 43].

Figure 9 shows a geometric representation of the gamma analysis tool for one and two-dimensional dose distribution evaluation. The calculation of the gamma value is described in

references [14], [39] and [43]. The acceptance criteria are denoted by ΔD for the dose difference and Δd for DTA. All evaluated points will receive a penalty value Γ given by

$$\Gamma(\vec{r}_r, \vec{r}_e) = \sqrt{\frac{r^2(\vec{r}_r,\vec{r}_e)}{\Delta d} + \frac{\delta^2(\vec{r}_r,\vec{r}_e)}{\Delta D}} \tag{2.8}$$

where Equation 2.8 describes an orthogonal space defined by a DTA dimension and a dose difference dimension with

$$r(\vec{r}_r, \vec{r}_e) = |r_m - r_e| \tag{2.9}$$

and

$$\delta(\vec{r}_r, \vec{r}_e) = D_e(\vec{r}_e) - D_r(\vec{r}_r) \tag{2.10}$$

where $D_e(\vec{r}_e)$ and $D_r(\vec{r}_r)$ are the evaluated and reference doses at positions $\vec{r}_e$ and $\vec{r}_r$, respectively.

Gamma value can be defined as the minimum generalized Γ function in the set of evaluated points and obtained by

$$\gamma(\vec{r}_r) = min\{\Gamma(\vec{r}_r, \vec{r}_e)\} \; \forall \; \{\vec{r}_c\}. \tag{2.11}$$

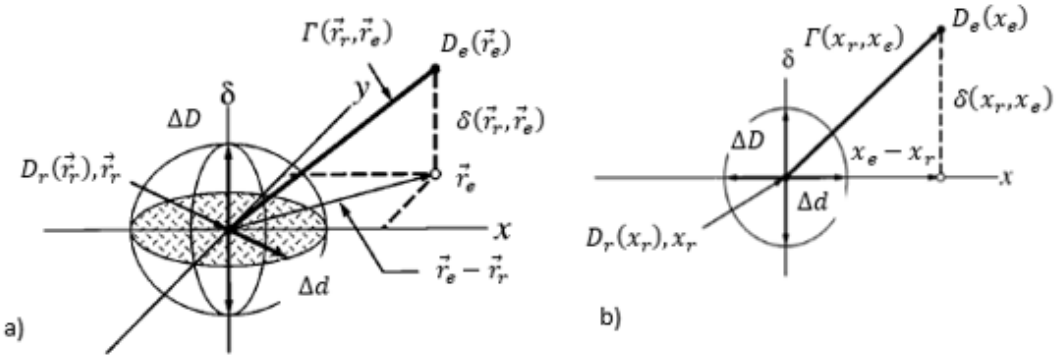

Figure 21 – Geometric representation of the theoretical concept of gamma evaluation method. a) Two-dimensional representation. b) One-dimensional representation. Adapted from [39], using [43] nomenclature.

In order to simplify gamma analysis procedure, a filter cascade process was employed to determine whether γ is greater or less than 1, instead of computing the value of γ. The search is restricted to regions near the reference point and, as soon as one pixel is found for which $\Gamma(\vec{r}_e, D_e)$ is smaller than unity, calculation is stopped and the reference point is classified as accepted. When such pixel is not found, a further analysis is performed, since in regions of high dose gradient, it is possible that the evaluated dose distribution intersects the ellipsoid but the datapoints sampling the distribution are situated outside the ellipsoid of acceptance [39]. The advantage of this approach is that it is significantly faster than the original algorithm, but it does not provide information regarding the magnitude of failure [44].

Gamma analysis is performed in clinical practice using analysis software, as Portal Dosimetry from Varian Medical Systems, Inc., which will be used as an example of the calculation of gamma evaluation in a TPS, for a 3.0%, 3.0 mm criterion for dose difference and DTA. First, both predicted (evaluated) and measured (reference) images are scaled to have a unit of 3.0% of the maximal value (after clipping 0.1% off the high valued end of the histogram) of the predicted dose, since virtual circles with radius 1 (corresponding to 3.0 mm in spatial direction and 3.0% of the near maximum of the predicted dose) are drawn around each point of the measured dose. After scaling, the difference between measured and predicted images is calculated, creating a preliminary gamma image that contains only the dose dimension. The surrounding region around the pixel is scanned on the outline of squares (shells) with increasing size. The pixels lying on the outline of the current square are scanned non-sequentially starting from the pixels nearest to the center towards the four edges. For each set of eight pixels on the square outline with the same distance from the center the pixel with the smallest dose difference from the center pixel is searched. The gamma value of the center pixel is then updated using the expression

$$\gamma = \sqrt{d^2 + D^2} \tag{2.12}$$

where d is the distance and D is the dose difference, if this is smaller than the current one. Before starting with a new search within each new set of eight pixels, the best possible gamma value for this set is compared with the current gamma value and, if it is larger than the current value, the algorithm moves forward to the next square. If the first set of investigated pixels on this square have also larger gamma values than the current value, the gamma search for the current pixel is finished and the procedure is started for the next pixel until for all the pixels the optimal gamma value has been found. In order to prevent long calculation times, a saturation value of 10 was defined, so that the algorithm do not search farther than 10 x DTA mm around each pixel [45].

Gamma analysis is commonly performed using a 3.0%, 3.0 mm criterion for dose difference and DTA, but different criterions can be used, depending on the purpose of the analysis and on the decision of the medical physicist or the institution. A similar situation occurs with acceptance tolerance limits, since definitive limits have not been established. However, institutions use reference tolerance values to evaluate the acceptability of treatments for verifications performed with gamma analysis. Some of these tolerance values for gamma passing percentage (percentage of points with γ>1), using a 3.0%, 3.0 mm gamma criterion for per-field measurements, obtained in studies performed to establish tolerance action levels for gamma analysis, as well as values used as reference tolerances in institutions, are summarized in Table 4.

Author / Institution	Tolerance limit for % of passing points
IPOLFG [25]	95.00%
Van Esch, Depuydt and Huyskens, 2004 [49]	95.00%
Both *et al*, 2007 [46]	95.00% for prostate 90.00% for other treatments
Howell, Smith & Jarrio, 2007 [38]	Average within 1 SD of institutional mean (IM) 25% of fields in a treatment within 2 SD of IM Average within 1 SD if areas with γ>1 outside the field.
Santa Maria Nuova Hospital (Italy) [47]	90.00%
Lund University Hospital (Sweden) [47]	90.00%
Ezzell *et al.*, 2009 [48]	90.00%

Table 4 - Summary of tolerance limits for percentage of gamma passing points suggested by some authors and used as reference in some institutions [25, 49, 46, 38, 47, 48].

Although an acceptance criterion of 95.0% for the percentage of passing points is used in IPOLFG and in other institutions for 3.0%, 3.0 mm gamma criterion, action levels of 90.0% of the points passing the criterion has been reported as acceptable in the literature for per-field measurements [50].

Chapter 3

Materials and Methods

3.1. The IMRT system

In this study, three Varian 2100C/D linear accelerators with photon energies of 6 MV and of a higher energy (10 MV or 15 MV) and several electron energies, installed at the Instituto Português de Oncologia Francisco Gentil de Lisboa were used for the data acquisition for the dosimetric equivalence evaluation. The three linear accelerators are denominated as DHX01, DHX02 and DHX03, according to the time of installation, as represented in Figure 22.

The DHX02 and DHX03 linacs were installed as dosimetrically equivalent in the treatment planning system (TPS), whereas DHX01 is dosimetrically similar, but is not defined as equivalent in the TPS.

Figure 22 - Schematic representation of linear accelerators used in the study.

The three linear accelerators are used to perform IMRT treatments, by means of a multileaf collimator Millenium MLC with 120 leaves, divided by two banks with 60 leaves each. Moreover, all linear accelerators are also equipped with an electronic portal image device (EPID), aS-500 model, used for verification of IMRT plans. These devices include an amorphous silicon detector (a-Si), an image acquisition system that supports all the detection electronics and interface hardware and the workstation *Portal Vision* for evaluation of results.

All verification tests and treatments are performed with a 6 MV photon beam.

3.2. Basic Dosimetry

Basic dosimetry evaluation included analysis of the data acquired in daily and trimestral quality controls during the year of 2014 for 6 MV photon energies. Measurements for MLC quality assurance were also included in this evaluation. The results obtained with the three linear accelerators were analyzed using SPSS Statistics Package and an overall intercomparison was performed in order to understand if the results obtained in quality controls compromise the dosimetric equivalence in study.

3.2.1. Daily Quality Control

From daily quality control the dosimetric parameters were evaluated, including dose in central axis (CAX), flatness, symmetry in X (left-right) and Y axis (gun-target) and beam quality factor (BQF).

These parameters were performed using a PTW portable constancy check device, Quickcheck[webline]. The equipment is used for quality assurance and constancy checks of linear accelerators used in radiation therapy. It consists of a detector block, an electronic system and a display showing the dosimetrical values. All measured values are stored in an internal memory and they can be downloaded to the computer for posterior evaluation and monitoring [49].

The measurements were performed using a static field of 10 x 10 cm^2 and a dose rate of 600 MU/min. For this field size, five measuring ionization chambers are used: CAX, G10, T10, L10 and R10, represented in Figure 23, where G stands for gun, T for target, L for left and R for right.

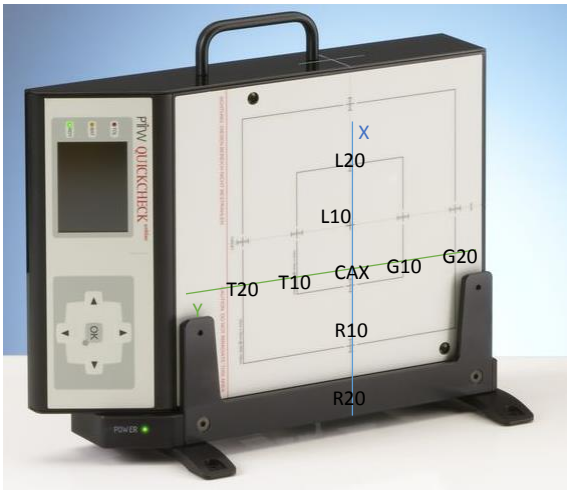

Figure 23 - PTW QUICKCHECK[webline] with ionization chamber position. [Adapted from http://www.ptw.de/support_quickcheck_webline.html]

For the determination of the dosimetric parameters evaluated in daily control, the dose in each one of the five measuring chambers, D_i, is calculated using the following expression [49]:

$$D_i = M_i \cdot N_i \cdot K_{TP} \tag{3.1}$$

where M_i is the measured charge of measuring chamber i, N_i is the ^{60}Co calibration factor of measuring chamber i and K_{TP} is the correction factor for air density correction, calculated as follows [49]:

$$K_{TP} = \frac{(273.2+T)P_0}{(273.2+T_0)P} \tag{3.2}$$

where P (hPa) and T (°C) are the air pressure and temperature at the time of the measurement and P_0 and T_0 are the calibration conditions, 1013.5 hPa and 20°C, respectively.

The central axis dose, flatness, symmetries and beam quality factor are then calculated using the dose values in the chambers and a normalization factor, K_{norm}, which is determined from target values selected by the user. The data used in this study was obtained defining target values of 100% to CAX, symmetries and beam quality factor and approximately 3% for flatness.

The evaluation values displayed by the device are then calculated using the following expressions:

Central Axis Dose CAX

$$CAX = (K_{norm})_{CAX} \cdot D_{CAX} \tag{3.3}$$

where $(K_{norm})_{CAX}$ is the normalization factor for the central axis dose and D_{CAX} is the central chamber dose calculated according to equation 3.1 [49].

Flatness F

$$F = 100 \cdot (K_{norm})_{Flat} \cdot \frac{(D_{max}-D_{min})}{(D_{max}+D_{min})} \tag{3.4}$$

where $(K_{norm})_{Flat}$ is the normalization factor for flatness, D_{max} and D_{min} is the maximum and minimum dose value of the five used measuring chambers, respectively [49].

Symmetry S

$$S_{LR} = 100 \cdot (K_{norm})_{SymLR} \cdot \underset{x = L_{10}}{\overset{L}{Max}} \left[\frac{Max\,[D_{-x},D_x]}{Min\,[D_{-x},D_x]}\right] \tag{3.5}$$

$$S_{GT} = 100 \cdot (K_{norm})_{SymGT} \cdot \underset{x = G_{10}}{\overset{G}{Max}} \left[\frac{Max\,[D_{-x},D_x]}{Min\,[D_{-x},D_x]}\right] \tag{3.6}$$

where $(K_{norm})_{SymLR}$ and $(K_{norm})_{SymGT}$ are the normalization factor for S in L-R and G-T direction, respectively, and D_{-x}, D_x are the dose values for the ionization chambers at the chamber positions x or –x, which are symmetrical to the central beam (if x = L_{10}, then –x = R_{10}, for instance) [49].

Index for the Radiation Quality BQF

$$BQF = (K_{norm})_{BQF} \cdot Polynom\left(\frac{D_{E_i}}{D_{CAX}}\right) \quad (3.7)$$

where $(K_{norm})_{BQF}$ is the normalization factor for BQF, D_{E_i} is the dose of the corresponding ionization chamber for radiation quality and D_{CAX} is the dose in the central chamber [49].

For the current study, the previously mentioned constancy values obtained with QUICKCHECK^{webline} for 6 MV photon beams throughout the year of 2014 are evaluated for the DHX01 and DHX02 machines. For the DHX03 accelerator, due to loss of the data obtained in the first eight months of the year, the values acquired in the first months of 2015 were added to the study, in order to observe the DHX03 constancy behavior during a higher time period. For this reason, DHX03 measures are not comparable in time with the results obtained with the other two linear accelerators, since the time of acquisition is not coincident. However, this does not compromise the results, since the goal of the present study is to evaluate the constancy behavior of the linear accelerators and not to perform intercomparisons.

A tolerance of 2.00% is considered for the stability of the parameters acquired in the daily QA.

3.2.2. Trimestral Quality Assurance

From all the parameters evaluated in trimestral QA performed during the year of 2014, four were selected to further analysis and comparison between linear accelerators: dose calibration factor, symmetry, MLC transmission factor and dosimetric leaf separation (DLS). As for daily quality checks, the main goal of the performed analysis was to determine if significant deviations are present in each one of the linear accelerators.

Dose Calibration Factor

The first of the parameters analyzed is the dose calibration factor. It is measured in a liquid water phantom (MP3 Phantom Tank) for a 10 x 10 cm^2 field and a SSD = 100 cm, with an Waterproof Farmer ionization chamber (PTW30013 of 0.6 cc sensitive volume) placed at a depth of 10 cm, supplied with a polarization voltage of 400 MV from an electrometer. The phantom is irradiated with 100 MU and the charge in the ionization chamber is collected by the electrometer. The corresponding dose value is obtained using the equation [25]:

$$D[Gy] = Charge\ reading\ (nC) \times K_{P,T} \times K_s \times K_p \times K_Q \times N_{D,W} \quad (3.8)$$

where K_s is the ion recombination factor, which corrects the response of the ionization chamber for the lack of complete charge collection due to ion recombination, K_p is the polarization factor, which corrects the response for a change in polarity if the polarizing voltage applied to the ionization chamber, K_Q is a factor that corrects for the difference between the response of an ionization chamber in the reference beam quality used for the calibration of the chamber and the actual beam quality and $N_{D,W}$ is a calibration factor in terms of absorbed dose to water at a reference beam quality. The values of these factors are specific of the ionization chamber and electrometer used. The dose calibration factor, in cGy/MU, is obtained by determining the quotient of the measured dose and the initial 100 MU [23].

Symmetry and Flatness

In trimestral quality assurance, symmetry and flatness are determined for a 30 x 30 cm^2 field, SSD = 100 cm and a 10 cm depth, using a MP3 water phantom tank and ionization chamber (PTW31010 of 0.125 cc sensitive volume) to obtain dose profiles in x and y direction [25]. Symmetry and flatness values are determined from the obtained dose profiles as [25]:

$$F = 100 \cdot \frac{(D_{max} - D_{min})}{(D_{max} + D_{min})} \quad (3.9)$$

and

$$S = 100 \cdot \frac{(D_x - D_{-x})}{(D_x + D_{-x})} \quad (3.10)$$

MLC Transmission Factor

For the determination of MLC transmission factor, a MP3 water phantom and an ionization chamber with a cavity volume of 0.6 cc at a depth of 5 cm, with an SSD = 95 cm, are used. The ionization chamber is irradiated at the central axis first with 1000 MU with the leaf bank A blocking a 10 x 10 cm^2 field. Afterwards, the same measurement was made using 1000 MU blocking the leaf bank B. Finally, the charge value for an open field of 10 x 10 cm^2 with 200 MU was registered. The average leaf transmission is calculated from the equation [25]:

$$T(transmission) = \frac{MLC_{closed}}{MLC_{open}} \cdot 100 \quad (3.11)$$

where MLC_{closed} is the average charge measured with leaf banks closed and MLC_{open} is the charge measured with the open field.

Dosimetric Leaf Separation (DLS)

For the determination of DLS value, a measurement (M) with an ionization chamber placed in the center of a 10 x 10 cm^2 field at a 5 cm depth (SSD = 95 cm) is irradiated with 200 MU at a dose rate of 600 MU/min. For several fields the leaf pairs are forced to move with a constant velocity and a fixed gap that varies between 0.5 mm and 20 mm. Measurements with closed MLC (M_t), but with the same setup are also performed and a graph in which ($M-M_t$) is represented in function of the respective gap width is created. The obtained line is then extrapolated for $M_t-M=0$ and the DLS value is directly determined [25].

Parameter	Tolerance Values
Dose calibration factor	2.00%
Beam symmetry	2.00%
MLC transmission factor	2.00% ± 0.50% difference from baseline
Dosimetric leaf separation	Recommended tolerance of 0.20 mm Action level of 0.50 mm

Table 5 - IPOLFG established tolerance values for trimestral quality assurance parameters [22, 25].

IPOLFG established tolerance values for trimestral quality assurance parameters are summarized in Table 5. The analysis of the trimestral verifications results will be performed using these tolerances as reference values.

3.2.3. MLC stability check using EPID images

Garden fence and chair tests, using EPID, are performed routinely in the service as MLC quality assurance. The results obtained for these tests during 2014 were analyzed in order to understand if significant variations occurred and for an overall comparison of the behavior of the three linear accelerators, since large variations in these tests can influence the results of IMRT treatments.

Besides these two tests for MLC verification, another two tests using EPID were performed in order to understand if the predicted output factors match the actual output factors of the EPID: field size dependence and linearity tests [51]. Due to lack of equipment availability for data acquisition, these two tests were performed only for DHX01 and DHX02, in order to evaluate if significant variations occur for static fields when a change of equipment is done.

3.2.3.1 Garden Fence Test

The Garden Fence Test is used to demonstrate the stability of the MLC leaves movements. This test is performed with the MLC leaf pairs moving with a constant velocity, with a 1mm gap between the leaves, along a 12cm width field. The MLC movement is stopped at ± 12 cm, ± 8

cm, ± 6 cm, ± 4 cm, ± 2 cm and ± 0.1 cm positions, which creates “hot lines” with 1 mm width. This test should be done weekly, for gantry rotations of 0°, 90°, 180° and 270° [25].

The garden fence is a qualitative test and its verification is done by visual inspection for discernable deviations such as an increase in interleaf transmission [22]. However, the verification of this test was performed comparing the portal images obtained with a reference image, using gamma analysis in order to understand if the agreement values obtained are stable. Gamma analysis was performed with the 3.0 %, 3.0 mm and the 3.0 %, 0.5 mm criteria (the last one is suggested in [25]). The utilization of two different criteria has the goal of understanding if there are similarities in the agreements values obtained for the different linear accelerators.

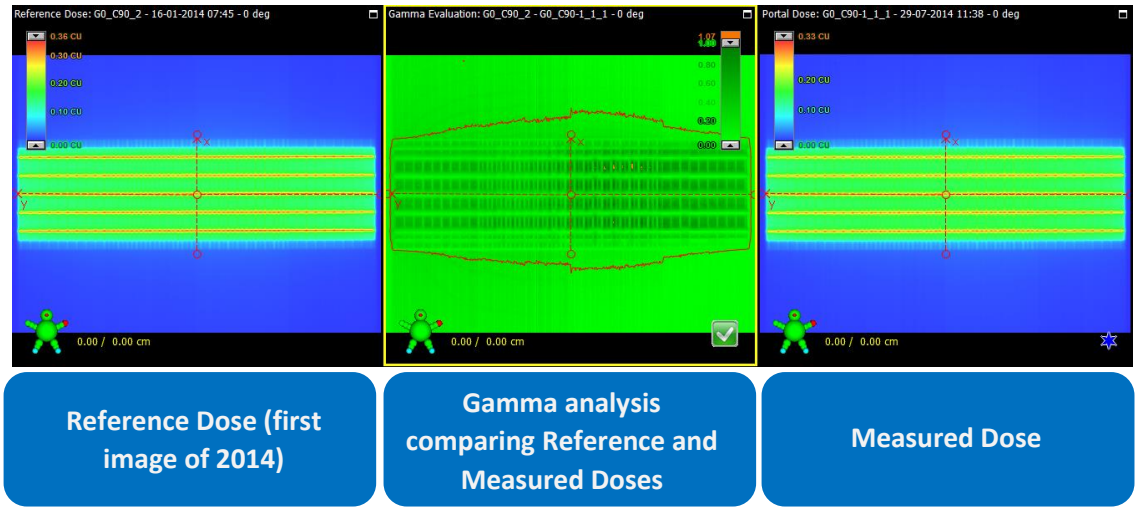

Figure 24 - Gamma Analysis for Garden Fence Test in Varian Portal Dosimetry

3.2.3.2. Chair Test

The chair test is used to differentiate the impact of the transmission factor and of the dosimetric leaf separation. A fluence distribution is obtained and can be divided in three parts, as shown in Figure 10, that allow to evaluate different issues [25]:

- Left part: Estimation of transmission factor precision. The area with null dose corresponds to the transmission through the leaves.
- Central part: Used for absolute dose verification with ionization chamber.
- Right part: In the area between the chair feet the leaves move with maximum velocity and the actual fluences are influenced by the transmission factor and the dosimetric leaf separation.

The chair test is performed for 0° gantry angle, 90° collimator angle and a source-detector distance of 100 cm. The verification of this test is done with a 3.0 %, 3.0 mm gamma analysis, comparing the measured portal image with the TPS predicted image [25].

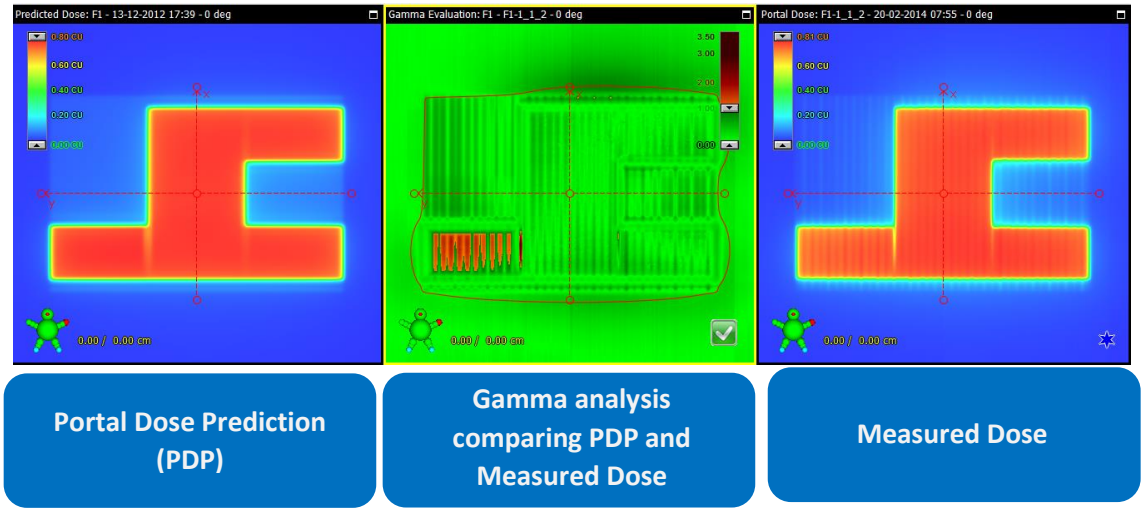

Figure 25 - Gamma analysis for Chair Test in Varian Portal Dosimetry

3.2.3.3. Field Size Dependence Test

The field size dependence test was performed in order to verify whether the output factors obtained from the EPID acquisition match the output factors from the predicted dose image (PDIP) when field size and dose rate change.

To perform this verification, the *Point Dose* tool from Varian *Portal Dosimetry* software is used to obtain the central axis output factors (CAX). The relative difference between the measure and predicted output factors should be less than ± 1% [50].

For the realization of the field size dependence test, portal imaging verification plans were created for a SSD = 100 cm and field sizes of 3x3, 5x5, 10x10, 15x15, 25x25 and 15x25 cm^2. The test was performed for two different dose rates, 400 and 600 MU/min, in order to understand if there is a relation between the dose rate and the field size dependence [51, 52].

3.2.3.4. Linearity Test

The linearity test was also performed *Point Dose* tool, but the portal imaging verification plans were created for a SSD = 100 cm and a fixed field size of 10x10 cm^2, but varying the amount of monitor units delivered to the field from 10 to 200 MU, in order to understand the linearity of the detector response as a function of the number of monitor units. This test was also performed for both 400 and 600 MU/min dose rates [51, 52].

3.3. IMRT Planning Dosimetry

The analysis of IMRT planning dosimetry was performed by verifying treatment plans, created with Eclipse™ TPS of Varian Medical Systems, Inc., of head and neck and prostate treatments using EPID. For this purpose, samples containing patients treated in each one of the linear accelerators for each one of the treatment categories were selected, in a total of six samples.

Besides the EPID verification performed before the beginning of the treatment with the original equipment, verifications of the original plan with the other two linear accelerators, i.e. without change of treatment unit in the TPS. An analysis of the dose distributions calculated in the TPS was also performed, by changing the treatment unit and recalculating dose for all the patients in each one of the samples. This may help to determine if significant differences in calculated dose (as number of monitor units, for instance) occur with this change. This last analysis has the purpose of understanding if possible deviations in the agreement values result from the small or big differences of dosimetric characteristics between the linear accelerators.

3.3.1. Head and Neck Radiotherapy Samples

The study was performed for three samples of Head and Neck IMRT treatments, one for each of the linear accelerators: DHX01, DHX02 and DHX03. These samples include patients treated for Head & Neck with IMRT dose prescriptions of 70 Gy for PTV, divided in 33 or 35 fractions. For some patients, a single PTV is defined, receiving the total dose prescription of 70 Gy. However, for other patients, more PTVs are defined, receiving different dose values: one of PTV receiving the total dose prescription of 70 Gy and the other receiving lower prescribed doses, which are 54, 59.4, 63 or 66 Gy.

Table 6 shows the total number of patients, the average and range age considered for each linac:

	Number of patients	**Average Range**	**Range Age**	**Percentage of female (%)**
DHX01	27	55.26 ± 15.73	[14,85]	25.93%
DHX02	25	56.44 ± 11.21	[37, 81]	0.00%
DHX03	20	56.85 ± 10.84	[34,78]	15.00%

Table 6 - Summary of the characteristics of Head and Neck samples.

The percentage of patients for different range age for the three linear accelerators are shown in Figures 26 to 28.

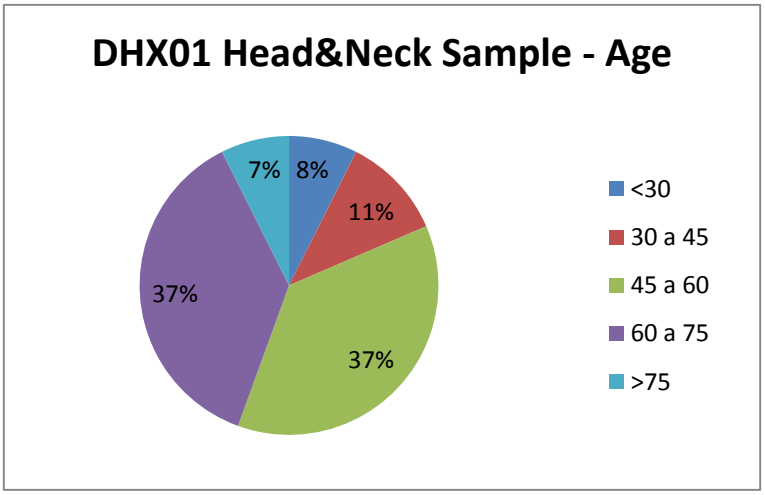

Figure 26 - Graphical representation of the age of DHX01 Head & Neck sample patients.

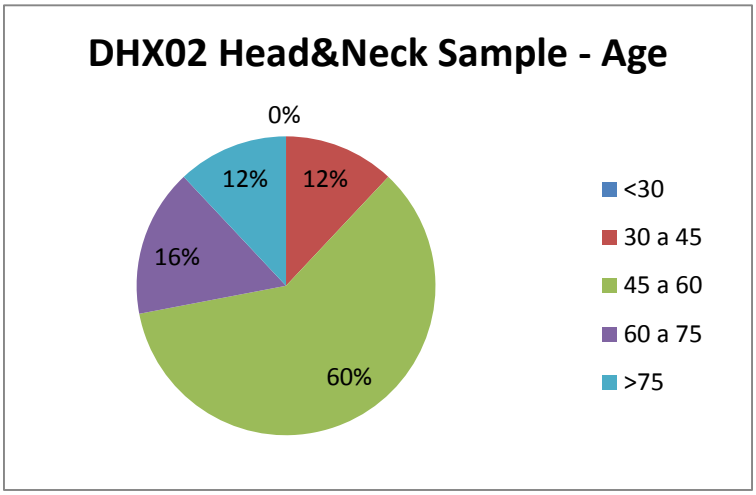

Figure 27 - Graphical representation of the age of DHX02 Head & Neck sample patients.

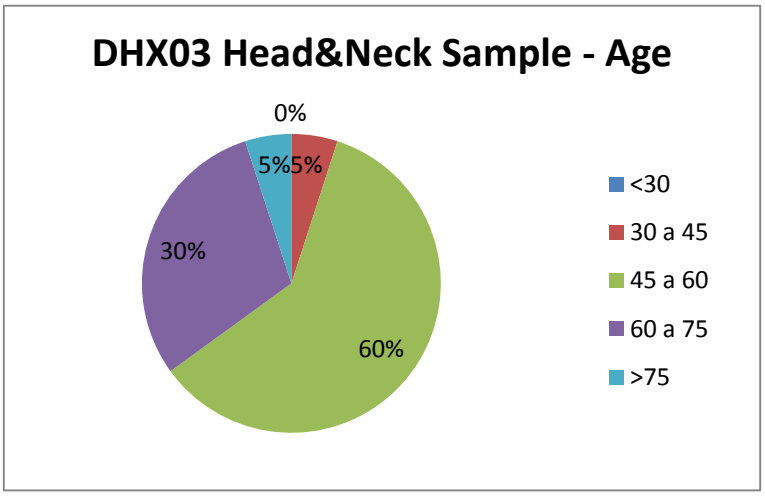

Figure 28 - Graphical representation of the age of DHX03 Head & Neck sample patients.

For the TPS dose analysis, the deviation between the dose values before and after change of treatment unit in the TPS was calculated for the parameters present in [53] : D_{min}, D_{max}, D_{mean} and $V_{95\%}$ for PTV54, PTV59.4 and PTV70 (three different PTVs are delineated in the plan, each one receiving different dose values), D_{max} for critical structures (brainstem, right and left optical nerves, optical chiasm and spinal cord) and part of the organs-at-risk (right and left eyes and right and left lenses), D_{mean} for the remaining organs-at-risk referred in the protocol (right and left parotides, larynx, esophagus and pharynx) and, besides the dose values, the sum of monitor units was also compared for all the patients in the three samples, in order to understand if significant dose delivery deviations occur when a change of treatment unit is performed.

In relation to the EPID verifications, a gamma analysis was performed with a 3.0 %, 3.0 mm criterion and the average agreement values were calculated using this criterion for all the patients in the samples. However, as for some patients the agreement values were lower than 95.0% were obtained, the gamma analysis was repeated for this patients with a 3.5 %, 3.0 mm and 4.0 %, 4.0 mm criteria in order to determine if, with these criteria, the average agreement value for the patient increase to a value above 95.0%. Correlation coefficients between the different verifications performed for each sample were also determined, using SPSS Statistics package.

For H&N samples, an additional verification with ionization chamber was performed for DHX01 and DHX02 samples, in order to detect possible influence of EPID panel on the EPID verifications results.

3.3.2. Prostate Samples

The study was performed for three samples of Prostate IMRT treatments, one for each of the linear accelerators: DHX01, DHX02 and DHX03. These samples include patients treated for prostate with IMRT dose prescriptions between 74 and 78 Gy for PTV. For some patients, a single PTV is defined, receiving the total dose prescription, divided in 37 to 39 fractions. However, usually the treatment consists of two or three planning courses, each one with a different PTV. In the case of a treatment divided by two planning courses, the treatment is performed in two stages. In the case of a total dose prescription of 78 Gy, for instance, the prescribed dose is divided by the two treatment stages, usually with a prescription of 50 Gy in 25 fractions for the first stage of the treatment, in which a PTV that includes the prostate and ganglia is defined, and a prescription of 28 Gy in 14 fractions for the second stage of the treatment, in which a PTV including only the prostate is defined. For a treatment consisting of three planning courses, the treatment includes three stages. Considering a total dose prescription of 77 Gy, the first stage of the treatment may have a dose prescription of 45 Gy in 25 fractions, for instance, for a PTV including the prostate, the ganglia and seminal vesicles. Dose prescriptions of 16 Gy in 8 fractions are defined for the two remaining treatment stages, one with a PTV including the prostate and ganglia and the other with a PTV including only the prostate.

Table 7 shows the total number of patients, the average and range age considered for each linac:

	Number of patients	Average Range	Range Age
DHX01	12	69.42 ± 5.65	[58, 77]
DHX02	11	70.45 ± 8.09	[54, 79]
DHX03	10	66.80 ± 6.43	[52, 76]

Table 7 - Summary of the characteristics of Head and Neck samples.

The percentage of patients for different range age for the three linear accelerators are shown in Figures 29 to 31.

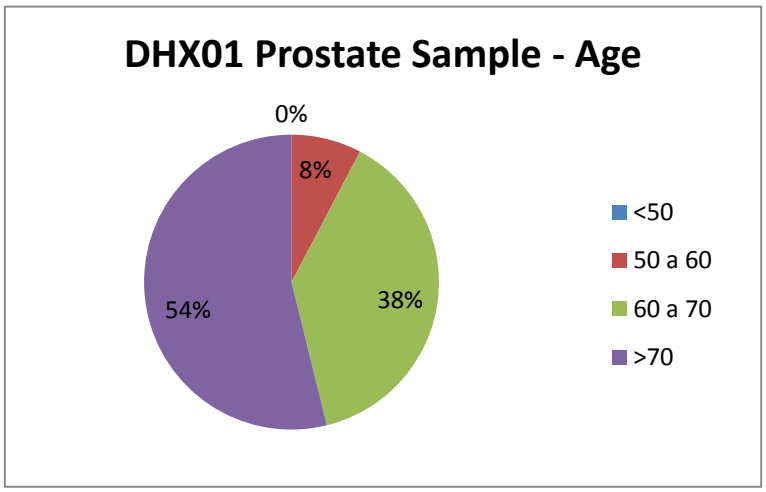

Figure 29 - Graphical representation of the age of DHX01 prostate sample patients.

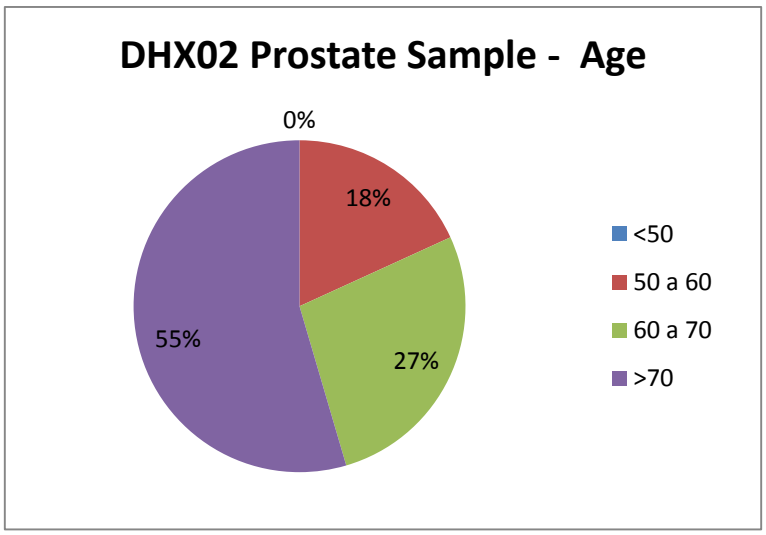

Figure 30 - Graphical representation of the age of DHX01 prostate sample patients.

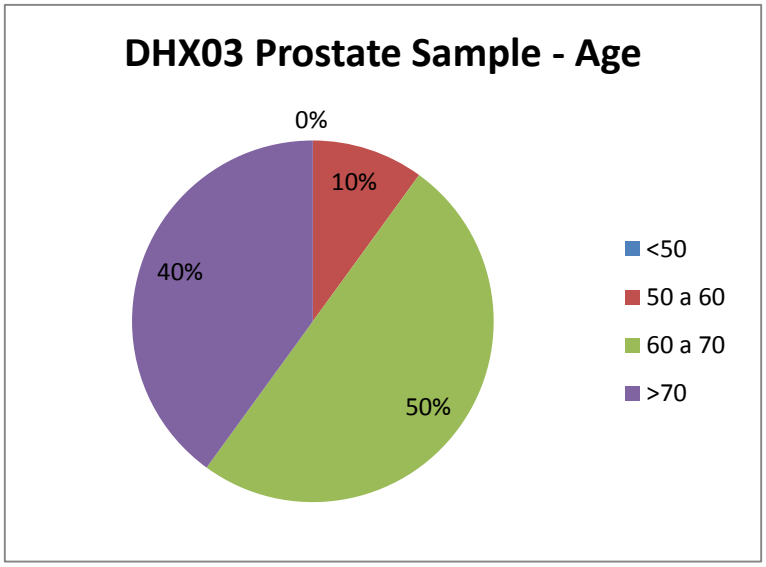

Figure 31 - Graphical representation of the age of DHX01 prostate sample patients.

For the three prostate samples a procedure similar to the used for H&N samples was applied. In relation to the comparison of doses before and after change of treatment unit for the three prostate samples, dose deviations were calculated for the parameters present in the IPOLFG prostate protocol of tolerances [54]: D_{min}, D_{max}, D_{mean} and $V_{95\%}$ for PTVs (which were separated in intervals of dose values prescribed in order to have enough patients in each category for a viable comparison, which was possible only for PTV45 to PTV50 and PTV74 to PTV78, since for DHX02 and DHX03 samples the majority of the patients has only two PTVs prescribed), $D_{30\%}$ and $D_{50\%}$ for bladder, $D_{20\%}$ and $D_{50\%}$ for rectum, $D_{5\%}$ for right and left femur heads and D_{mean} for penile bulb. The difference of monitor units before and after the change of equipment in the TPS was also calculated.

Analysis of the EPID verifications for the three linear accelerators, using *Portal Dosimetry* for the determination of gamma analysis agreement values, was also performed for prostate samples. The gamma analysis was performed with a 3.0 %, 3.0 mm criterion and the average agreement values were calculated using this criterion for all the patients in the samples. Correlation coefficients were also determined between the EPID verifications performed for each of the prostate samples, using SPSS Statistics package.

3.3.3. Ionization Chamber Verification

The ionization chamber verification consisted in the measurement of absolute dose using an ionization chamber and a solid water phantom.

The main goal of this test is, in addition to the verification of the dose calculated by the TPS, to understand if possible discrepancies in the EPID gamma analysis result from uncertainties in the treatments (due to the linear accelerators in the TPS, for instance) or from the EPID panel (as calibration factor or panel wear).

To perform this test, 12 patients were choose from each of the DHX01 and DHX02 H&N samples. The measures were performed irradiating a solid water phantom with the fields of the treatment plans. This solid water phantom consists of a series of water equivalent (same absorption and scatter properties as water) material (RW3) plate. For these measures, a PTW 30013 cylindrical ionization chamber with 0.6 cc sensitive volume was placed inside the solid water phantom. The ionization chamber is connected to an electrometer, which is used for charge measurement and as a power supply for the polarization voltage of the ionization chamber [23, 25].

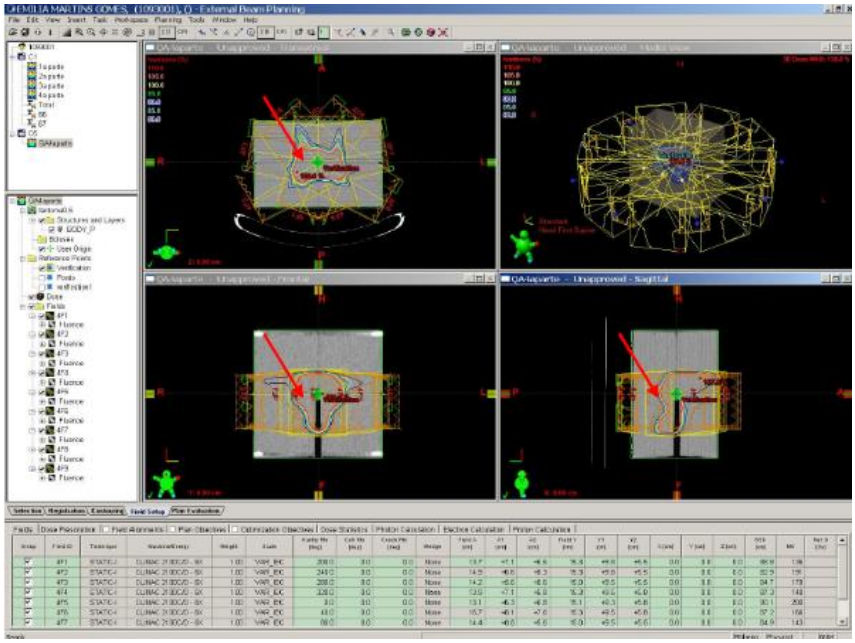

Figure 32 - Verification plan for ionization chamber, created with Varian Eclipse software [25].

Figure 33 - Solid water phantom for verification with ionization chamber [25]

First, a verification plan is created for each of the patients, consisting in calculating the dose from the original treatment plan into a CT of solid water phantom used for the dose measurement [25].

The phantom is assembled on the treatment couch in the accelerator, overlapping the RW3 plates and taking into account the laser and phantom marks (corresponding to the geometrical center of the ionization chamber), in order to have the plate in which the ionization chamber is

inserted at a SDD (Source-Detector Distance) = 100 cm and the upper plate at an SSD = 95 cm. After the assembling of the phantom, the temperature and the atmospheric pressure in the room should be verified for the determination of the correction factor for air temperature and air pressure, K_{TP}, which corrects the response of an ionization chamber for the effect of the possible difference between the standard reference temperature and pressure specified by the standards laboratory and the actual temperature and pressure of the chamber in the environmental conditions in the moment of the verification and is given by equation 3.2. The electrometer should be set to the charge acquisition mode (nC), with the polarization voltage recommended for the ionization chamber in use (400V for the ionization chamber used for this verification) [5, 23, 25].

The phantom with the ionization chamber is then irradiated with the verification plans for a gantry angle of 0° and, for each of the patients, the charge read by the electrometer is recorded and used to determine the dose, which is given by equation 3.8.

After the determination of the doses for each of the patients using the original linear accelerator, both the samples were verified in the other equipment (DHX01 sample verified with DHX02 and DHX02 sample verified with DHX01) and the measured doses were compared with the TPS doses and, for each of the samples, both experimental verifications were compared. It is recommended that the differences do not exceed a tolerance of +/-3% [25].

Chapter 4

Results and Discussion

4.1. Basic Dosimetry

In the next sections, the results of the analysis of daily and trimestral quality assurance parameters obtained in the verifications performed with the three linear accelerators are presented.

4.1.1. Daily Quality Assurance

In this chapter, the results obtained from the analysis performed for a one year-term behavior of the parameters registered daily during the QA control for the three linear accelerators are presented. The analyzed parameters include dose in the central axis (CAX dose), flatness, symmetry (X and Y) and beam quality factor.

4.1.1.1. CAX Dose

The CAX dose values (minimum, maximum, mean and standard deviation) obtained daily using the Quickcheck[webline] device for the three linear accelerators are summarized in Table 8.

CAX				
Equipment	Minimum	Maximum	Mean	Std. Deviation
DHX01	97,93%	100,86%	99,72%	0,52%
DHX02	98,72%	101,45%	100,19%	0,57%
DHX03	97,47%	100,22%	98,99%	0,40%

Table 8 - Descriptive Statistics for daily QA CAX dose

In Figure 34, it is possible to observe the one year-term behavior over one year of the dose value at the central axis for the three linear accelerators.

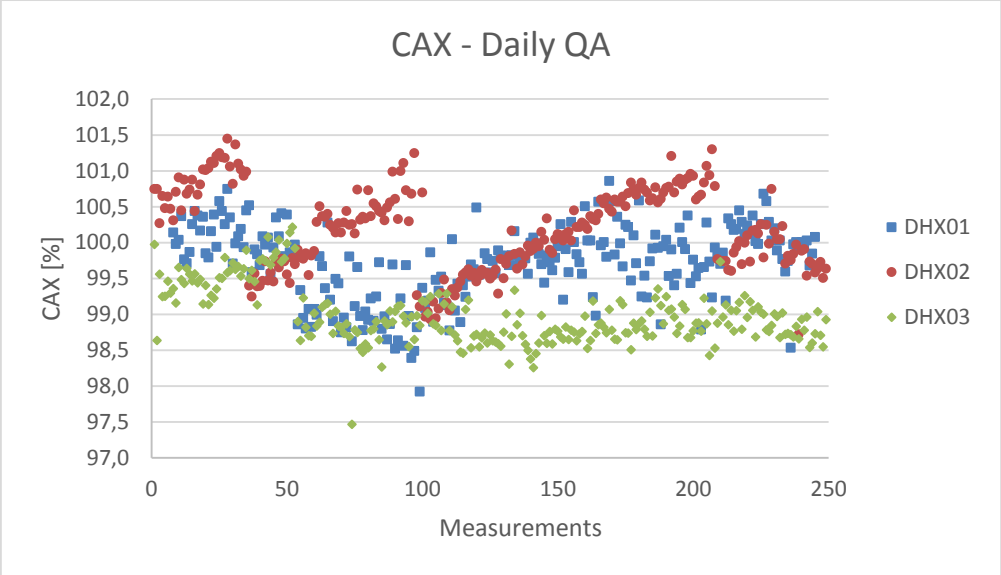

Figure 34 – Long-term assessment over one year of CAX dose results registered daily during the QA control.

From the analysis of CAX dose data, it was verified that the measurements are within the tolerance limit of 2.00%, except for two values that are slightly below 98.00%. This discordance with the tolerance in these two points can result from sporadic measuring conditions and the error associated with this measuring method.

In general, for DHX01 linac an average CAX dose of 99.72% was obtained, which is close to the reference value of 100.00%. A slight decrease tendency is present in the first values, corresponding with the first months of 2014. It can correspond to a seasonal variation (negative in winter), as described in the literature [55].

In the case of DHX02 linac, a clear increasing tendency is observed during the whole year, with abrupt decreases that correspond to the adjustments performed in the trimestral quality assurance days. It is important to state that, although an abnormal behavior was observed, the variations are not significant, since the average CAX dose is 100.19% and the minimum and maximum measured values are 98.72% and 101.45%, respectively, which are clearly within the tolerance limits. Another important observation relates with the measured values after the last trimestral quality assurance of 2014, which suggest that the increasing tendency was not maintained in the end of the year.

For DHX03 linac, although the differences are not critical, lower CAX dose values are observed than for the other two linear accelerators, with an average value of 98.99% and minimum and maximum CAX dose values of 97.47% and 100.22%, respectively, which are within the tolerance limits, except for one CAX value (97.47%). It is important to mention that a direct intercomparison of the results obtained with the three linacs is not possible, since, due to the loss of part of the results obtained with DHX03 linac, the period analyzed for this equipment is not the same than for DHX01 and DHX02 linacs. In spite of this, an overall tendency for lower

values is observable for DHX03, which can require careful verification of the evolution of this tendency in the future.

It can be concluded, in relation to CAX dose, that, although different behaviors were observed to each one of the linear accelerators in study, major differences (above 2.00%) were not present and the measurements are within the tolerance limits. From the overall analysis of CAX dose values, it is not expected that the differences observed between DHX01 and DHX02 linacs in relation to this parameter influence significantly the results of the analysis of dosimetric equivalence for IMRT treatments. In the case of DHX03, as the measurements were performed in a different period due to loss of data, it is not possible to conclude if the CAX dose measurements obtained in daily QA can influence directly the global results of this study. However, the one year term data analyzed for this linear accelerator suggests a good stability for this parameter.

4.1.1.2. Flatness

In relation to the flatness, the minimum, maximum, mean and standard deviation of the values obtained for the three linear accelerators using the PTW Quickcheck[webline] device are summarized in Table 9.

Flatness [%]

Equipment	Minimum	Maximum	Mean	Std. Deviation
DHX01	2,93	3,63	3,25	0,13
DHX02	3,02	4,17	3,46	0,16
DHX03	2,91	3,74	3,16	0,13

Table 9 - Descriptive statistics for daily QA flatness.

In Figure 35, it is possible to observe the results obtained in each of the daily verification for the three linear accelerators.

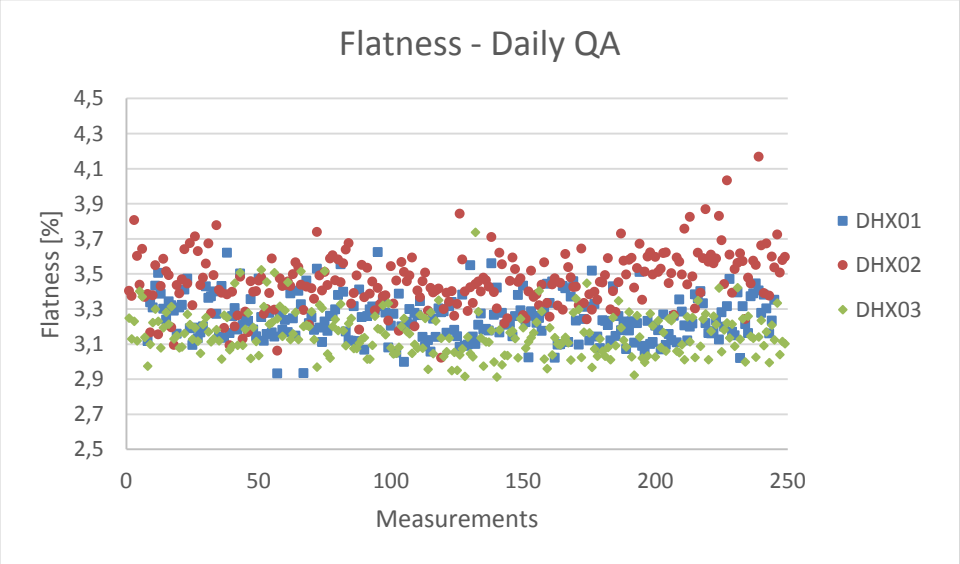

Figure 35 – Long-term assessment over one year of flatness results registered daily during the QA control.

The results obtained in the daily quality assurance were also in clear accordance with the 2.00% stability tolerance, considering a flatness reference value of approximately 3.00% for the three linear accelerators.

For DHX01 linac, an average flatness of 3.25% was obtained, with minimum and maximum values of 2.93% and 3.63%, respectively. From these results, it can be concluded that the flatness values for DHX01 linac are very stable, with a variation between minimum and maximum inferior to 1.00 %.

The values obtained with DHX02 linac are slightly higher than for the other two linear accelerators, although the difference is not significant, as the average flatness value is 3.45% and the minimum and maximum values are 3.02% and 4.17%, respectively. It can be perceived that, for this equipment, a higher variation between minimum and maximum was obtained. However, it is a variation of 1.15%, which is clearly lower than the stability tolerance of 2.00% and, for this reason, DHX02 flatness behavior can be considered identical to the observed for the other two linear accelerators.

In spite of the different acquisition period, DHX03 linac present a flatness behavior similar to the other two machines, especially to DHX01, with an average flatness value of 3.16% and minimum and maximum values of 2.91% and 3.74%, respectively.

The previous results demonstrate a good stability in relation to the flatness values measured in the daily quality assurance, with a good agreement with the recommended tolerance. In general, a high similarity in terms of flatness is observed between the three machines in study, allowing to infer that this parameter will not compromise the dosimetric equivalence in study.

4.1.1.3. X-axis Symmetry

The minimum, maximum, mean and standard deviation for X-axis symmetry (Left-Right direction) values obtained for the three linear accelerators using PTW Quickcheck[webline] are summarized in Table 10.

Symmetry X

Equipment	Minimum	Maximum	Mean	Std. Deviation
DHX01	100,00%	102,60%	100,78%	0,48%
DHX02	100,01%	102,51%	100,78%	0,53%
DHX03	100,02%	103,05%	100,83%	0,57%

Table 10 - Descriptive Statistics for daily QA x-axis symmetry.

In Figure 36, it is possible to observe the results obtained in each of the daily verification for the three linear accelerators.

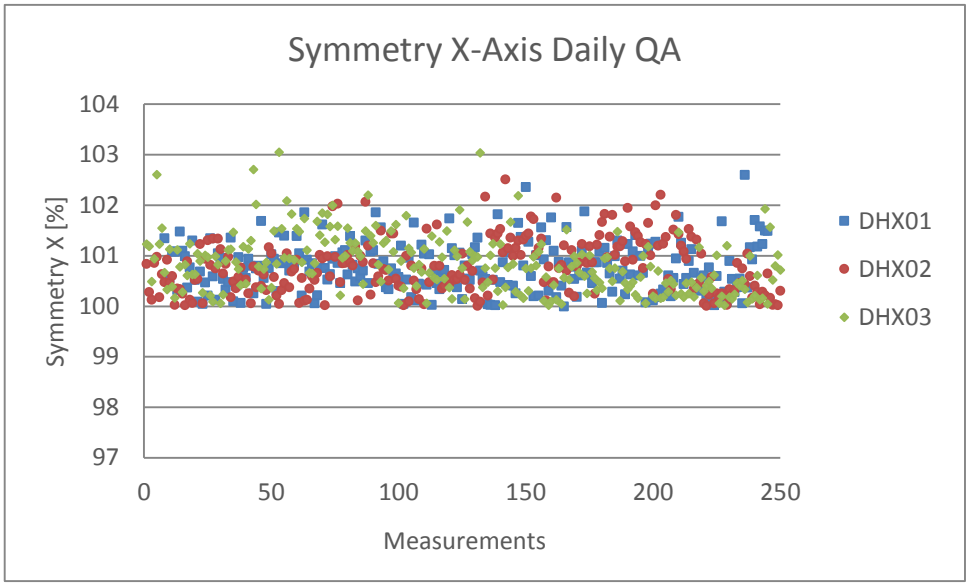

Figure 36 – Long-term assessment over one year of X-axis symmetry results registered daily during the QA control.

In relation to the X-axis symmetry results, it is important to observe that some points exceed the established tolerance of 2.00%. However, it is a reduced number of points compared to the total number of measurements (approximately 2.00%) and their occurrence is, apparently, arbitrary, not suggesting a tendency.

The symmetry values obtained with DHX01 linac are in accordance with the recommended tolerances, except for two points above 102.00%, with a maximal value of 102.60%, which, as discussed above, are not significant, as the remaining values are in accordance with the established limits, with an average value of 100.78% and a minimum value of 100.00%.

For DHX02 linac, the obtained results are very similar to the obtained with DHX01, with an average symmetry value in X-axis of 100.78% and minimum and maximum values of 100.01% and 102.51%, respectively. Although the maximum exceeds the tolerance limit of 2.00%, the exceeding values are sporadic, corresponding only to approximately 2.50% of the total DHX02 points, and, as for DHX01 linac, the average value is in accordance with the recommendations.

DHX03 linac is the equipment with more points (approximately 3.00%) exceeding 102.00%, although it does not suggest an increasing tendency, as stated before. In spite of these higher values, the average symmetry value for the X-axis is 100.98%, which is in accordance with the recommended tolerance of 2.00% and does not diverge significantly from the average values obtained with the other two linear accelerators.

4.1.1.4. Y-axis Symmetry

The minimum, maximum, mean and standard deviation for Y-axis symmetry (Gun-Target direction) values obtained for the three linear accelerators using the PTW Quickcheck^{webline} device are summarized in Table 11.

Symmetry Y				
Equipment	Minimum	Maximum	Mean	Std. Deviation
DHX01	100,02%	102,32%	100,83%	0,47%
DHX02	100,05%	103,16%	101,10%	0,55%
DHX03	100,00%	102,25%	100,81%	0,43%

Table 11 - Descriptive Statistics for daily QA y-axis symmetry.

In Figure 37, it is possible to observe the results obtained in each of the daily verification for the three linear accelerators.

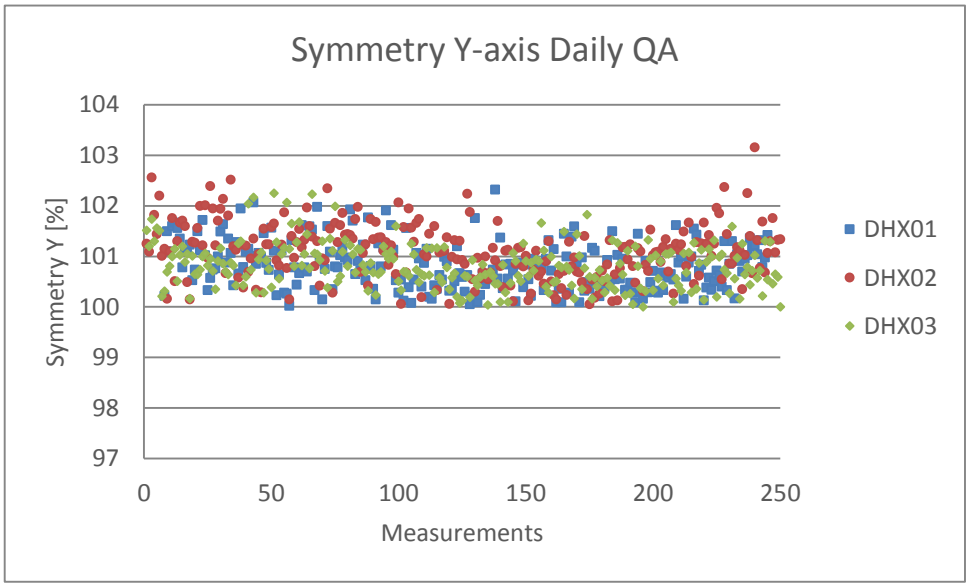

Figure 37- Long-term assessment over one year of Y-axis symmetry results registered daily during the QA control.

For the Y-axis symmetry (G-T direction), the results obtained were similar to the described for X-axis symmetry, with some points also exceeding the 102.00% recommended limit. However, as previously, the number of exceeding points is reduced (approximately 2.00% of the total points) and does not suggest a behavior tendency.

For DHX01 linac, an average Y-axis symmetry of 100.83% was obtained, with minimum and maximum values of 100.02% and 102.32%, respectively.

In the case of DHX02 linac, a slightly higher average was obtained, 101.10%, which result from a greater number of points (approximately 4.50%) exceeding the 2.00% tolerance obtained with this equipment, with a maximum value of 103.16% and minimum value of 100.05%, but, as stated before, this observation is not significant and the results indicate a good level of stability during the year. However, as a precaution procedure, an adjustment of symmetry was performed in the end of the third month of measurements.

The results obtained with DHX03 linac are similar to the previous, with an average value of 100.81% and minimum and maximum values of 100.00% and 102.25%, respectively, presenting a stable behavior.

From the previous analysis it can be concluded that, in terms of beam symmetry, the behavior of the three linear accelerators is stable and in accordance with the established tolerance values. For this reason, it is not expected that this parameter compromise the dosimetric equivalence of the three linear accelerators in study. However, in spite of not suggesting a behavior tendency, it is recommended the careful analysis of the future symmetry measures, in order to detect an eventual increasing tendency.

4.1.1.4. Beam Quality Factor

The minimum, maximum, mean and standard deviation for beam quality factor are summarized in Table 12.

BQF				
Equipment	Minimum	Maximum	Mean	Std. Deviation
DHX01	98,40%	102,27%	100,39%	0,62%
DHX02	97,43%	101,34%	99,46%	0,86%
DHX03	97,82%	102,57%	99,90%	0,55%

Table 12 - Descriptive Statistics for daily QA Beam Quality Factor.

In Figure 38, it is possible to observe the results obtained in each of the daily verification for the three linear accelerators using the PTW Quickcheck^{webline} device.

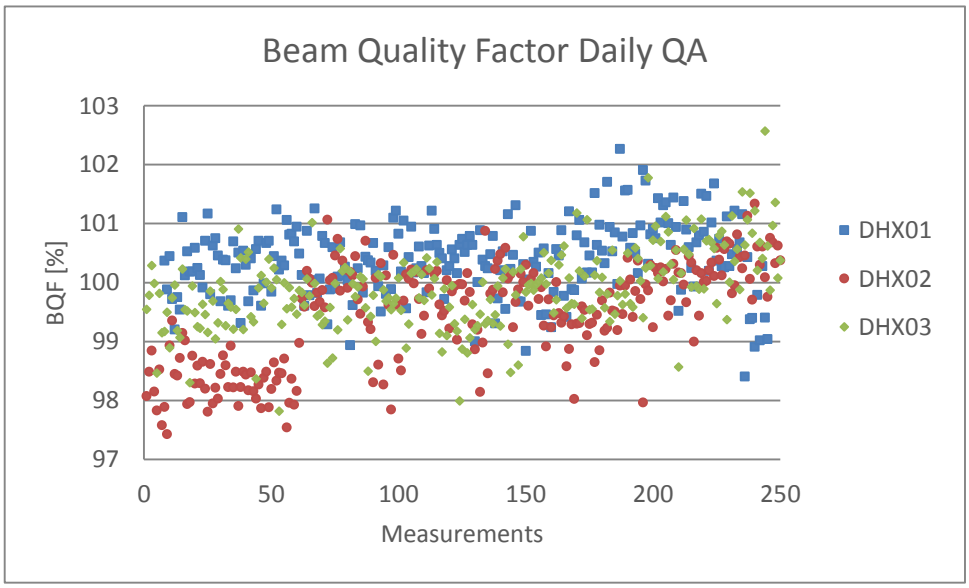

Figure 38 – Long-term assessment over one year of beam quality factor results registered daily during the QA control.

In relation to beam quality factor, some points outside the tolerance limits were observed (approximately 2.00% of the total number of points) and the behavior of the linear accelerators is considerably different. However, the behavior of each one of the linear accelerators is relatively stable, not suggesting a tendency to exceed the tolerance limits.

For DHX01 linac, an average beam quality factor of 100.39% was obtained, with minimum and maximum values of 98.40% and 102.27%, respectively. Although distributed in a relatively large interval of values, the beam quality factor measurements tend to present a stable behavior during the year, as well as a general accordance with the established tolerance limits (approximately 2.00% of the points exceed the tolerance limit, but these points present a sporadic distribution throughout the year, not suggesting a tendency to exceed the tolerance).

On the other hand, DHX02 linac present a more complex behavior during the year, with lower values in the first quarter of the year (around 98.00%) and approximately 5% of the points in disagreement with the tolerance limits. However, after the symmetry adjustment performed for this equipment, the beam quality factor values tend to distribute around the reference value (100.00%), with only approximately 2.00% of the points outside the tolerance limits. In general, an average beam quality factor of 99.46% was obtained for DHX02 linac, which was influenced by the lower values obtained in the beginning of the year, and minimum and maximum values of 97.43% and 101.34% were obtained, respectively.

For DHX03 linac, the measured beam quality factors does not diverge significantly from the reference value, with an average value of 99.90% and minimum and maximum values of 97.82% and 102.57%, respectively, which describe a stable behavior and are in accordance with the tolerance. However, throughout the year a slight increasing tendency was observed for this equipment (with an overall approximate increase of 1.00%), that do not compromise the dosimetric equivalence of the DHX03 linac in the present, but should be monitored in the future measurements.

From an overall comparison between the results obtained with the three linear accelerators it is recommended that the future behavior of DHX02 linac in terms of beam quality factor should be carefully verified in order to anticipate possible critical variations and avoid possible significant deviations from the reference values. Although not so critical, this verification should also be performed for DHX03. In spite of that recommendations, it is not expected that this parameter could compromise the dosimetric equivalence between the two linear accelerators.

4.1.2. Trimestral Quality Assurance

The results obtained during the trimestral verifications for dosimetrical parameters, such as dose calibration factor, symmetry (X and Y), MLC transmission and dosimetric leaf separation verifications are summarized in the next subchapters. The reference values, obtained by an external entity, are also represented in Figures 39-43 as measurement 0.

4.1.2.1. Dose Calibration Factor

The dose calibration factor minimum, maximum, mean and standard deviation values obtained for the three linear accelerators are summarized in Table 13 and represented over one and a half year in Figure 39.

Dose Calibration Factor [cGy/MU]

Equipment	Minimum	Maximum	Mean	Std. Deviation
DHX01	1,0004	1,0090	1,0042	0,0033
DHX02	0,9956	1,0100	1,0031	0,0046
DHX03	1,0002	1,0100	1,0029	0,0036

Table 13 - Descriptive statistics for trimestral QA dose calibration factor.

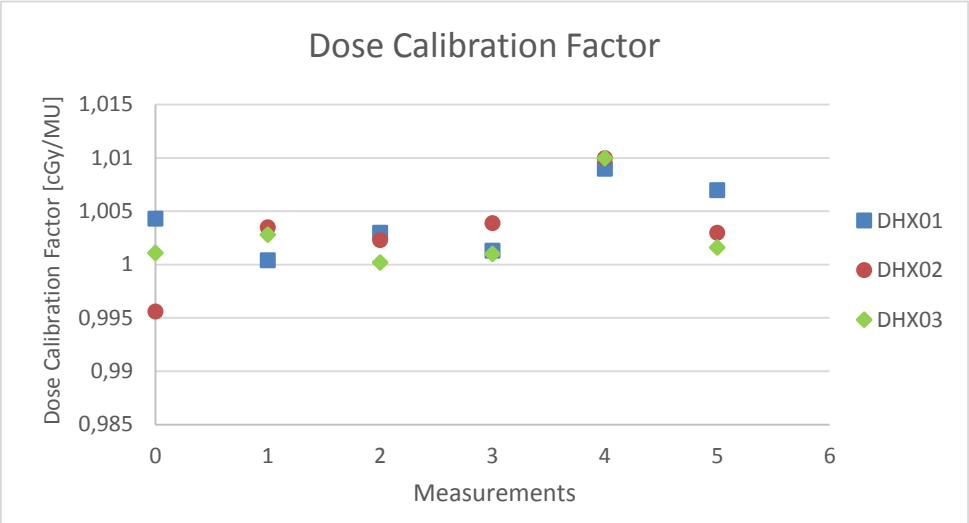

Figure 39- Graphical representation of dose calibration factor obtained in trimestral QA.

From the results, it is verified that the dose calibration factor is below the tolerance limit (2%) for all the three linear accelerators, with average values very close to unity and minimum and maximum values that do not exceed a deviation of 1.00%.

This observation allows to conclude that there are very small alterations of the equivalence between DHX02 and DHX03 linacs, in relation to absolute dose and also that the dose calibration factor results obtained with DHX01 linac are similar to the obtained with the other two linear accelerators, suggesting an equivalence between the three linear accelerators in relation to absolute dose. An increase of around 0.50% in this factor was obtained in the fourth measurement for the three linear accelerators, which was corrected in the next measurement. In spite of that correction, a further detailed analysis of the behavior of this parameter is required, in order to understand if a tendency to increase is present.

4.1.2.2. X- axis Symmetry and Y-axis Symmetry

The X-axis symmetry minimum, maximum, mean and standard deviation values obtained for the three linear accelerators are summarized in Table 14 and shown in Figure 40 over the period of one and a half year.

X-axis symmetry

Equipment	Minimum	Maximum	Mean	Std. Deviation
DHX01	100,69%	101,09%	100,92%	0,16%
DHX02	100,64%	101,89%	101,00%	0,53%
DHX03	100,42%	100,82%	100,58%	0,19%

Table 14 - Descriptive Statistics for trimestral QA x-axis symmetry.

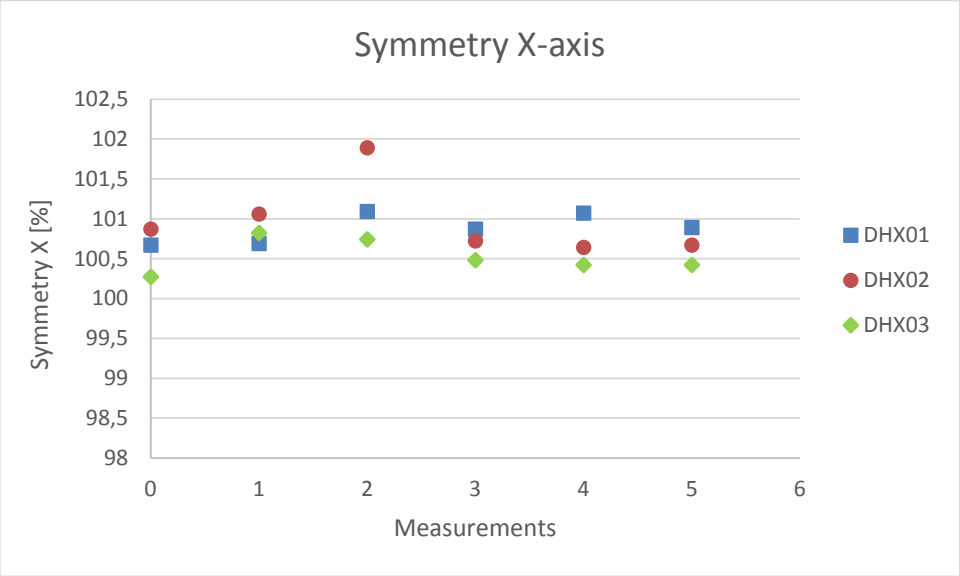

Figure 40 - Graphical representation of X-axis symmetry obtained in trimestral QA.

The X-axis beam symmetry is within the tolerance limit for DHX01 and DHX03 linacs, with a maximum deviation of approximately 1.00% from the baseline (which corresponds to a 100.00% symmetric field) and values relatively stable with time. However, it was observed a change of 1.00% between two successive measurements for DHX02 linac to an X-symmetry value of 101.89%. Although this value is within the tolerance limit, it is very close to the maximum acceptable value and, for this reason, a symmetry adjustment was performed by a Varian engineer and the X-axis symmetry values obtained in the subsequent periodic QA were relatively stable and with a deviation below 1.00%. This observation is an additional motivation to perform a further analysis, as DHX02 and DHX03 linacs were adjusted as dosimetrically equivalent in the TPS and their symmetry behavior over time is slightly different, which accentuate the importance of evaluating the possible implications of these slightly differences in IMRT treatments.

The Y-axis symmetry minimum, maximum, mean and standard deviation values obtained for the three linear accelerators are summarized in Table 15 and shown in Figure 41.

Y-axis symmetry

Equipment	Minimum	Maximum	Mean	Std. Deviation
DHX01	100,25%	100,85%	100,51%	0,28%
DHX02	100,09%	101,14%	100,49%	0,39%
DHX03	100,46%	100,79%	100,56%	0,13%

Table 15 - Descriptive statistics for trimestral QA y-axis symmetry.

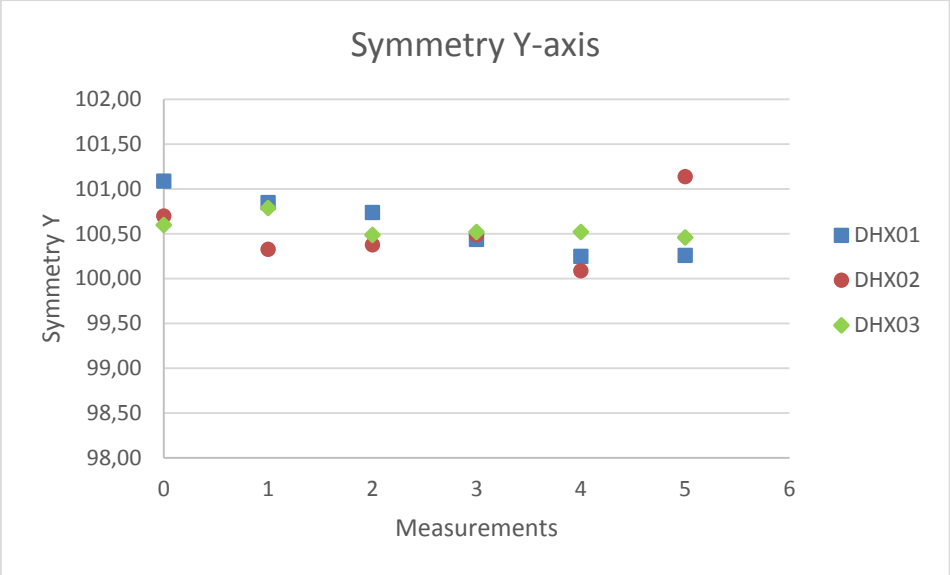

Figure 41 - Graphical representation of Y-axis symmetry obtained in trimestral QA.

The Y-axis symmetry is also within the tolerance limit for the three linear accelerators, with relatively stable values, except for the last measurement of DHX02 linac, in which an increase from a value near 100.00% in the previous measure to a value of 101.14% was observed.

Although the deviation values are clearly within the tolerance limits and very similar average values were obtained (approximately 100.50%) for the three linear accelerators, is important to monitor the evolution of this parameter in the following measures, to understand if the increase observed for DHX02 was a single higher measurement or results from tendency to an increase in Y- axis symmetry.

4.1.2.3. MLC Transmission

The MLC transmission minimum, maximum, mean and standard deviation values obtained for the three linear accelerators are summarized in Table 16.

MLC Transmission

Equipment	Minimum	Maximum	Mean	Std. Deviation
DHX01	1,45%	1,48%	1,46%	0,02%
DHX02	1,39%	1,41%	1,40%	0,08%
DHX03	1,43%	1,44%	1,44%	0,04%

Table 16 - Descriptive statistics for trimestral QA MLC transmission.

In Figure 42 it is possible to observe the MLC transmission results obtained in each of the trimestral verification for the three linear accelerators compared to the transmission value considered by the TPS.

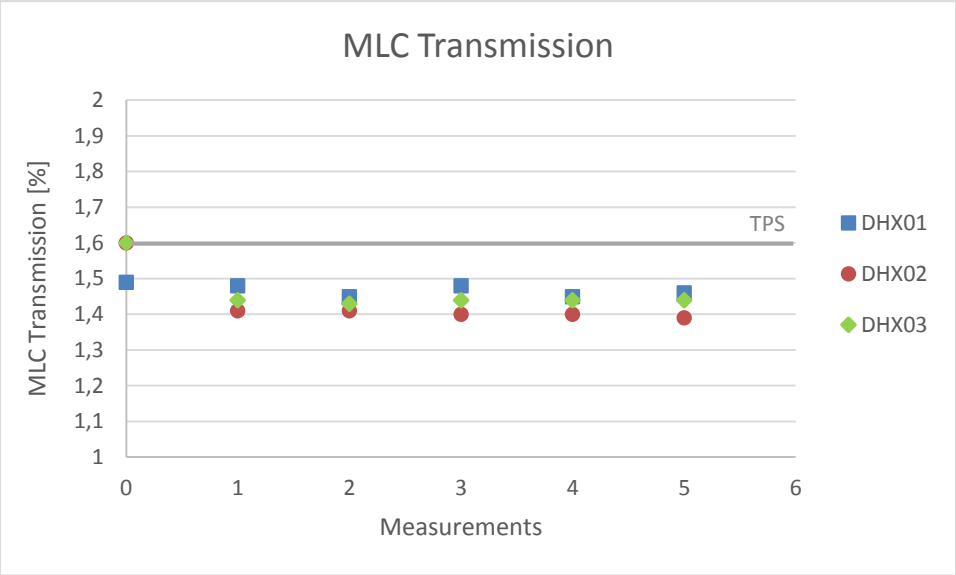

Figure 42 - Graphical representation of MLC transmission obtained in trimestral QA.

The MLC transmission is also below the tolerance value and present similar values for all the linear accelerators, although slightly lower than the reference (measurement 0, which were performed by an external entity, so the values could be approximated or averaged, creating a deviation from the values measured during periodic QA) and TPS values.

Although the deviation between measurements and the TPS is small (approximately 0.20%, which is lower than the 0.50% difference tolerance), the MLC transmission show a tendency for maintaining these lower values.

4.1.2.4. Dosimetric Leaf Separation

The dosimetric leaf separation minimum, maximum, mean and standard deviation values obtained for the three linear accelerators are summarized in Table 17 and the long-term assessment is shown and compared to the dosimetric leaf separation values considered by the TPS in Figure 43.

DLS (mm)				
Equipment	Minimum	Maximum	Mean	Std. Deviation
DHX01	2,05	2,13	2,07	0,03
DHX02	2,36	2,47	2,42	0,04
DHX03	2,27	2,35	2,30	0,03

Table 17 - Descriptive statistics trimestral QA dosimetric leaf separation.

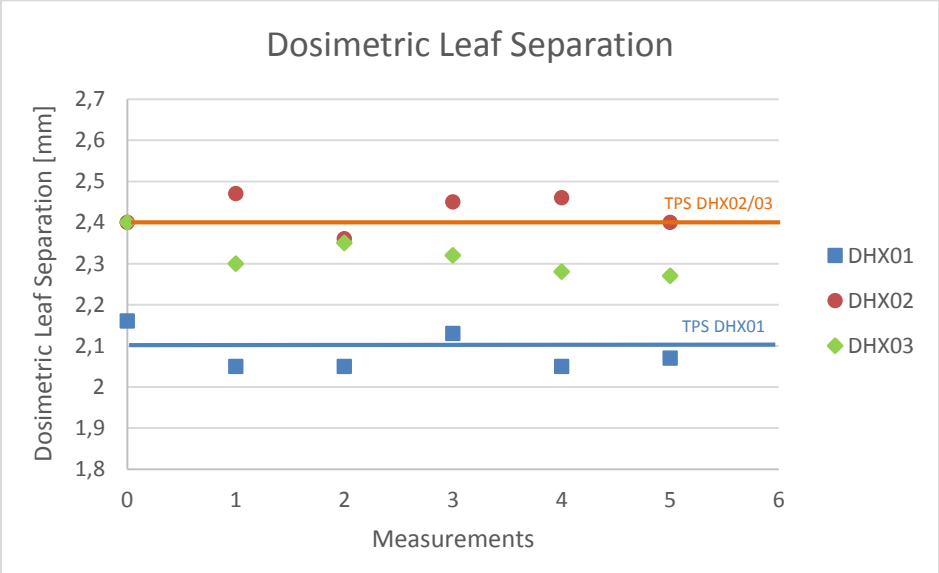

Figure 43- Graphical representation of dosimetric leaf separation obtained in trimestral QA.

The dosimetric leaf separation values obtained with DHX02 and DHX03 linacs are very similar, with DHX02 presenting a tendency to have greater values of DLS than DHX03 linac. However, the differences observed are inferior to the tolerance value of 0.20 mm for all the measurements, so it can be concluded that the equivalence between the two linear accelerators is also maintained in relation to the dosimetric leaf separation.

However, when the dosimetric leaf separation values obtained with DHX01 linac are considered, it can be concluded that, although these values stood very stable around the TPS value (2.10 mm), with differences lower than 0.10 mm for all the measurements, more investigation is needed to consider DHX01 linac equivalent to the other two linear accelerators in respect to DLS as, in spite of having differences lower than the action level of 0.50 mm, these are higher than the tolerance value of 0.20 mm and these differences may result in more significant discrepancies when IMRT treatments are performed indistinctly (without replanning) with DHX01 or DHX02/03 linacs.

4.1.3. EPID Tests

4.1.3.1. Garden Fence Test

The minimum, maximum, mean and standard deviation values of the agreement in gamma analysis obtained for Garden fence test using criteria of 3.0%, 3.0 mm and 3.0%, 0.5 mm are summarized in Table 18.

Garden Fence Test

Gamma criterion	Equipment	Minimum	Maximum	Mean	Std. Deviation
3.0%, 3.0 mm	DHX01	95,60%	100,00%	99,61%	0,89%
	DHX02	99,90%	100,00%	99,99%	0,03%
	DHX03	99,60%	100,00%	99,93%	0,11%
3.0%, 0.5 mm	DHX01	63,10%	100,00%	95,67%	8,52%
	DHX02	67,40%	100,00%	97,18%	6,51%
	DHX03	91,60%	100,00%	98,26%	1,93%

Table 18 - Descriptive statistics for agreement value of the Gamma analysis for Garden Fence test.

The results obtained for the Garden Fence test using gamma criteria of 3.0%, 3.0 mm and 3.0%, 0.5 mm can be observed in Figures 44 and 45, respectively.

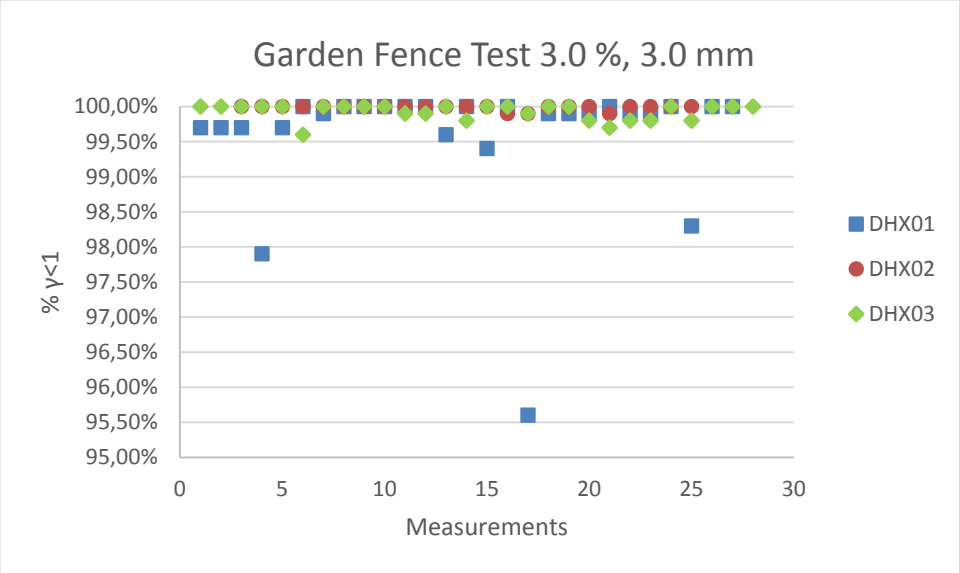

Figure 44 - Gamma analysis agreement values for Garden Fence test using 3.0 %, 3.0 mm criteria.

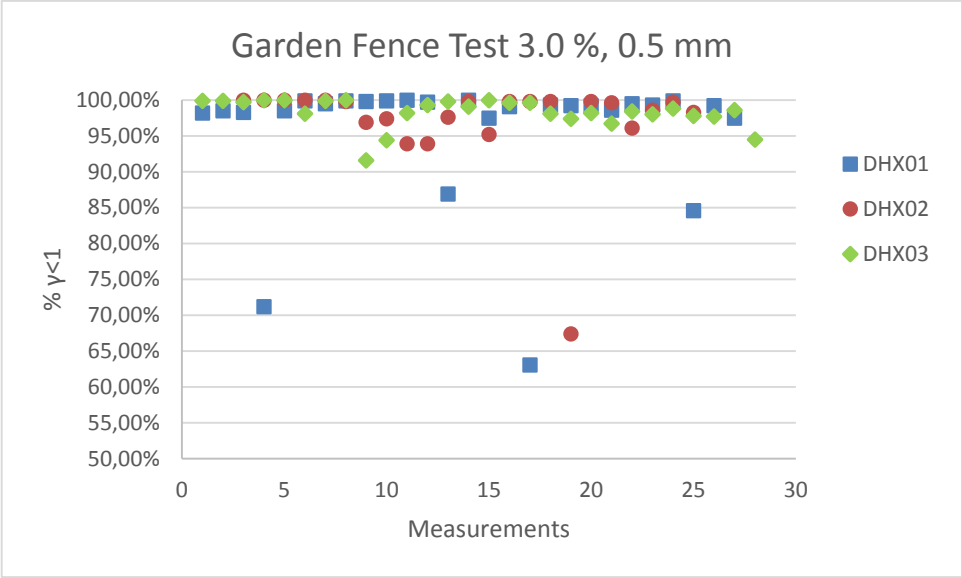

Figure 45 - Gamma analysis agreement values for Garden Fence test using 3.0 %, 0.5mm criterion.

Using the gamma analysis with 3.0 %, 3.0 mm criteria, it can be observed that the agreement between the experimental images and the reference image (first image obtained in 2014) is approximately 100.00% in all measurements for DHX02 and DHX03 linacs, which means that the MLC of both linear accelerators have a very stable behavior. However, for DHX01 linac, although most results are near 100.00% agreement, in some of the measurements performed lower agreements were obtained with this criteria, all of them above 95.00% and with an average agreement value of 99.59% for this criterion, which have a non-significant difference in relation to the average agreement values of 99.99% and 99.93% obtained for DHX02 and DHX03 linacs, respectively. For this reason, although having a non-ideal behavior, the results of the Garden Fence test for DHX01 linac are relatively stable using the 3.0 %, 3.0 mm gamma criterion.

Changing the gamma criteria to 3.0 %, 0.5 mm, the agreement values obtained for the garden fence test using a gamma comparison with a reference image (first image of 2014) are globally lower than with the 3.0 %, 3.0 mm criterion. However, the agreement values obtained for DHX03 linac are above 90.00% for all the measures, with the majority of the values above 95.00%, which can be classified as a good result using this criteria. For DHX02 linac, the results are similar, except for one value (67.40%), which is not significant, as it is a single lower value that is not observed in the following measurements. On the other hand, although the majority of the agreement values are also above 95.00%, four lower values (86.90%, 84.60%. 71.20% and 63.10%) are observed for DHX01 linac. In spite of not having a very significant meaning, as the majority of the values are within the acceptance limits (above 95.00%) and the average agreement, 95.79%, is not significantly lower than for the other linear accelerators (97.10% for DHX02 and 98.33% for DHX03), these results justify further analysis for DHX01 linac, in order to understand if it is related with imprecisions in irradiation or EPID acquisition.

4.1.3.2. Chair Test

The minimum, maximum, mean and standard deviation values obtained for Chair test using criteria of 3.0%, 3.0 mm are summarized in Table 19.

Chair Test

Gamma criterion	Equipment	Minimum	Maximum	Mean	Std. Deviation
3.0%, 3.0 mm	DHX01	80,60%	96,70%	89,71%	5,53%
	DHX02	85,00%	95,35%	90,54%	5,12%
	DHX03	92,30%	94,20%	93,23%	0,84%

Table 19 - Descriptive statistics for agreement value of the Gamma analysis for Chair test.

The results obtained for the garden fence test using gamma criteria of 3.0%, 3.0 mm can be observed in Figure 46.

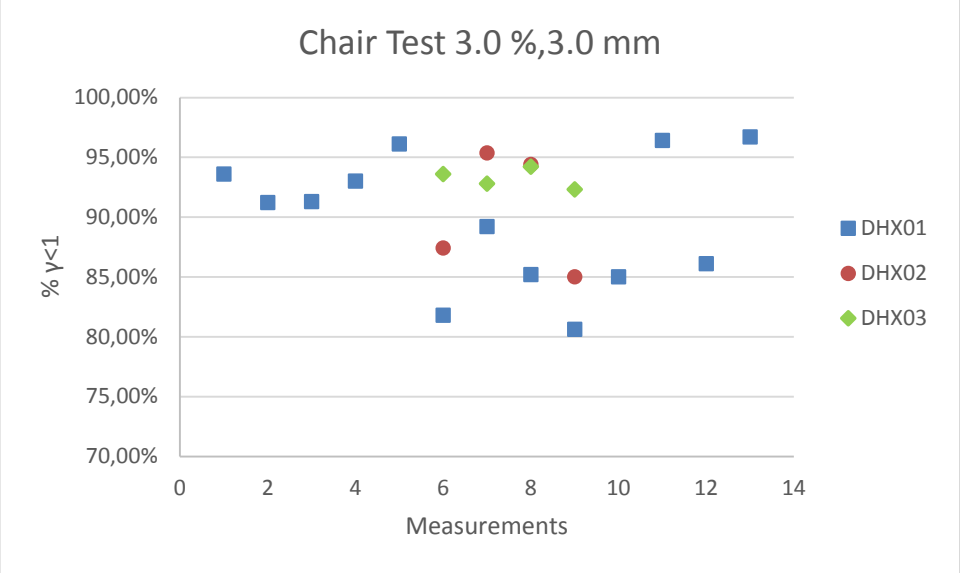

Figure 46 - Gamma analysis agreement values for Chair test with a 3.0 %, 3.0 mm criteria.

In first place, it is important to state that the number of measurements for the three linear accelerators is clearly unequal, with more measurements for DHX01 linac than for DHX02 and DHX03 linacs, which results, on one hand, from the previous installation of DHX01 linac, which have, for this reason, a higher time of functioning, creating more predisposition for alterations of MLC constancy. On the other hand, it was previously observed that DHX02 and DHX03 linacs have a more constant MLC behavior, which leads to a less frequent need of monitoring. In order to compare the results obtained with the three linear accelerators, the results were organized in the graphic such that measurements near in time are presented in the same X-axis positions.

It is also important to mention that the reference values for the Chair test, acquired during the linear accelerators validation process by an external entity, although higher than 90.00%, were relatively low.

From the previous observation, it can be concluded that the results obtained for DHX03 linac were very stable and show a good agreement with the reference value (91.30%), as for all the measurements the agreement values obtained in the gamma analysis were above this value, with an average deviation of 2.06%.

In the case of DHX02 linac, for which the reference gamma agreement value is 91.80%, two measurements above and two measurements below the reference value were obtained, with an average absolute deviation of 4.88%.

For DHX01 linac, the results obtained present poor stability. In the first five measurements (all performed in January, 2014) the agreement values obtained were above the reference value of 92.20%. In the following measurements, results below the reference value were obtained and the average absolute deviation from the reference value is 5.52%, which is a more significant deviation. However, it is not observed a tendency for decrease of the gamma agreement, since the value obtained in the last measurement of 2014 was 96.70%, which is above the reference value.

Both in case of DHX01 and DHX02 linacs the results are not conclusive, due to oscillation between acceptable and non-acceptable values. For this reason, a further analysis is recommended, in order to understand if an unstable behavior is maintained in the future. It is important to mention that, for all the measurements with poorer results, the low agreement region coincides with the left part of the Chair test portal image, in which the leaves move with a higher speed, allowing a higher transmission, decreasing the agreement with the TPS predicted image.

4.1.3.3. Field Size Dependence Test

The results of the Field Size Dependence test, performed for DHX01 and DHX02 linacs, for dose rates of 400 MU/min and 600 MU/min can be observed in Figures 47 and 48, respectively.

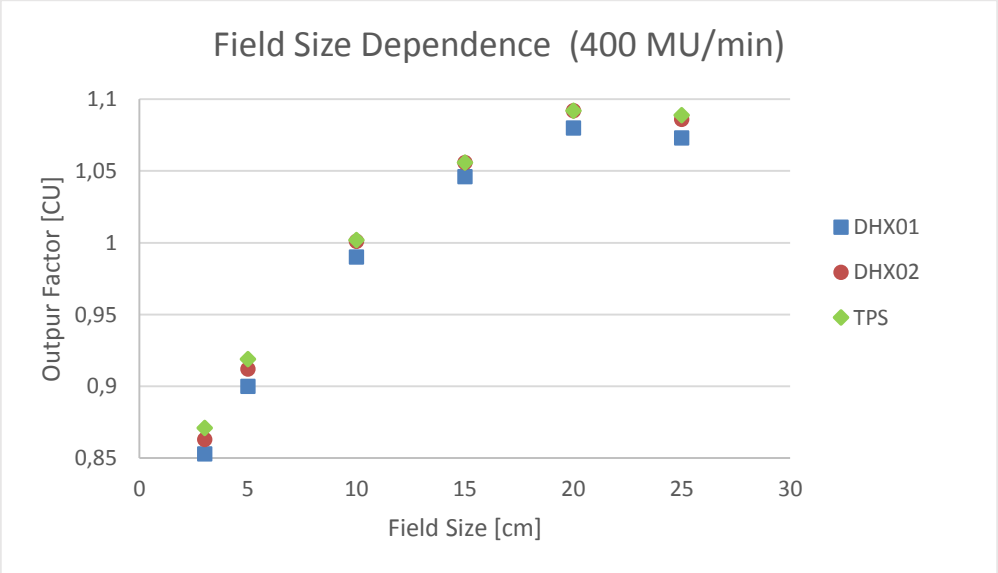

Figure 47 – Field size dependence test output factors for a dose rate of 400 MU/min.

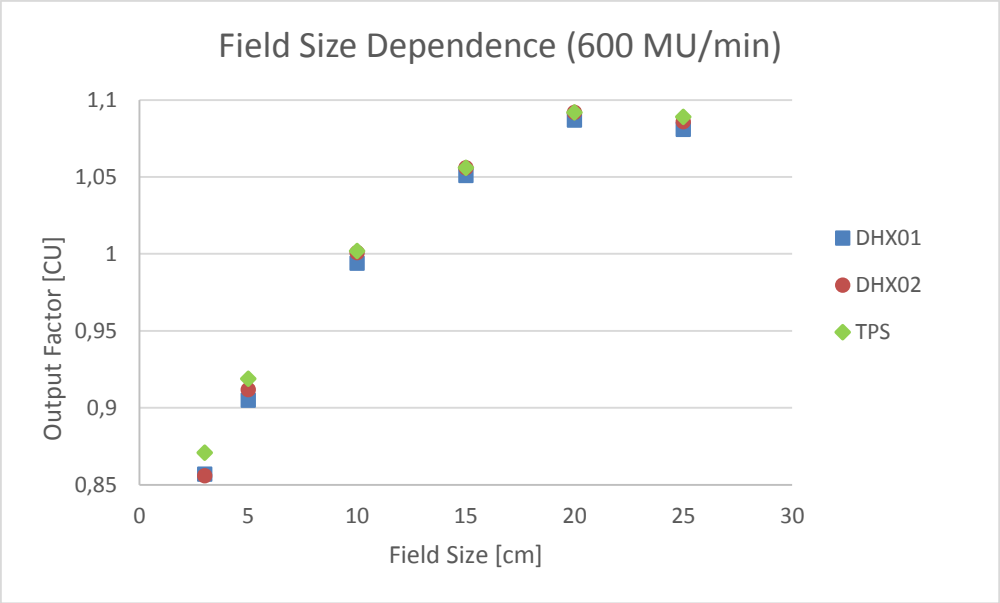

Figure 48 - Field size dependence test output factors for a dose rate of 600 MU/min.

The minimum, maximum, mean and standard deviation values for the absolute deviations obtained from the comparison of the DHX01, DHX02 and TPS Field Size Dependence test results, for dose rates of 400 MU/min and 600 MU/min, are summarized in Table 20.

Field Size Dependence Test Absolute Deviations [%]

Dose Rate	Comparison	Minimum	Maximum	Mean	Std. Deviation
400 MU/min	DHX01/TPS	0,96%	2,11%	1,50%	0,50%
	DHX02/TPS	0,00%	0,93%	0,35%	0,40%
	DHX01/DHX02	0,96%	1,33%	1,15%	0,12%
600 MU/min	DHX01/TPS	0,46%	1,63%	0,94%	0,52%
	DHX02/TPS	0,00%	1,75%	0,48%	0,68%
	DHX01/DHX02	0,12%	0,77%	0,50%	0,23%

Table 20 - Descriptive statistics for field size dependence test absolute deviations.

First of all, it is important to mention that the output factors calculated by the TPS were the same for DHX01 linac and DHX02 linacs, without variations with the change of treatment unit in the TPS. For this reason, in the analysis only one set of TPS output factor values was considered, which is valid for both linear accelerators.

From the results, it is observed that, in general, larger deviations occur for the 400 MU/min dose rate (which is the more used clinically) than for the 600 MU/min.

Comparing both experimental verification from DHX01 and DHX02 for this dose rate, an average absolute deviation of 1.15% was obtained, which is higher than the average absolute deviation of 0.46% obtained between the two linear accelerators for a dose rate of 600 MU/min. However, for both dose rates, higher output factors were obtained for DHX02 than for DHX01 for all the field sizes.

A good agreement was obtained in the comparison between the experimental verification with DHX02 linac and the TPS prediction, with an average absolute deviation of 0.35% for the 400 MU/min dose rate and of 0.48% for the 600 MU/min dose rate, values that are clearly below the tolerance of 1.00%. On the other hand, the deviation values were slightly higher when comparing the experimental verification with DHX01 linac with the TPS prediction, with an average absolute deviation of 1.50% for the 400 MU/min dose rate and of 0.94% for the 600 MU/min dose rate. It was also observed that the TPS predicted output factors were higher or equal to the experimental output factors for all the field sizes, for both the linear accelerators.

From the observations stated above, it is possible to conclude that, for a dose rate of 600 MU/min, the results are in accordance with the expected, since the average deviations obtained for the three linacs were within the tolerance limit of ± 1.00%. Another important aspect to mention is that a slightly higher average deviation value was obtained for DHX01 linac, resulting partially from significantly higher deviation values obtained for the lower field sizes (3x3 and 5x5 cm^2), which are not included in the tolerance of ± 1.00%, since this tolerance recommendation is valid for fields with dimensions above 5x5 cm^2. Despite of this result for DHX01 linac, when comparing the experimental results obtained with both the linear accelerators for this dose rate, an average absolute deviation of approximately 0.48% was obtained, which is below the tolerance and can be considered a good result.

When performing the same test for a dose rate of 400 MU/min, the deviations were slightly more accentuated. As stated before, the results obtained in the comparison between DHX02 experimental and TPS predicted output factors were also satisfactory, with a 0.35% average absolute deviation. However, when comparing the TPS predicted output factors with the obtained experimentally with DHX01 linac, an average absolute deviation of 1.50% was obtained, with values above 1.00% for all the field sizes, except for the 15x15 cm^2 field, for which a deviation of 0.96% was obtained. Although not so evidently as in relation to the TPS values, the differences are maintained when comparing the output factors obtained with DHX01 linac with the obtained with DHX02 linac, with an average absolute deviation of 1.15%, also with a single deviation value lower than 1.00%, for the 15x15 cm^2 field.

Further investigation was performed in order for this test to be conclusive in relation to the analysis of the equivalence of both the linear accelerators. The test was performed with a verification plan created for DHX02 and eventual deviations in the TPS predicted output factors, although not expected, were evaluated by changing the treatment unit in the TPS from DHX02 to DHX01 linac. The predicted output factors remained the same after this change, supporting the hypothesis that, for static fields, output factor deviations in the TPS does not occur.

Another observation from this test to take into account is that the dose rate influences the field size dependence, with higher deviation for the more clinically used dose rate of 400 MU/min when a change of equipment in relation to the defined in TPS occurs.

4.1.3.4. Linearity Test

The results of the Linearity test, performed for DHX01 and DHX02 linacs for dose rates of 400 MU/min and 600 MU/min are summarized in Figures 49 and 50, respectively.

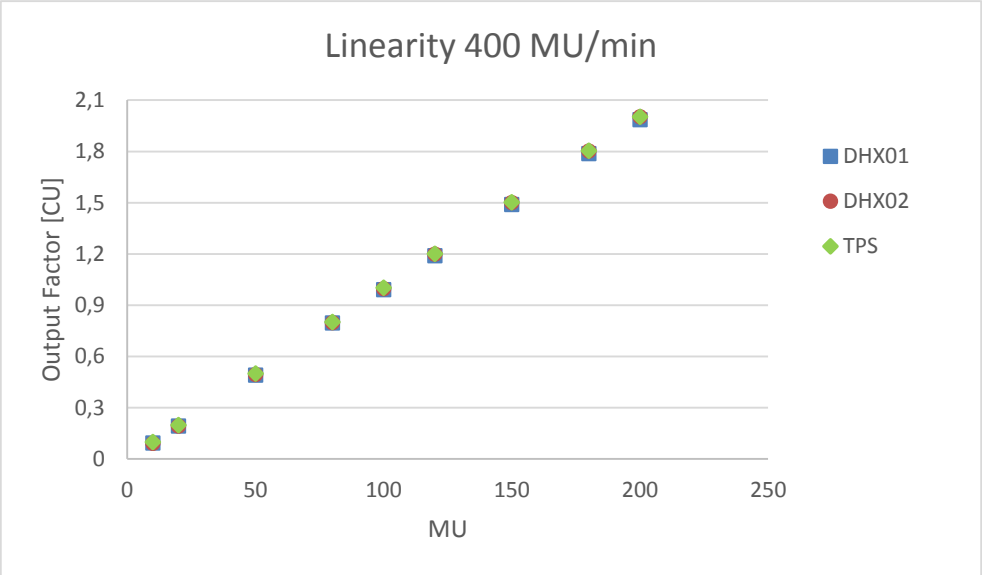

Figure 49 - Linearity test output factors for a dose rate of 400 MU/min.

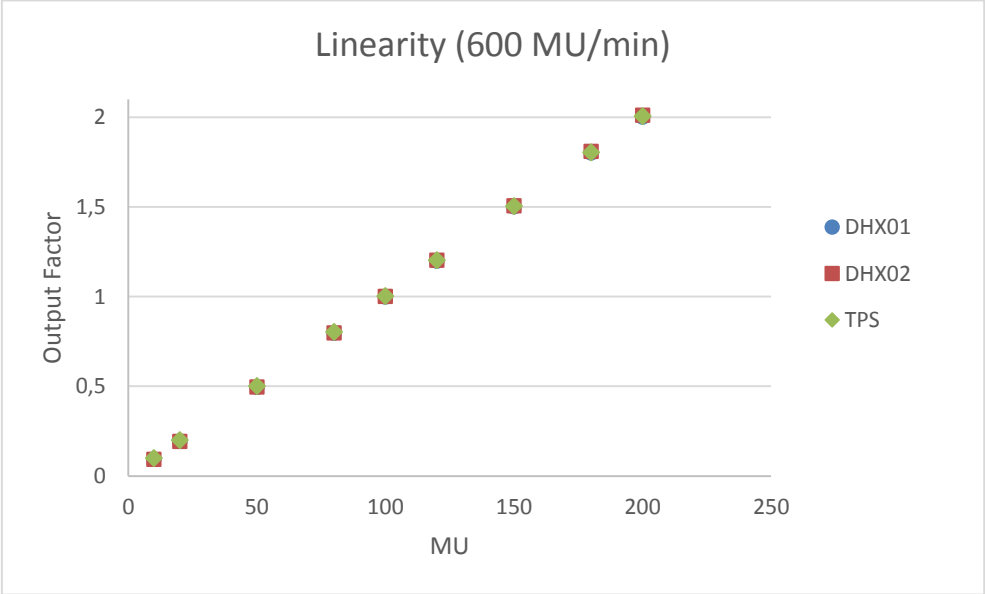

Figure 50 - Linearity test output factors for a dose rate of 600 MU/min.

The minimum, maximum, mean and standard deviation values for the absolute deviation obtained from the comparison of the DHX01, DHX02 and TPS linearity test results, for dose rates of 400 MU/min and 600 MU/min, are summarized in Table 21.

Linearity Test Absolute Deviations [%]

Dose Rate	Comparison	Minimum	Maximum	Mean	Std. Deviation
400 MU/min	DHX01/TPS	0,63%	5,26%	1,79%	1,60%
	DHX02/TPS	0,00%	8,70%	1,63%	2,89%
	DHX01/DHX02	0,00%	3,16%	0,89%	0,90%
600 MU/min	DHX01/TPS	0,22%	7,53%	1,77%	2,50%
	DHX02/TPS	0,00%	8,70%	1,64%	2,87%
	DHX01/DHX02	0,25%	1,08%	0,54%	0,23%

Table 21 - Descriptive statistics for linearity test absolute deviations.

First of all, it is important to mention that, as for Field Size Dependence test, the output factors calculated by the TPS were the same for DHX01 and DHX02 linacs, without variations with the change of treatment unit in the TPS. For this reason, in the analysis only one set of TPS output factor values was considered, which is valid for both linear accelerators.

The results indicate relatively high deviations in the comparison of the TPS predictions with the experimental output factors obtained with DHX01 and DHX02 linacs, as can be observed in Table 21.

For a dose rate of 400 MU/min, the differences obtained were also slightly higher than for 600 MU/min, although with smaller deviations than for the Field Size Dependence test.

In the comparison between the experimental output factors obtained in the verifications with DHX01 and DHX02 linacs for a 400 MU/min dose rate, an average absolute deviation of 0.89% was obtained, with higher output factors obtained with DHX02 than with DHX01 for all MU values, except for 10 MU, which is also the only value for which an average deviation higher than 1.00% (3.16%) was obtained in the comparison of both experimental verifications. This disagreement in relation to the tolerance limits for lower MU values, including 10 MU, is present in the literature, in which a deviation up to 10.00% is mentioned [51]. The same behavior is observed for the same experimental comparison for the verifications performed with a dose rate of 600 MU/min, for which an average absolute deviation of 0.54% was obtained. The output factors obtained with DHX02 linac were only lower than the obtained with DHX01 linac for the 10 MU value and only for this MU value a deviation between the measured output factors above 1.00% was obtained (1.08%), although considerably lower than for the 400 MU/min dose rate. From the reported results relative to the comparison between the output factors obtained experimentally with DHX01 and DHX02, it can be concluded that these results are in agreement with the recommended tolerance limits and both the linear accelerators can be considered experimentally equivalent in relation to linearity for both the dose rates.

However, when the experimental results obtained with each of the linear accelerators were compared with the TPS predicted output factors, the deviations obtained were higher. In the case of DHX02 linac, average absolute deviations of 1.63% for the 400 MU/min dose rate and of 1.48% for the 600 MU/min dose rate were obtained from the comparison with TPS predicted output factors. These deviation values are above the recommended tolerance limit of 1.00%, which can be justified by the fact that high deviations were obtained only for the lower values

of MU, with values below 1% for all the MU values above 50 MU. For this reason, as for the fact that the deviations obtained for the lower MU values are below the tolerance value of 10.00% found in the literature [51], it can be considered that the comparison between the output factors measured with DHX02 and the TPS output factors predicted for DHX02 are in accordance with the expected, without significant deviations, since the deviation values obtained were below 1.00% for MU values above 50 MU and did not exceed 8.70% for MU values below 50 MU.

For the experimental verification performed with DHX01, the results obtained in the comparison with the TPS predicted output factors are very similar for both dose rates, with average absolute deviations of 1.79% for 400 MU/min and of 1.77% for 600 MU/min. For the 600 MU/min dose rate, it is also verified that the deviation is higher than 1.00% only for MU values lower than 50 MU. On the other hand, although for this MU values the deviations obtained were higher for 600 MU/min, which is in accordance with the results found in the literature, that states that the higher deviations were obtained for lower MU and higher dose rate [51], for the 400 MU/min dose rate deviations slightly above 1.00% were obtained for MU values above 80 MU. Although the tolerance limit of 1.00% is not significantly exceeded, these results indicate that, for a dose rate of 400 MU/min (more used clinically), deviations between measured and TPS predicted output factors slightly above 1.00% were obtained for MU values of approximately 100, which are used clinically. Although the deviation is not significantly high, the exceeding of the tolerance deviation values requires careful analysis of the results obtained with DHX01 linac.

4.2. Head and Neck IMRT Treatments

4.2.1. Change of Treatment Machine in Eclipse™ TPS: Dose evaluation

In this chapter, the results of the analysis of the differences in the doses calculated by the TPS in the different volumes used for treatment evaluation, as well as in the total MU number, after change in treatment machine in Eclipse™ TPS are shown and discussed. The results are divided by three categories:

- DHX01 Head and Neck sample, in which the treatment planning was originally performed for DHX01 linac and for which the dose and MU number differences were calculated in relation to a second plan that consisted in a copy of the original plan, followed by change of treatment machine in the TPS for DHX02/DHX03 linacs (which are equivalent in the TPS) and dose and monitor unit recalculation;
- DHX02 Head and sample, in which the treatment planning was originally performed for DHX02 linac and for which the dose and MU number differences were calculated in relation to a copy of the original plan, with dose and MU number recalculation for DHX01 linac; and

- DHX03 Head and Neck sample, in which the treatment planning was originally performed for DHX03 and for which the procedure for the determination of dose and MU number difference after change of treatment machine in the TPS was similar to the used to DHX02.

The average deviations obtained for the total MU number and dose calculated by the TPS for the different volumes in study for the three Head and Neck samples are summarized in Table 22.

PTV54			
	DHX01 Sample	DHX02 Sample	DHX03 Sample
D_{min}	0.130%	0.220%	0.183%
D_{max}	0.152%	0.138%	0.159%
D_{mean}	0.062%	0.050%	0.072%
$V_{95\%}$	0.010%	0.013%	0.008%

PTV59.4			
	DHX01 Sample	DHX02 Sample	DHX03 Sample
D_{min}	0.160%	0.155%	0.174%
D_{max}	0.099%	0.129%	0.143%
D_{mean}	0.044%	0.030%	0.046%
V95%	0.010%	0.006%	0.005%

PTV70			
	DHX01 Sample	DHX02 Sample	DHX03 Sample
D_{min}	0.134%	0.134%	0.099%
D_{max}	0.104%	0.009%	0.140%
D_{mean}	0.031%	0.031%	0.033%
V95%	0.012%	0.006%	0.021%

D_{max} OAR			
	DHX01 Sample	DHX02 Sample	DHX03 Sample
R Eye	0.514%	0.308%	0.407%
L Eye	0.277%	0.244%	0.490%
R Lens	0.403%	0.284%	0.689%
L Lens	0.746%	0.378%	0.584%

D_{max} Critical Structures			
	DHX01 Sample	DHX02 Sample	DHX03 Sample
Brainstem	0.329%	0.294%	0.358%
Right ON	0.165%	0.204%	0.461%
Left ON	0.173%	0.228%	0.314%
Chiasm	0.195%	0.117%	0.188%
Spinal Cord	0.409%	0.237%	0.450%

D_{mean} OAR			
	DHX01 Sample	DHX02 Sample	DHX03 Sample
R Parotid	0.136%	0.250%	0.241%
L Parotid	0.122%	0.227%	0.260%
Larynx	0.199%	0.174%	0.365%
Esophagus	0.237%	0.250%	0.251%
Pharynx	0.121%	0.273%	0.293%

MU			
	DHX01 Sample	DHX02 Sample	DHX03 Sample
MU	0.567%	0.507%	0.617%

Table 22 - Average absolute TPS dose and total Monitor Units deviations for H&N samples TPS change of treatment unit.

From Table 22, it can be observed that significant deviations are not observable with the change of treatment unit, since all the absolute average deviations obtained for the three samples are lower than 1.00%. For the PTVs (target volumes), all the parameters analyzed present low deviations (inferior to 0.25%). In the case of organs-at-risk and critical structures, slightly higher deviations (up to approximately 0.75%) were obtained for the structures with lower volumes in the plans, since a small volume are more sensitive to a slight dose variation, although these variations are not significant, since they present values lower to 1.00% and do not compromise the accordance of the dose values with the protocoled tolerances.

Dosimetrical differences between DHX01 original plans and recalculated plans for DHX02/DHX03

The deviation values calculated for dose and MU values before and after the change of treatment unit in the TPS are shown in Figures 51 to 56.

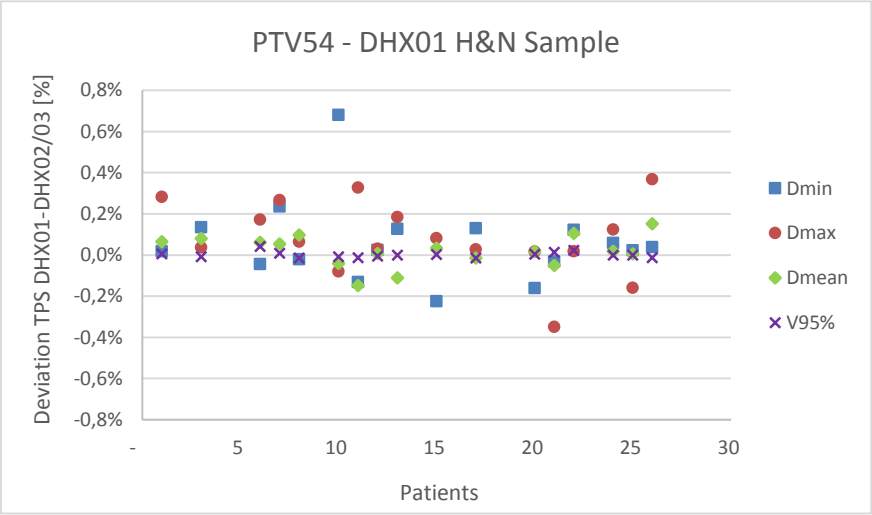

Figure 51 – Graphical representation of DHX01 H&N sample TPS dose deviations for PTV54 between DHX01 original plans and DHX02/DHX03 recalculated plans.

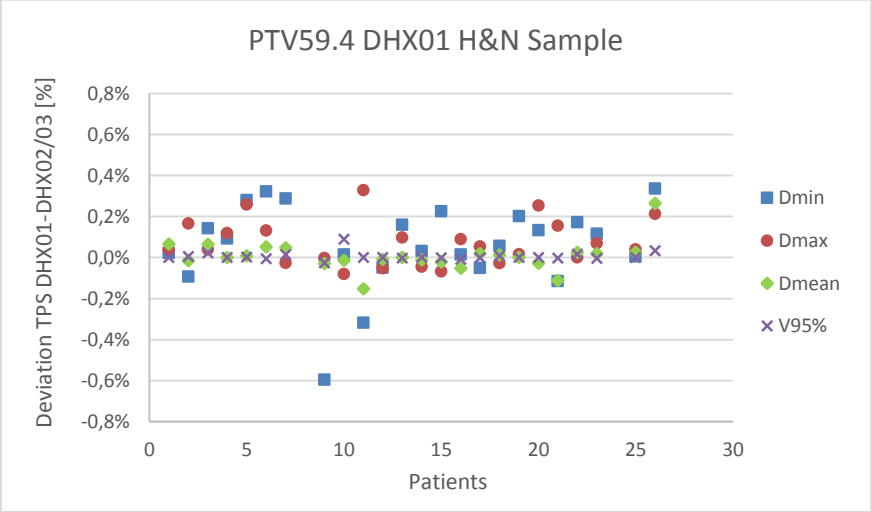

Figure 52- Graphical representation of DHX01 H&N sample TPS dose deviations for PTV59.4 between DHX01 original plans and DHX02/DHX03 recalculated plans.

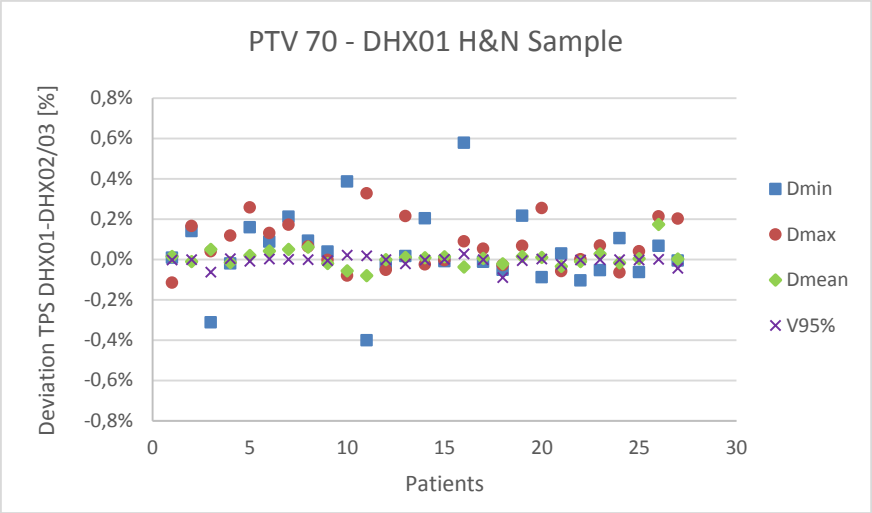

Figure 53 - Graphical representation of DHX01 H&N sample TPS dose deviations for PTV70 between DHX01 original plans and DHX02/DHX03 recalculated plans.

From the analysis of the results obtained for the PTVs of DHX01 sample, it can be observed that the differences obtained with the change of treatment unit were small, with average absolute deviations lower than 0.20% for all the PTV parameters in study. In relation to the deviation values obtained for each of the patients in the sample, the values are distributed within the interval of ± 0.80%, with deviations higher than 0.50% only for D_{min}, for which, in general, higher deviations were verified. For $V_{95\%}$, which is the parameter that deserves more attention in the evaluation of a treatment plan, the deviations obtained with the change of treatment unit were approximately null for all the patients in DHX01 sample.

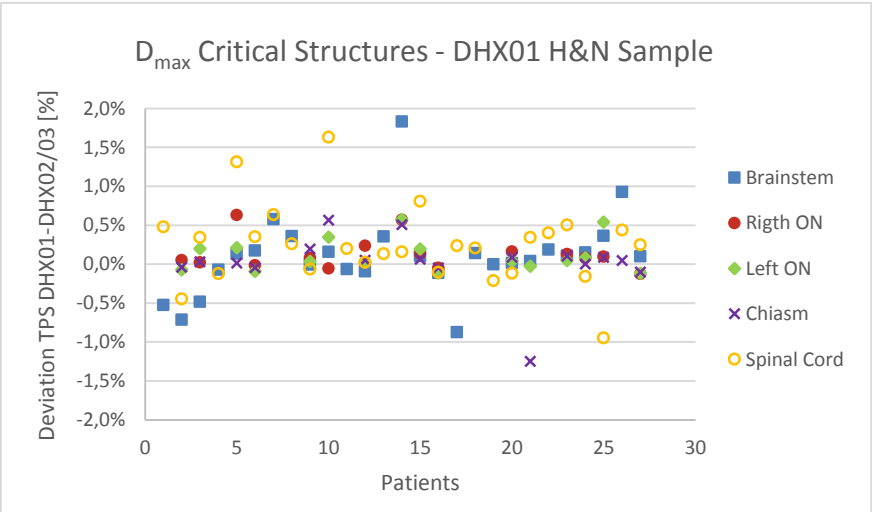

Figure 54 - Graphical representation of DHX01 H&N sample TPS dose deviations for critical structures D_{max} between DHX01 original plans and DHX02/DHX03 recalculate plans.

In relation to the critical structures, the analysis of D_{max} parameter has resulted in average absolute deviations lower than 0.50%. From the respective dispersion graph, it can be observed that the deviations are within the interval of ± 2.00%, not describing significant variations and not compromising the accordance with the established protocol. However, the cases in which deviations above 1.00% occurred were analyzed with more detail and it was concluded that the presence of this higher variations are coincident with a low volume of the structures and also with a high proximity between the given critical structures with the target volumes that results in a higher dose gradient and a consequent higher susceptibility to dose variances.

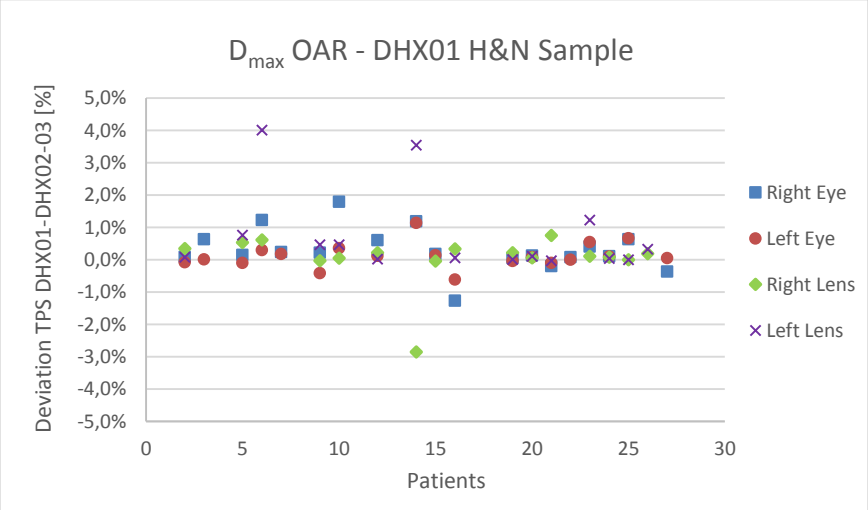

Figure 55 - Graphical representation of DHX01 H&N sample TPS dose deviations for organs-at-risk D_{max} between DHX01 original plans and DHX02/DHX03 recalculated.

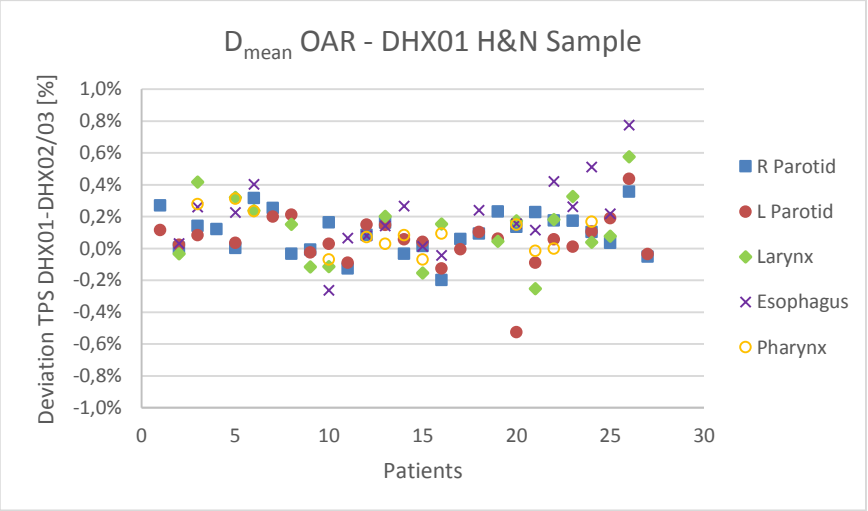

Figure 56 - Graphical representation of DHX01 H&N sample TPS dose deviations for organs-at-risk D_{mean} between DHX01 original plans and DHX02/DHX03 recalculated.

The parameter D_{max} for the organs-at-risk presents average absolute deviations lower than 1.00%, although above 0.50%, resulting from the occurrence of larger deviations for the organs for which this parameter was evaluated, eyes and lenses, which range from approximately -3.00% to 4.00%. In spite of these high deviations, this observation is not critical, since the doses in these organs present low values (inferior to 10 Gy), increasing the sensibility to small variations. For the organs-at-risk for which the D_{mean} parameter was evaluated, the average absolute deviations obtained were low to all the organs, with values within the ± 1.0% interval.

The total number of monitor units of the treatment plan presents an average absolute deviation of 0.57% between the original plan and the plan after change of treatment unit, demonstrating that the significant variations are not significant. Further analysis of the behavior observed for the patients in the sample was not performed, since the monitor unit number variations after recalculation for a different equipment result from the TPS optimization algorithm that does not define an exact monitor unit number, attributing random values within an interval that does not alter the dose values, since the same algorithm is used for the three linear accelerators. The small dose deviations obtained result from the dosimetric leaf separation (DLS) that is the only parameter that is different for DHX01 and the beam-matched linear accelerators (DHX02 and DHX03). Since a higher DLS value was defined for DHX02 and DHX03 in the TPS than for DHX01, it is expected that higher doses are obtained with DHX02 and DHX03, what is in accordance with the observed results, as the TPS doses were slightly higher after the change from DHX01 to DHX02/03.

Dosimetrical differences between DHX02 original plans and recalculated plans for DHX01

The deviation values calculated for dose and MU values before and after the change of treatment unit in the TPS for DHX02 H&N sample are shown in Figure 57 to 62.

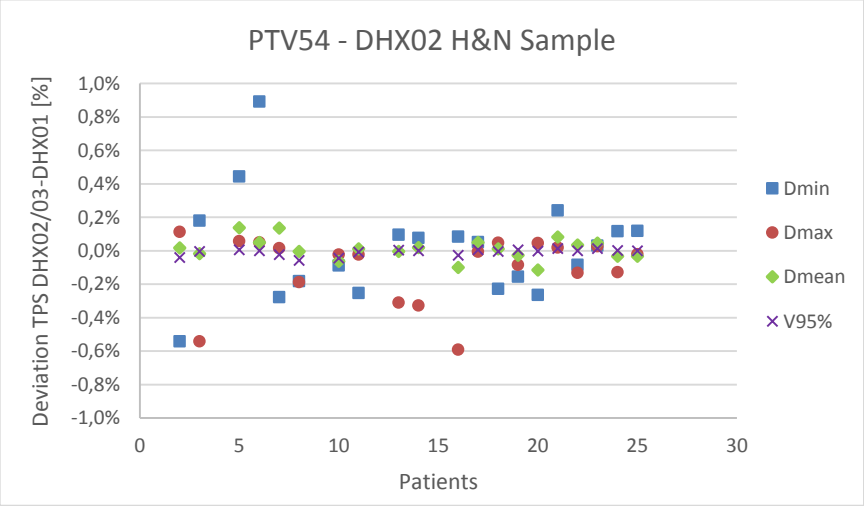

Figure 57 - Graphical representation of DHX02 H&N sample TPS dose deviations for PTV54 between DHX02 original plans and DHX01 recalculated plans.

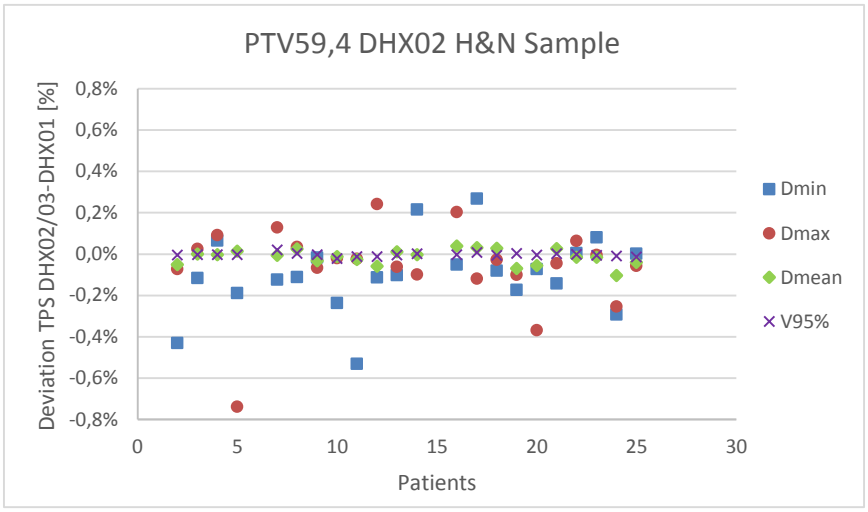

Figure 58 - Graphical representation of DHX02 H&N sample TPS dose deviations for PTV59.4 between DHX02 original plans and DHX01 recalculated plans.

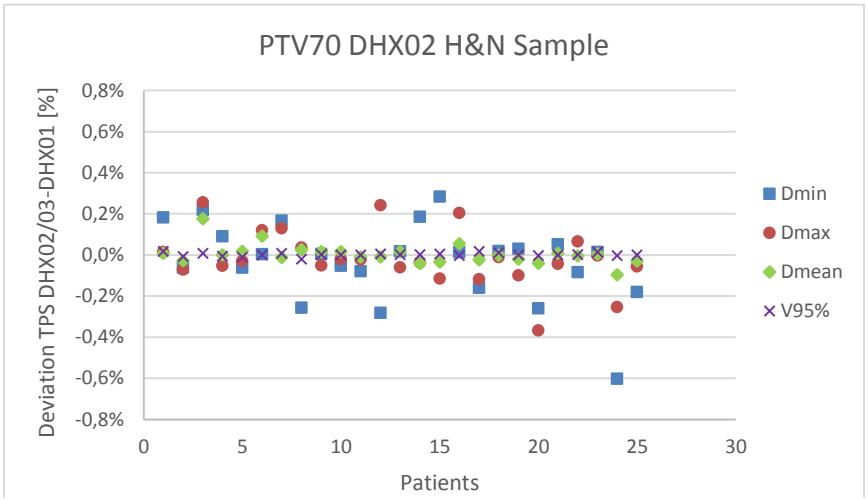

Figure 59 - Graphical representation of DHX02 H&N sample TPS dose deviations for PTV70 between DHX02 original plans and DHX01 recalculated plans.

Focusing first on the doses in PTVs, the average absolute deviations are lower than 0.25% for all the PTV parameters analyzed with deviation values within the interval of ± 1.00% for all DHX02 sample patients and PTV parameters in study. As for DHX01 sample, it was verified that the highest deviations occur to D_{min}, although without relevant variations, and that $V_{95\%}$ presents deviations very close to 0.00%.

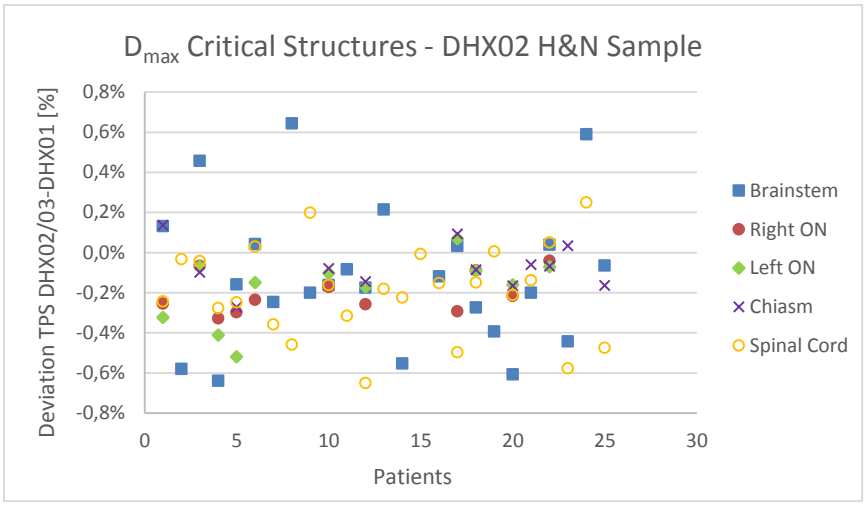

Figure 60 - Graphical representation of DHX02 H&N sample TPS dose deviations for critical structures D_{max} between DHX02 original plans and DHX01 recalculated plans.

For the critical structures in study, the parameter D_{max} is also associated with a low average absolute deviation (lower than 0.30%), with deviation values distributed in the interval ± 0.80%, not indicating significant variation due to the change of treatment unit.

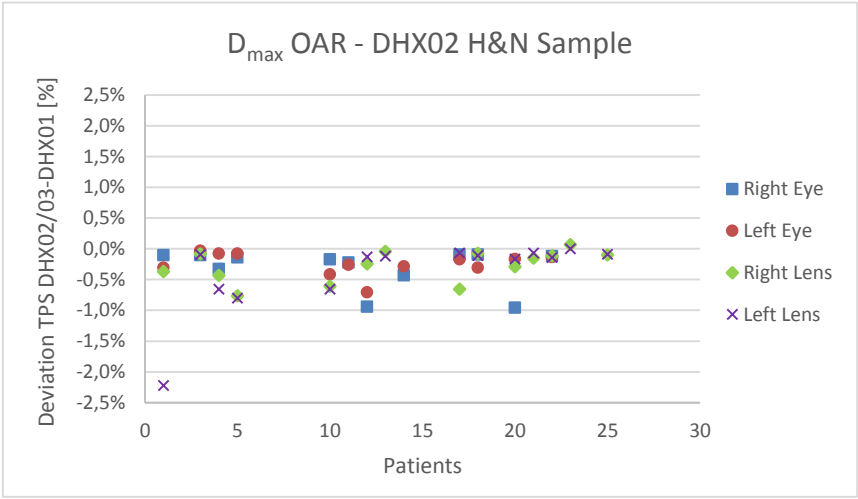

Figure 61 - Graphical representation of DHX02 H&N sample TPS dose deviations for organs-at-risk D_{max} between DHX02 original plans and DHX01 recalculated plans.

In relation to the organs-at-risk, for D_{max} the average absolute deviation values are lower than 0.40%, with deviation values distributed between - 1.00% and 0.10%, excepting for one patient, for which a deviation of - 2.20% was obtained. However, this value does not require alarm, since, as mentioned for DHX01 sample, the organs evaluated with this parameter present low volumes and dose values, increasing the sensibility to small dose variations.

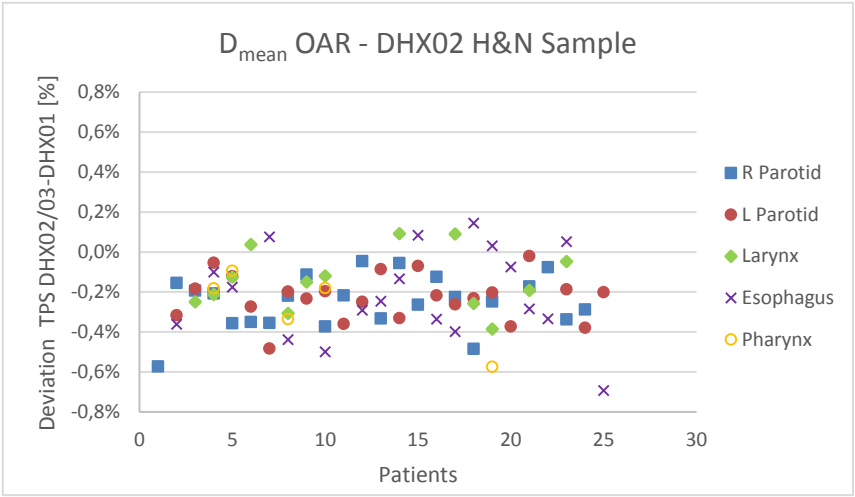

Figure 62 - Graphical representation of DHX02 H&N sample TPS dose deviations for organs-at-risk D_{mean} between DHX02 original plans and DHX01 recalculated plans.

For the organs-at-risk evaluated with D_{mean}, the average absolute deviation values are lower than 0.40% for all the organs evaluated, with deviations ranging from – 0.80% to 0.20%, which represents low variations due to the change of treatment unit.

The comparison of the total monitor unit number before and after the change of treatment unit resulted in an average absolute deviation of 0.51%, which is similar to the value obtained for the DHX01 sample, although, for the same reason, a detailed evaluation was not performed, since the observed variations were due to the same reason. In relation to the deviations obtained for doses, the results are also in accordance with the expected, since higher TPS doses were observed in the original plans for DHX02/03 than after the change to DHX01.

Dosimetrical differences between DHX03 original plans and recalculated plans for DHX01

The deviation values calculated for dose and MU values before and after the change of treatment unit in the TPS for DHX03 H&N sample are shown in Figures 63 to 68.

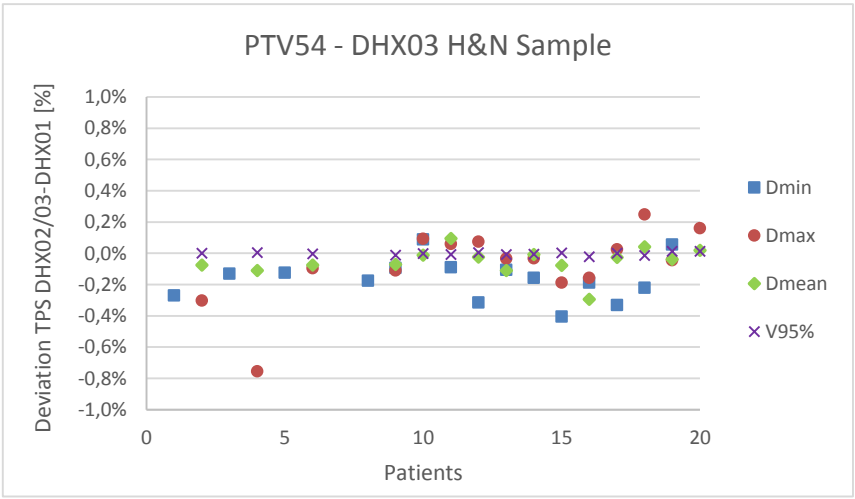

Figure 63 - Graphical representation of DHX03 H&N sample TPS dose deviations for PTV54 between DHX03 original plans and DHX01 recalculated plans.

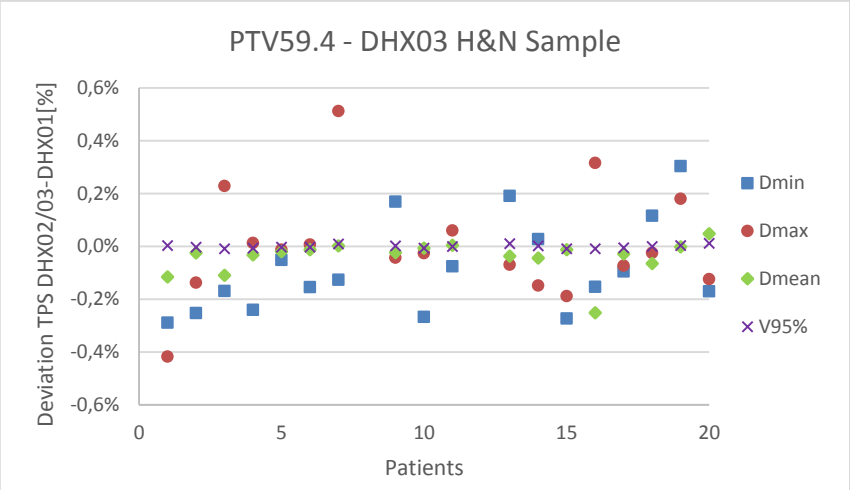

Figure 64 - Graphical representation of DHX03 H&N sample TPS dose deviations for PTV59.4 between DHX03 original plans and DHX01 recalculated plans.

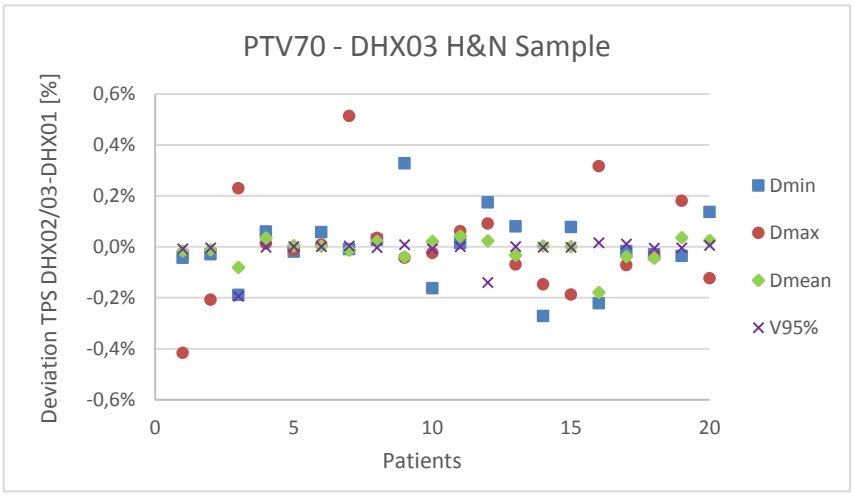

Figure 65 - Graphical representation of DHX03 H&N sample TPS dose deviations for PTV70 between DHX03 original plans and DHX01 recalculated plans.

From the analysis of DHX03 sample results, it was observed that the results does not differ significantly from the obtained for DHX02 sample. In relation to the average absolute deviations, similar values were obtained, not passing 0.20% for all the parameters and PTVs in analysis, although for this sample the deviations are larger for D_{max} than for D_{min}, but also with variations that does not are not relevant for the conclusions of this comparison, since the dose deviations for all the patients do not exceed ± 1.00%.

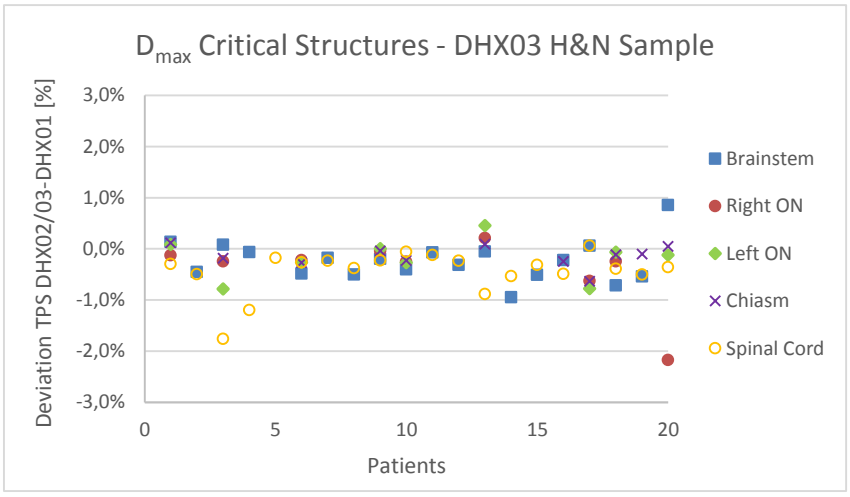

Figure 66 - Graphical representation of DHX03 H&N sample TPS dose deviations for critical structures D_{max} between DHX03 original plans and DHX01 recalculated plans.

In relation to the critical structures, significant deviations are also not present, with average absolute deviations that not exceed 0.50%, resultant from a majority of deviations with reduced values, with exception for three points above 1.00%, resultant from the already mentioned conditions of low volume of the structures and proximity to the target volumes and, for this reasons, are not considered as significant deviations.

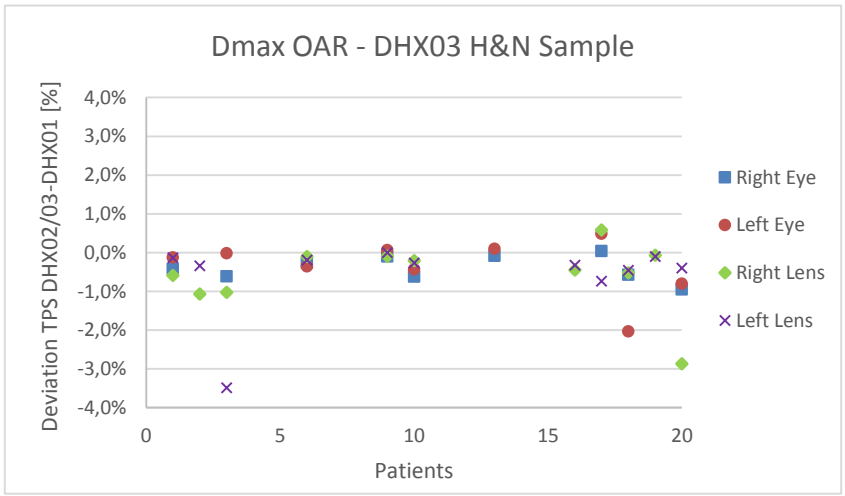

Figure 67 - Graphical representation of DHX03 H&N sample TPS dose deviations for organs-at-risk D_{max} between DHX03 original plans and DHX01 recalculated plans.

An identical situation was verified to organs-at-risk when analyzing the D_{max}, since all the organs evaluated with this parameter have very low volumes and the prescribed doses are also low for the majority of these organs, increasing the probability of large dose variations, which does not compromise the conclusions of this study, since the organs-at-risk tolerances are not exceeded after the change of treatment unit and the prescribed doses to the target volumes are not significantly altered.

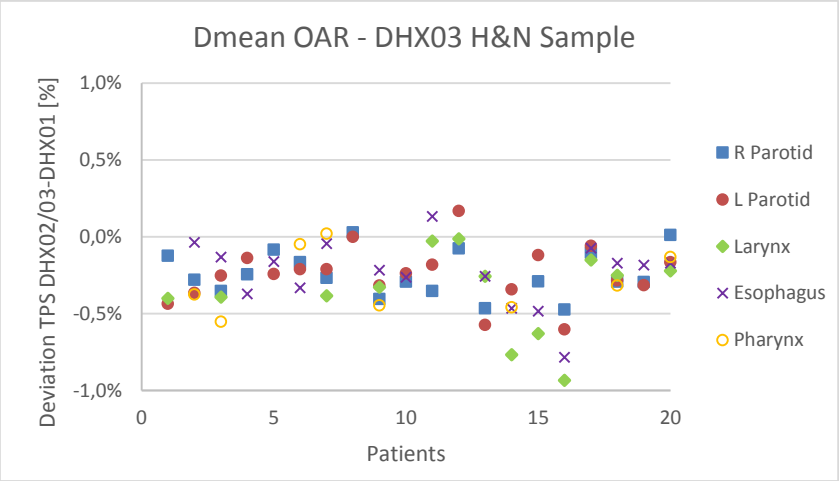

Figure 68 - Graphical representation of DHX03 H&N sample TPS dose deviations for organs-at-risk D_{mean} between DHX03 original plans and DHX01 recalculated plans.

For the organs-at-risk evaluated with D_{mean}, a more stable behavior was observed, with average absolute deviations that do not exceed 0.40%, resultant from deviations ranging from – 1.00% to 0.20%.

The MU average absolute variation obtained is the highest from the three H&N samples, with a value of 0.62%, although this result is not significant, as mentioned for the two previous samples. Analyzing the results referent to dose variations, the behavior is similar to the obtained for DHX02 sample, which is in accordance with a higher DLS value defined in the TPS.

4.2.2. EPID Verifications

For the verification of the Head and Neck IMRT treatments with EPID, a similar approach was used: the treatment plans, which were verified before the treatment using the original linear accelerator, were also verified using the other two linear accelerators. As in the case of the analysis of the dose calculated by the TPS, the results are presented divided by three categories:

- DHX01 Head and Neck sample, in which the original planning and verification were performed for DHX01 linac and posterior verifications were done without replanning using DHX02 and DHX03 linacs, in order to compare the three verifications and determine the differences obtained with the change of linear accelerator;
- DHX02 Head and Neck sample, in which the original planning and verification were performed for DHX02 linac and posterior verifications were done without replanning using DHX01 and DHX03 linacs, in order to compare the three verifications and determine the differences obtained with the change of linear accelerator;
- DHX03 Head and Neck sample, in which the original planning and verification were performed for DHX03 linas and posterior verifications were done without replanning using DHX01 and DHX02 linacs, in order to compare the three verifications and determine the differences obtained with the change of linear accelerators.

DHX01 H&N Sample Results

The results from the verification of DHX01 H&N sample, originally verified using DHX01 linac and posteriorly verified without replanning using DHX02 and DHX03 linacs, can be observed in Figure 69.

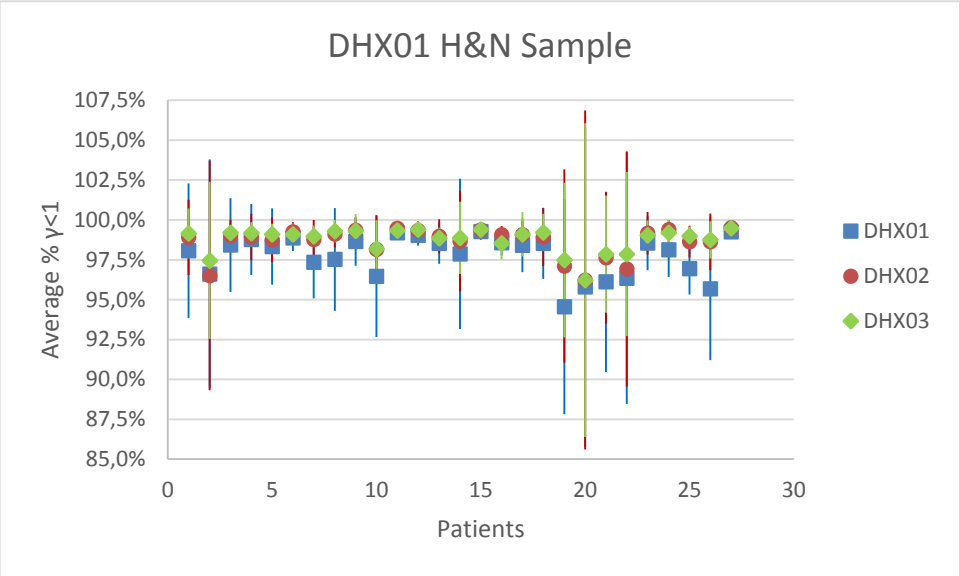

Figure 69 - Average gamma analysis agreement values for patient EPID verifications of DHX01 H&N sample using 3.0%, 3.0 mm criterion.

The minimum, maximum, mean and standard deviation values relative to the DHX01 H&N sample are shown in Table 23.

DHX01 H&N Sample

Equipment	Minimum	Maximum	Mean	Std. Deviation
DHX01	94,56%	99,27%	97,78%	1,27%
DHX02	96,24%	99,51%	98,63%	0,92%
DHX03	96,23%	99,49%	98,76%	0,77%

Table 23- Descriptive statistics for DHX01 H&N Sample EPID verifications.

For the original verification with DHX01 linac, an average agreement of 97.78% using the 3.0 %, 3.0 mm criterion was obtained, with agreement values higher than 90.00% for all the patients in the sample, with only one patient with an agreement value slightly lower than 95.00% (94.56%).

For the verification of this sample with DHX02 linac, an average agreement of 98.63% were obtained for a gamma criterion of 3.0 %, 3.0 mm , with agreement values above 95.00% for all the patients in the sample. This average agreement corresponds to an average absolute deviation in relation to the original verification with DHX01 of 0.87%, with a tendency for slightly higher agreement values than the obtained with DHX01, which is not significant, since the deviation is inferior to 1.00%.

The results obtained with DHX03 linac are similar to the obtained with DHX02, with an average agreement of 98.76% for a gamma criterion of 3.0 %, 3.0 mm, with agreement values above 95.00% for all the patients in the sample. The tendency for slightly higher agreement values than the obtained with DHX01 is maintained, as in the verification with DHX02. However, the difference for DHX03 is also not significant, since the average absolute deviation between this and the original verification is 1.00%.

It is also important to mention that, for some patients, although the average agreement value is in accordance with the recommended tolerance of 95.00%, the correspondent standard deviation is high, which results from low agreement values obtained for some fields that have small size and, consequently, low MU.

Although it is not the main goal of DHX01 sample analysis, it was observed that the results obtained with DHX02 and DHX03 are very similar (with an average absolute deviation of 0.24%), supporting the dosimetric equivalence between the two linear accelerators. However, this equivalence will be evaluated with more precision with the verification of the DHX02 and DHX03 samples with the three machines. As for DHX01, the agreement values obtained were slightly lower than for the other two linear accelerators, as mentioned above and, in spite of being a non-significant difference, it is important to understand the origin of this results, since they were obtained with a TPS plan created for DHX01 and it was expected that the best results were obtained with this equipment. However, from the trimestral quality assurance results, a discrepancy between the MLC transmission defined in the TPS and the experimental MLC transmission measures was verified. This results in a predicted dose higher than the dose that will be achieved experimentally, for all linear accelerators, since the TPS MLC transmission value is the same. However, since higher DLS values were measured for DHX02 and DHX03, higher experimental doses are obtained for these two linear accelerators, resulting in higher agreements in relation to the TPS predicted doses.

Although without a critical role for the evaluation of these sample, since the deviations obtained were very low, the behavior of the three linear accelerators was analyzed for this sample with the determination of correlation coefficients, considering as variables each of the EPID verifications for DHX01 sample. The results can be observed in Table 24.

		DHX01	**DHX02**	**DHX03**
DHX01	Pearson Correlation	1	0,816**	0,787**
	Sig. (2-tailed)	----	0,000	0,000
DHX02	Pearson Correlation	0,816**	1	0,949**
	Sig. (2-tailed)	0,000	----	0,000
DHX03	Pearson Correlation	0,787**	0,949**	1
	Sig. (2-tailed)	0,000	0,000	----

**. Correlation is significant at the 0.01 level (2-tailed).

Table 24 – Correlation coefficients for DHX01 H&N sample EPID verifications.

Although without a critical role for the evaluation of these sample, since the deviations obtained were very low, the behavior of the three linear accelerators was analyzed for this sample with the determination of correlation coefficients, considering as variables each of the EPID verifications for DHX01 sample. Positive strong correlations were obtained between the three variables for a significance level of 0.01, with a higher coefficient, 0.949, between DHX02 and DHX03 verifications, as expected, since this two linear accelerators are beam-matched. For the comparisons DHX01/DHX02 and DHX01/DHX03 slightly lower correlation coefficients were obtained, although with values above 0.75, indicating that the verifications show similar behaviors.

These results are in accordance with the observations made for the gamma analysis results, supporting that, for this sample, DHX02 and DHX03 behaviors are very similar and, on the other hand, DHX01 show a slight deviation in relation to the other two linear accelerators, which is not significant, since relatively strong correlations were obtained and gamma analysis results are in accordance with the acceptance agreement value tolerance of 90.00%, presenting average absolute deviations not above 1.00% in relation DHX02 and DHX03.

DHX02 H&N sample results

The results from the verification of DHX02 H&N sample, originally verified using DHX02 linac and posteriorly verified using DHX01 and DHX03 linacs can be observed in Figure 70.

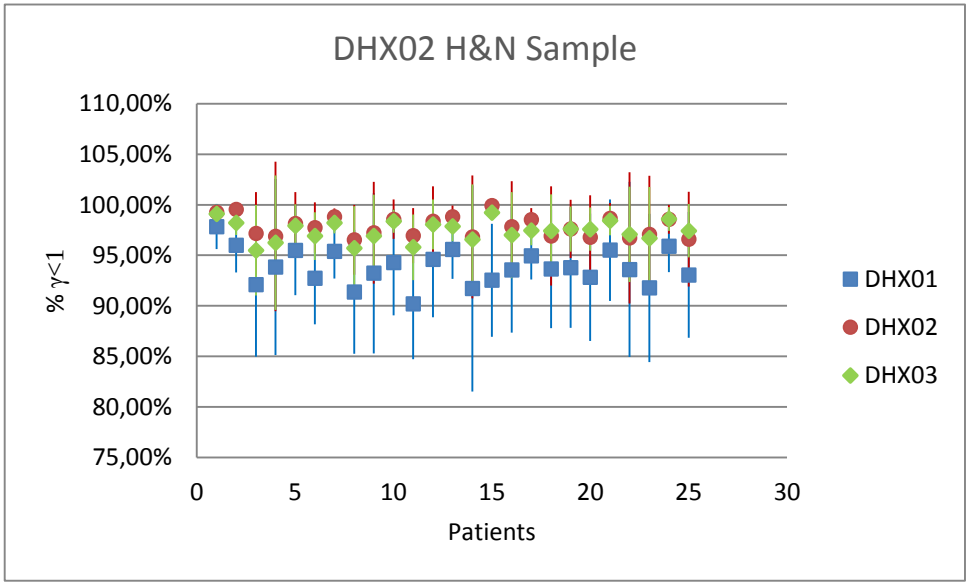

Figure 70 - Average gamma analysis agreement values for patient EPID verifications of DHX02 H&N sample, using 3.0 %, 3.0 mm criterion.

The minimum, maximum, mean and standard deviation values relative to the DHX02 H&N sample are shown in Table 25.

DHX02 H&N Sample

Equipment	Minimum	Maximum	Mean	Std. Deviation
DHX01	90,19%	97,85%	93,82%	1,76%
DHX02	96,53%	99,93%	97,85%	1,01%
DHX03	95,50%	99,23%	97,44%	1,01%

Table 25 – Descriptive statistics for DHX02 H&N sample EPID verifications.

For the original verification with DHX02, an average gamma analysis agreement value of 97.85% was obtained from the comparison with the TPS PDIP, with a minimum of 96.53%, which is in accordance with the target tolerance of 95.00%.

When the same sample is verified using DHX03, similar results were obtained, supporting the dosimetric equivalence between the two linear accelerators. This verification resulted in an average gamma analysis agreement value of 97.44%, representing a non-significant average absolute deviation of 0.63% in relation to the original verification with DHX02, with a minimum of 95.50%, which is also is accordance with the recommended tolerance of 95.00%.

However, when DHX02 H&N sample is verified with DHX01, a lower average gamma analysis agreement value of 93.82% was obtained, with a minimum agreement value of 90.19%. Although this result is not critical, since the agreement values obtained are above the established acceptance value of 90.00%, an average absolute deviation of 4.31% was obtained in this change. This deviation is not sufficiently large to definitely compromise the indistinct use of DHX01 when equipment changes are required, but suggests that caution is required in these change when recalculations are not performed.

As for DHX01 sample, large error bars were obtained for some of the patients due to the presence of lower gamma analysis agreement values for some fields with low dimensions and, consequently, low MU number.

Although it was expected, for this sample, that lower agreement values were obtained for the verification with DHX01, since it is not beam-matched with DHX02 and DHX03, the deviations observed can also be justified, as for DHX01 sample, with MLC transmission and DLS values. However, for this sample, the deviations obtained when performing the verification with DHX01 are higher than for the previous sample due to the definition of a higher DLS value in the TPS for DHX02 and DHX03, which results in a higher TPS predicted dose than for DHX01, in addition to the consequence of the higher TPS MLC transmission. Experimentally, the doses are lower, in the three verifications, than the predicted dose, due to the lower real MLC transmission values. However, as DLS measured values are similar to the implemented in the TPS, the experimental doses obtained with DHX02 and DHX03 are higher, becoming more concordant with the TPS prediction, while DHX01 experimental doses present higher deviations from the predicted.

Correlation coefficients were also determined for DHX02 H&N sample EPID verifications. The results are shown in Table 26 and demonstrate a positive correlation between the EPID verifications performed with the three linear accelerators in study for a significance level of 0.01.

		DHX01	DHX02	DHX03
DHX01	Pearson Correlation	1	0,682**	0,746**
	Sig. (2-tailed)	----	0,000	0,000
DHX02	Pearson Correlation	0,682**	1	0,806**
	Sig. (2-tailed)	0,000	----	0,000
DHX03	Pearson Correlation	0,746**	0,806**	1
	Sig. (2-tailed)	0,000	0,000	----

**. Correlation is significant at the 0.01 level (2-tailed).

Table 26 – Correlation coefficients for DHX02 H&N sample EPID verifications.

A correlation coefficient of 0.806 was obtained between the verifications with DHX02 and DHX03, which indicates a highly correlated behavior between both verifications. This observation, in addition to the good agreements obtained with the gamma analysis, suggests a high similarity, for this sample, between both linear accelerators. Between the verifications performed with DHX02 and DHX01, a correlation coefficient of 0.682 was obtained, indicating a relatively strong correlation between the behaviors of the two verifications, in spite of the agreement deviations observed.

Although the main goal of the verifications performed with this sample was not to compare DHX01 with DHX03, it was observed, with EPID verification gamma analysis and also with the obtained correlation coefficient of 0.746, that this equipment, although more similar to DHX02, presents an intermediate behavior in relation to the other two linear accelerators, since the largest deviations obtained in the intercomparisons were obtained between DHX01 and DHX02.

DHX03 H&N sample results

The results from the verification of DHX03 H&N sample, originally verified with DHX03 and posteriorly verified without replanning using DHX01 and DHX02 can be observed in Figure 71.

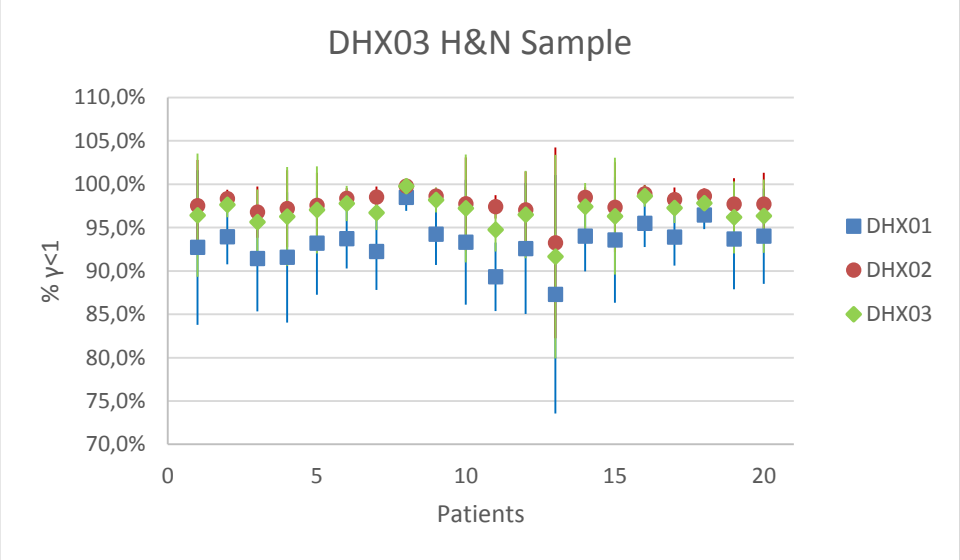

Figure 71 - Average gamma analysis agreement values for patient EPID verifications of DHX03 H&N Sample, using 3.0 %, 3.0 mm criterion.

The minimum, maximum, mean and standard deviation values relative to the DHX03 H&N sample are shown in Table 27.

DHX03 H&N Sample

Equipment	Minimum	Maximum	Mean	Std. Deviation
DHX01	87,31%	98,47%	93,26%	2,35%
DHX02	93,23%	99,79%	97,75%	1,29%
DHX03	91,65%	99,79%	96,78%	1,64%

Table 27 - Descriptive statistics for DHX03 H&N sample EPID verifications.

From the gamma analysis performed for the original EPID verification with DHX03, an average gamma agreement of 96.78% was obtained, with minimum and maximum values of 91.65% and 99.79%, respectively. This values are in accordance with the acceptance criterion of a 90.00% agreement value, but below the recommended tolerance of 95.00% for two patients (with agreement values of 91.65% and 94.76%).

The verification of this sample using DHX02 resulted in an average gamma agreement value of 97.75%, with minimum and maximum values of 93.23% and 99.79%, respectively. These values are similar to the obtained from the original verification with DHX03, with an average deviation of 1.00%. A single value, 93.23%, below the recommended agreement was observed, which is, however, above the acceptance criterion of 90.00%.

As for DHX02 H&N sample, larger deviations were obtained in the gamma analysis performed for the verification with DHX01, as an average gamma agreement value of 93.26% was obtained, with minimum and maximum values of 87.31% and 98.47%, respectively and an average deviation of 3.80% in relation to the original verification with DHX02. Average gamma agreements below the acceptance tolerance of 90.00% were obtained for two patients, with agreement values of 87.31% and 89.31%, which are not significantly lower than the established tolerance, but set reservations about the possibility of using DHX01 as dosimetrically equivalent to the beam-matched DHX02 and DHX03.

As observed for the previous samples, large error bars were obtained for some patients in the sample due to the presence of small fields that are more susceptible to dose variations.

In relation to the gamma comparisons between the three verifications, the results were similar than the obtained for DHX02 sample, supporting the dosimetric equivalence between DHX01 and with larger deviations, although not significant, for the verification performed with DHX01, which can be justified, in a similar way than for DHX02 sample, by MLC transmission and DLS TPS and experimental values.

Correlation coefficients were also determined for DHX03 H&N sample. The results are shown in Table 28.

		DHX01	DHX02	DHX03
DHX01	Pearson Correlation	1	0,851**	0,922**
	Sig. (2-tailed)	----	,000	,000
DHX02	Pearson Correlation	0,851**	1	0,942**
	Sig. (2-tailed)	,000	----	,000
DHX03	Pearson Correlation	0,922**	0,942**	1
	Sig. (2-tailed)	,000	,000	----

**. Correlation is significant at the 0.01 level (2-tailed).

Table 28 - Descriptive statistics for DHX03 H&N sample EPID verifications.

From the calculated correlation coefficients, it was observed that the three samples present similar behaviors, since high correlations were obtained, for a significance level of 0.01, for the three comparisons performed.

Between DHX03 and DHX02 a correlation of 0.942 was obtained, in accordance with the beam-matching between the two linear accelerators, from which similar behaviors are expected. For this sample, a high correlation was obtained between DHX03 and DHX01, with a value of 0.922, in spite of the relatively large deviations.

As further analysis, the correlation coefficient between DHX01 and DHX02 verifications for this sample was also determined, with a value of 0.851 that represents a high correlation between both verifications.

From the results above, it can be concluded that the three EPID verifications performed for this sample present very similar behavior patterns, in spite of the deviations obtained for DHX01.

4.3. Prostate IMRT Treatments

4.3.1. Change of Treatment Machine in Eclipse™ TPS: Dose evaluation

The analysis of the calculated dose and MU with change of treatment machine in the TPS performed for prostate IMRT treatments was similar to the described for the Head and Neck IMRT treatments. The results are also presented divided by three categories:

- DHX01 prostate sample, in which the original planning was performed for DHX01 linac and was followed by a change of treatment machine in the TPS and dose and MU recalculation for DHX02/03;
- DHX02 prostate sample, in which the original planning was performed for DHX02 linac and was followed by a change of treatment machine in the TPS and dose and MU recalculation for DHX01; and
- DHX03 prostate sample, in which the original planning was performed for DHX03 linac and the following procedure was similar to the described for DHX02 sample.

The average deviations obtained for the three prostate samples TPS dose analysis are summarized in Table 29.

PTV45-50			
	DHX01 Sample	DHX02 Sample	DHX03 Sample
D_{min}	0.156%	0.103%	0.152%
D_{max}	0.109%	0.046%	0.044%
D_{mean}	0.019%	0.012%	0.023%
$V_{95\%}$	0.000%	0.000%	0.001%

PTV74-78			
	DHX01 Sample	DHX02 Sample	DHX03 Sample
D_{min}	0.088%	0.121%	0.070%
D_{max}	0.108%	0.052%	0.044%
D_{mean}	0.019%	0.017%	0.020%
$V_{95\%}$	0.002%	0.005%	0.005%

OAR			
	DHX01 Sample	DHX02 Sample	DHX03 Sample
Bladder D30%	0.023%	0.110%	0.055%
Bladder D50%	0.039%	0.125%	0.082%
Rectum D20%	0.020%	0.041%	0.030%
Rectum D50%	0.030%	0.114%	0.062%

OAR			
	DHX01 Sample	DHX02 Sample	DHX03 Sample
RFemHead $D_{5\%}$	0.066%	0.067%	0.061%
LFemHead $D_{5\%}$	0.029%	0.072%	0.061%
BulbPen D_{mean}	0.086%	0.096%	0.078%

MU			
	DHX01 Sample	DHX02 Sample	DHX03 Sample
MU	0.794%	0.689%	0.506%

Table 29 - Average absolute TPS dose deviations for prostate samples TPS change of treatment unit

Low average absolute dose deviations were obtained (inferior to 0.20% for PTV parameters and to 0.15% for organs-at-risk parameters), indicating that the dose values remain almost unaltered after the treatment unit change in the TPS.

In relation to MU values, the absolute average deviations obtained were slightly higher for the same reason mentioned for the H&N samples. In spite of being higher, the deviations did not exceed 1.00% and do not lead to significant dose variations, since the error associated with monitor unit calculation by the optimization algorithm is small, in order to guarantee that large deviations would not occur in treatment delivery when recalculations in the TPS are performed.

Dosimetrical differences between DHX01 original plans and recalculated plans for DHX02/DHX03

The deviation values calculated for dose and MU values before and after the change of treatment unit to DHX02/03 in the TPS for DHX01 prostate sample are shown in Figures 72 to 75.

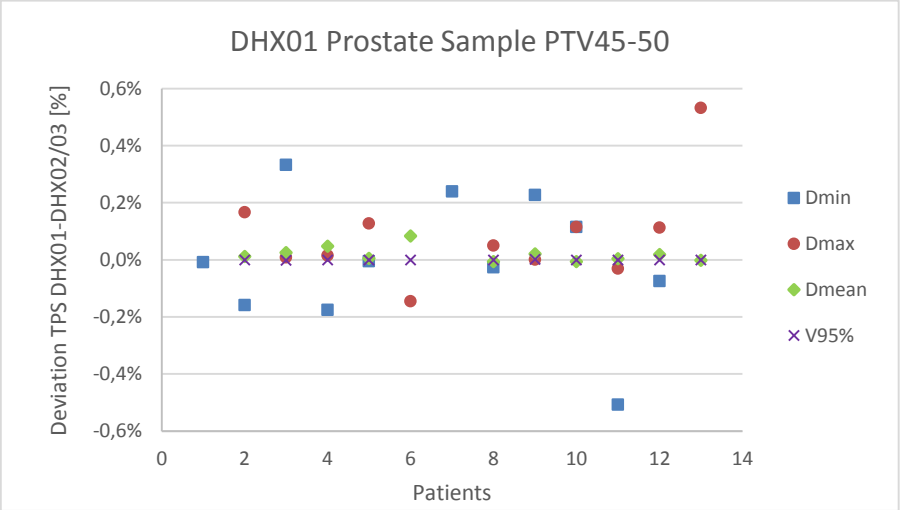

Figure 72- Graphical representation of DHX01 prostate sample TPS dose deviations for PTVs 45-50 between DHX01 original plans and DHX02/03 recalculated plans.

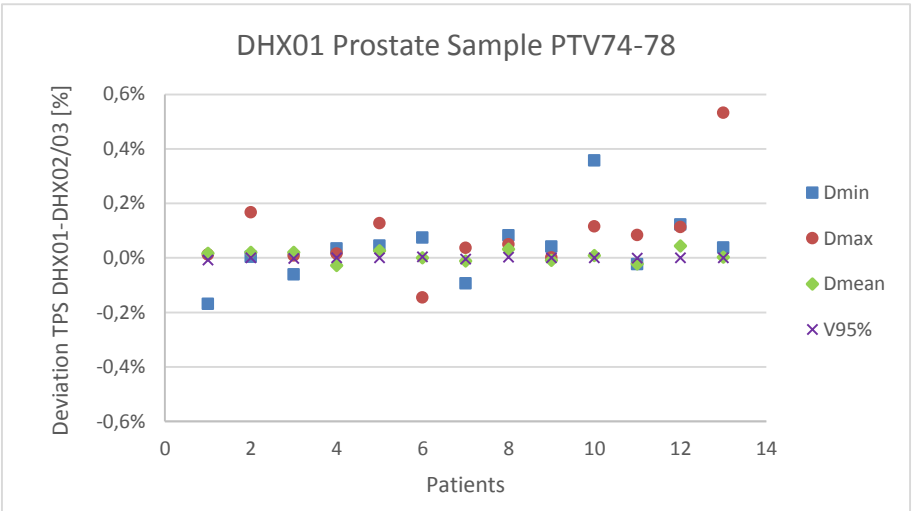

Figure 73 - Graphical representation of DHX01 prostate sample TPS dose deviations for PTVs 74-78 between DHX01 original plans and DHX02/03 recalculated plans.

For DHX01 prostate sample, PTV parameters in study presented dose deviations within ± 0.60% for all the patients, indicating a good agreement between the treatment units in the TPS. The main parameter used for the evaluation of dose in PTV, $V_{95\%}$, is approximately equal before and after the change of equipment in the TPS for all the patients in the sample, indicating that major differences are not obtained with the change.

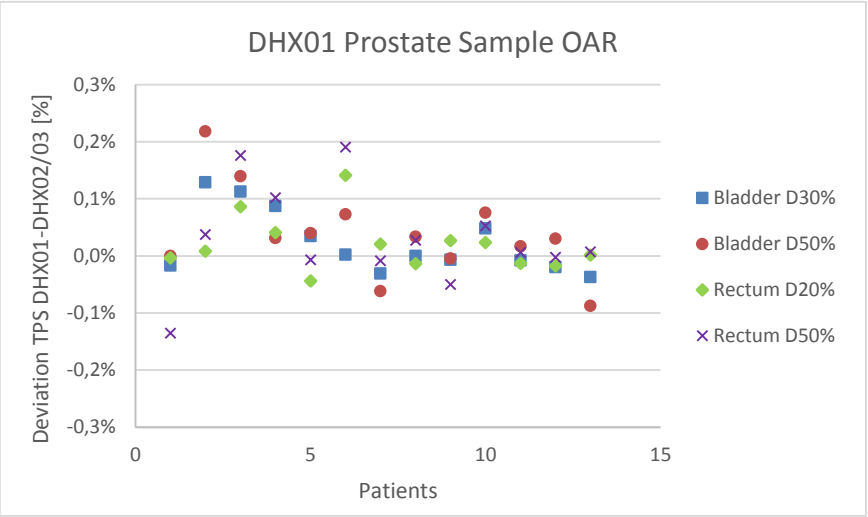

Figure 74 - Graphical representation of DHX01 prostate sample TPS dose deviations for organs-at-risk (bladder and rectum) between DHX01 original plans and DHX02/03 recalculated plans.

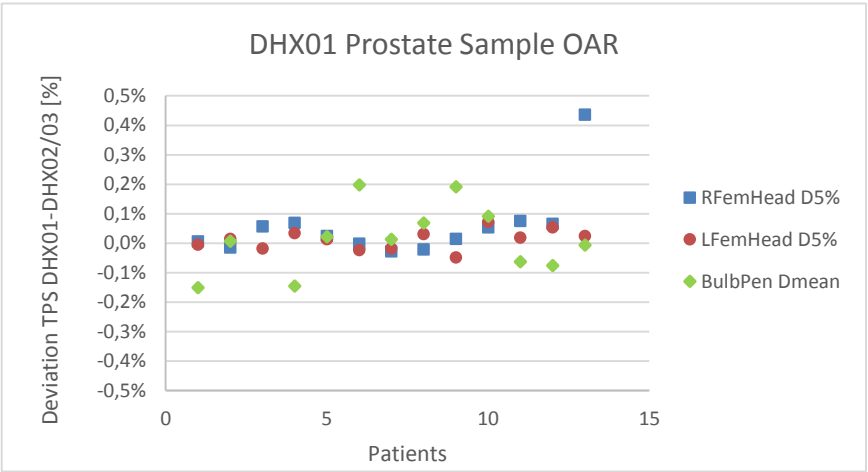

Figure 75 - Graphical representation of DHX01 prostate sample TPS dose deviations for organs-at-risk (femur heads and bulb of penis) between DHX01 original plans and DHX02/03 recalculated plans.

In relation to organs-at-risk, the differences observed after the change of treatment unit are also low, with values that vary between - 0.20% and 0.50%.

The overall variation behavior of this sample is very similar to the observed for DHX01 H&N sample, with a slight increase of dose values after the change from DHX01 to DHX02/03 in the TPS which, although clearly not significant, occurred for the majority of the patients in the sample and is coincident with the definition of a higher dosimetric leaf separation in the TPS for DHX02 and DHX03.

Dosimetrical differences between DHX02 original plans and recalculated plans for DHX01

The deviation values calculated for dose and MU values before and after the change of treatment unit to DHX01 in the TPS for DHX02 prostate sample are shown in Figures 76 to 79.

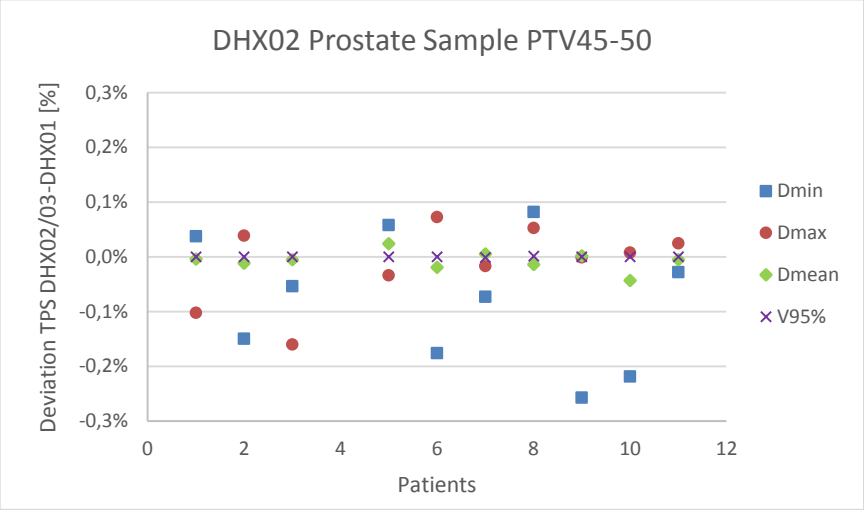

Figure 76 - Graphical representation of DHX02 prostate sample TPS dose deviations for PTVs 45-50 between DHX02 original plans and DHX01 recalculated plans.

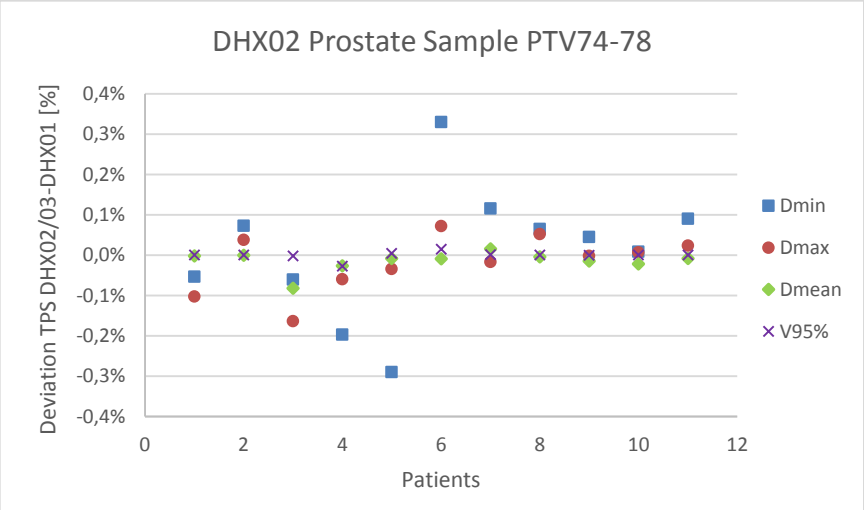

Figure 77 - Graphical representation of DHX02 prostate sample TPS dose deviations for PTVs 45-50 between DHX02 original plans and DHX01 recalculated plans.

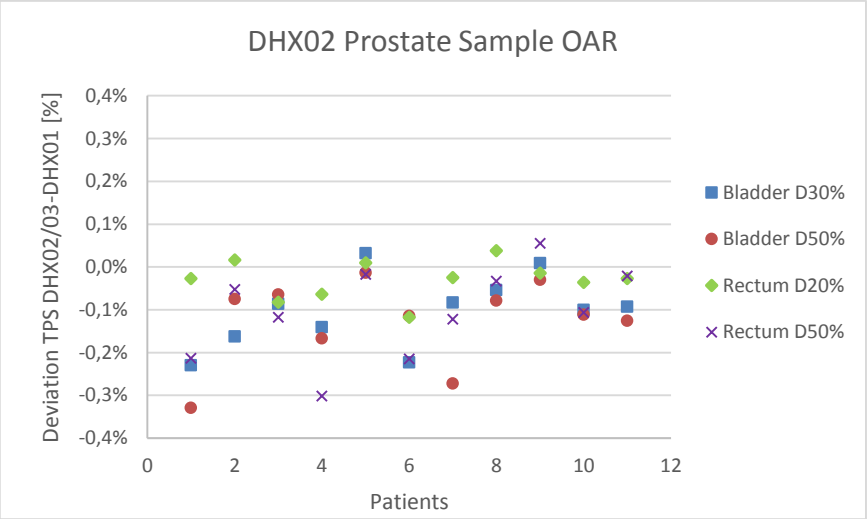

Figure 78 - Graphical representation of DHX02 prostate sample TPS dose deviations for organs-at-risk (bladder and rectum) between DHX02 original plans and DHX01 recalculated plans.

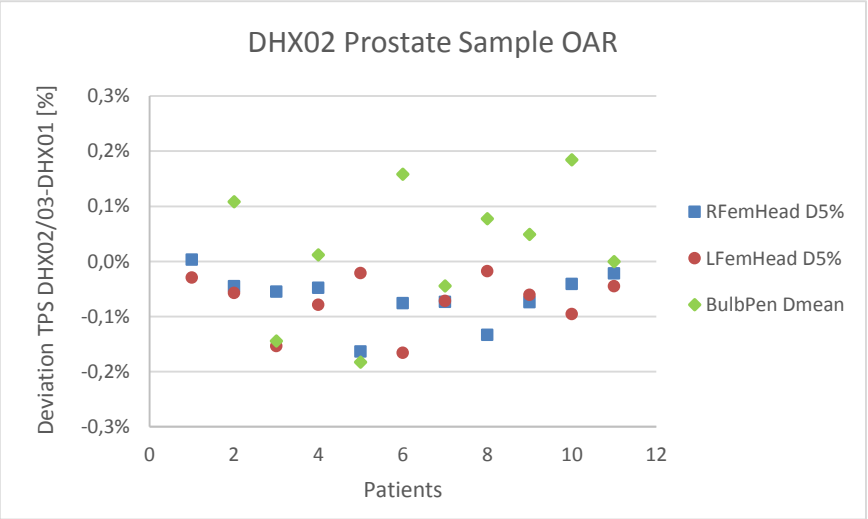

Figure 79 - Graphical representation of DHX02 prostate sample TPS dose deviations for organs-at-risk (femur heads and bulb of penis) between DHX02 original plans and DHX01 recalculated plans.

For DHX02 prostate sample, dose deviations within ± 0.40% were obtained for all the parameters analyzed, representing a high similarity between the TPS calculations for both the linear accelerators, without significant deviations due to the change of treatment unit.

In spite of the low deviations, a pattern of higher calculated doses for DHX02 and DHX03 were also obtained for this sample, which is, as mentioned for the previous sample, in accordance with the higher value of dosimetric leaf separation defined in the TPS for these two linear accelerators.

Dosimetrical differences between DHX03 original plans and recalculated plans for DHX01

The deviation values calculated for dose and MU values before and after the change of treatment unit in the TPS for DHX01 prostate sample are shown in Figure 59.

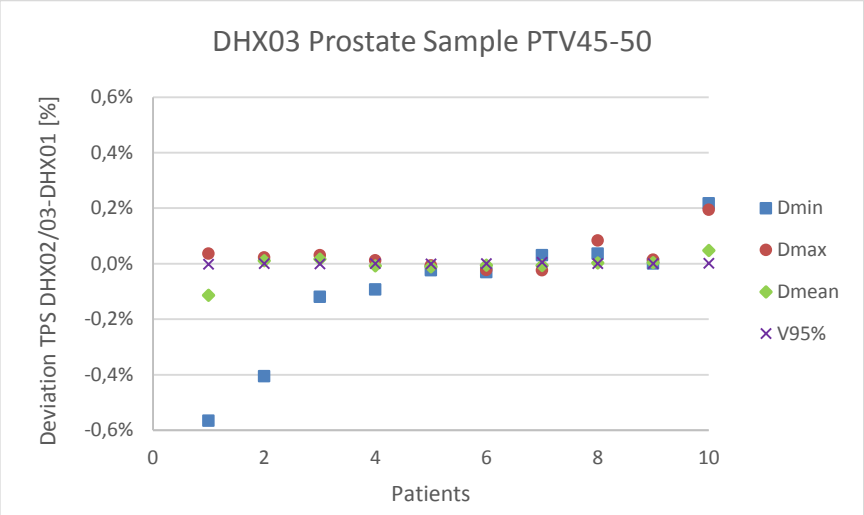

Figure 80 - Graphical representation of DHX03 prostate sample TPS dose deviations for PTVs 45-50 between DHX03 original plans and DHX01 recalculated plans.

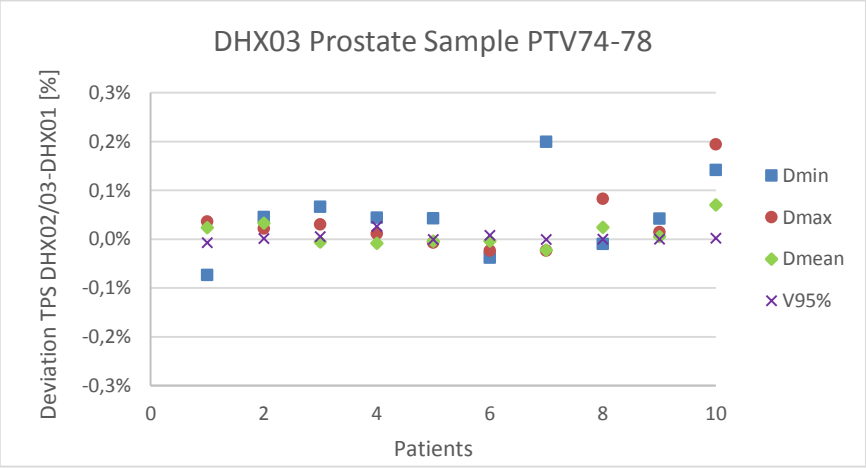

Figure 81 - Graphical representation of DHX03 prostate sample TPS dose deviations for PTVs 74-78 between DHX03 original plans and DHX01 recalculated plans.

In relation to the DHX03 prostate sample PTVs, dose deviation values between -0.2% and 0.2% were obtained for all the parameters in analysis, with exception to PTV D_{min}, which, as verified in the previous samples, is the PTV parameter with greater variations, presenting for this sample deviations ranging from – 0.60% to 0.30%.

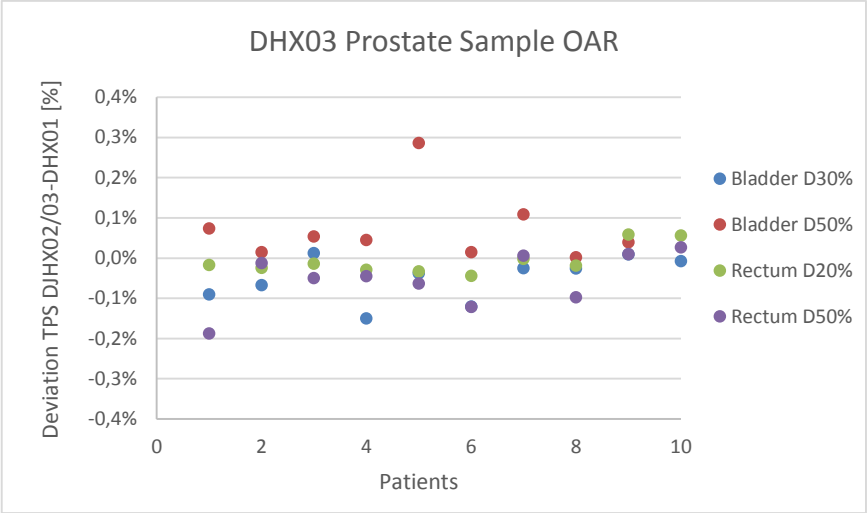

Figure 82 - Graphical representation of DHX03 prostate sample TPS dose deviations for organs-at-risk (bladder and rectum) between DHX03 original plans and DHX01 recalculated plans.

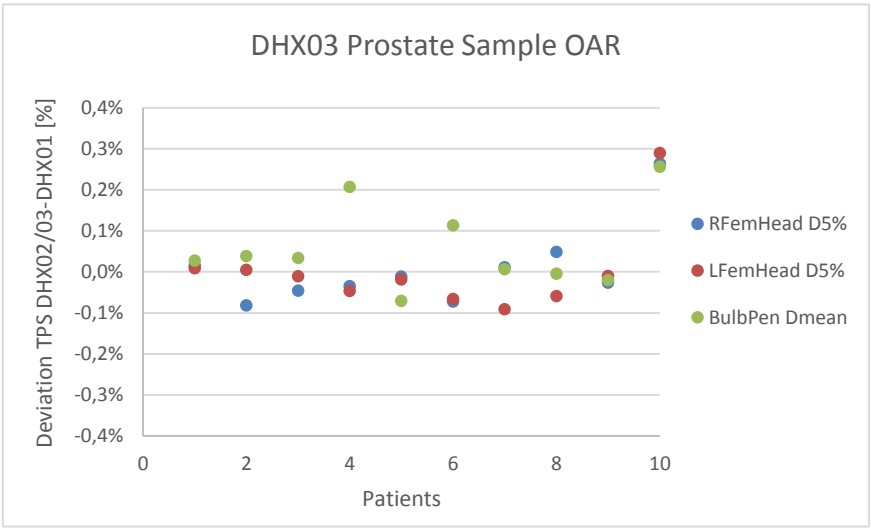

Figure 83 - Graphical representation of DHX03 prostate sample TPS dose deviations for organs-at-risk (femur heads and bulb of penis) between DHX03 original plans and DHX01 recalculated plans.

For the organs-at-risk, dose deviation values between – 0.20% and 0.30% were obtained, indicating that significant deviations does not occur for this sample with the change of equipment in the TPS.

4.3.2. EPID Verifications

For the verification of the prostate IMRT treatments with EPID, a similar approach was used: the treatment plans, which were verified before the treatment using the original linear accelerator, were also verified using the other two linear accelerators. As in the case of the analysis of the dose calculated by the TPS, the results are presented divided by three categories:

- DHX01 prostate sample, in which the original planning and verification were performed for DHX01 linac and posterior verifications were done without replanning

using DHX02 and DHX03 linacs, in order to compare the three verifications and determine the differences obtained with the change of linear accelerator;

- DHX02 prostate sample, in which the original planning and verification were performed for DHX02 linac and posterior verifications were done without replanning using DHX01 and DHX03 linacs, in order to compare the three verifications and determine the differences obtained with the change of linear accelerator;
- DHX03 prostate sample, in which the original planning and verification were performed for DHX03 linas and posterior verifications were done without replanning using DHX01 and DHX02 linacs, in order to compare the three verifications and determine the differences obtained with the change of linear accelerators.

DHX01 prostate sample results

The results from the verification of DHX01 prostate sample, originally verified using DHX01 linac and posteriorly verified using DHX01 and DHX03 can be observed in Figure 83.

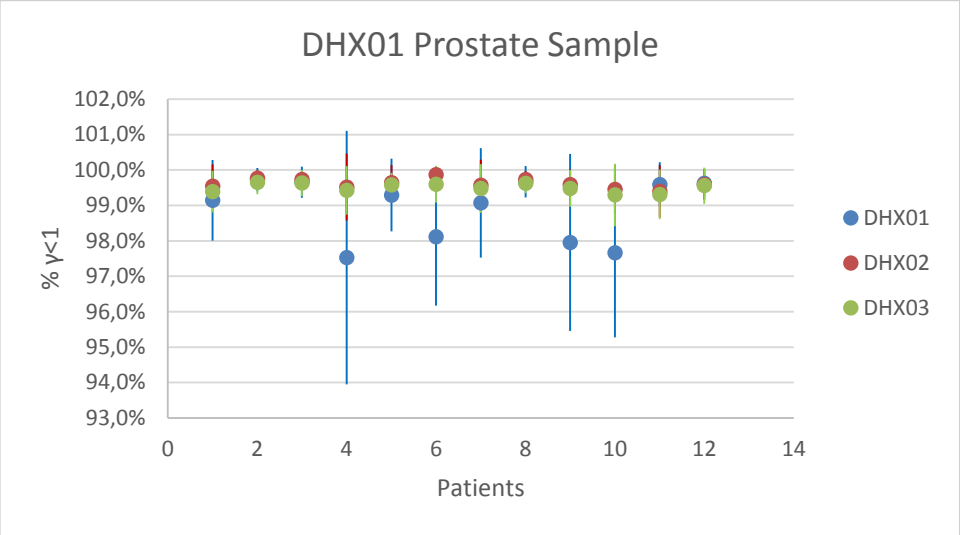

Figure 84 – Average gamma analysis agreement values for patient EPID verifications of DHX01 prostate sample, using 3.0 %, 3.0 mm criterion.

The minimum, maximum, mean and standard deviation values relative to the DHX01 prostate sample are shown in Table 30.

DHX01 prostate Sample

Equipment	Minimum	Maximum	Mean	Std. Deviation
DHX01	97,53%	99,73%	98,92%	0,86%
DHX02	99,40%	99,87%	99,62%	0,14%
DHX03	99,30%	99,65%	99,50%	0,12%

Table 30 – Descriptive statistics for DHX01 prostate sample EPID verifications.

For this sample, the average gamma agreement values obtained from each of the verifications performed are similar, without major deviations.

From the original verification with DHX01 linac, an average gamma agreement of 98.92% was obtained, with minimum and maximum values of 97.53% and 99.73%, respectively, indicating that the agreement values were in accordance with the recommended tolerance of 95.00 for all the patients of the sample.

When this sample was verified using DHX02 linac, an average gamma agreement of 99.62% was obtained, with minimum and maximum values of 99.40% and 99.87%, respectively, denoting a slight agreement improvement in relation to the TPS prediction, close to the optimal agreement of 100.00%. The results obtained using DHX03 linacwere very similar to the obtained with DHX02, with an average gamma agreement of 99.50% and minimum and maximum agreement values of 99.30% and 99.65%, respectively.

From the results above it can be observed that the agreement values obtained from the gamma analysis of the verifications performed with the three linear accelerators are above 95.00% for all the patients in the sample, which in accordance with the established tolerance. The deviations between the verifications performed with different linear accelerators are low, with an average absolute value of 0.75% for DHX02 and 0.59% for DHX03, in relation to the original verification performed with DHX01. Although higher deviations were obtained for some patients, their values did not exceed 2.00%, which do not represent significant variations. For these reason, the analysis performed for this sample suggests that, for prostate samples, significant variations are not observed with the experimental change of equipment.

The results also support the similarity between DHX02 and DHX03, since the average absolute deviation between gamma agreement values was 0.11% between the two linear accelerators, which is a very low variation.

However, it was observed, as for H&N samples, that the agreement values obtained with the original verification with DHX01 were, in general, slightly lower than the obtained with the other two verifications. This observation also results from the discrepancy between TPS and experimental MLC transmission values and the lower DLS values measured for DHX01 and is not highly relevant for this sample, since the deviations obtained were clearly not significant.

Correlation coefficients were also determined for DHX01 prostate sample. The results are shown in Table 31.

		DHX01	**DHX02**	**DHX03**
DHX01	Pearson Correlation	1	0,212	0,445
	Sig. (2-tailed)	----	0,508	0,147
DHX02	Pearson Correlation	0,212	1	0,899**
	Sig. (2-tailed)	0,508	----	0,000
DHX03	Pearson Correlation	0,445	0,899**	1
	Sig. (2-tailed)	0,147	0,000	----

**. Correlation is significant at the 0.01 level (2-tailed).

Table 31 – Correlation coefficients for DHX01 prostate sample EPID verifications.

The correlation coefficients were also determined for this sample and confirm, for this sample, the dosimetric equivalence between DHX02 and DHX03 linacs, since, besides the high concordance in the gamma agreement values, a strong correlation, with a value of 0.899, was obtained, for a significance level of 0.01, indicating a very similar behavior between DHX02 and DHX03 verifications.

In relation to the original verification with DHX01 linac, the results indicate that no correlation is present with the verifications performed with the other two linear accelerators. This observation, as mentioned before, does not compromise the indistinct use of the three machines, since low deviations were obtained with the experimental change of equipment without replanning, but it suggests that the behavior of DHX01 is not exactly equivalent when compared with the behaviors of the other two linear accelerators, as expected, since it is not beam-matched.

It is important to take into account that the determination of correlation coefficients has the single purpose of supporting the gamma analysis results and not an absolute value of comparison between the different verification, since the sample is small and, consequently, susceptible to uncertainties.

DHX02 prostate sample results

The results from the verification of DHX02 prostate sample, originally verified using DHX02 linac and posteriorly verified using DHX01 and DHX03 linacs, can be observed in Figure 84.

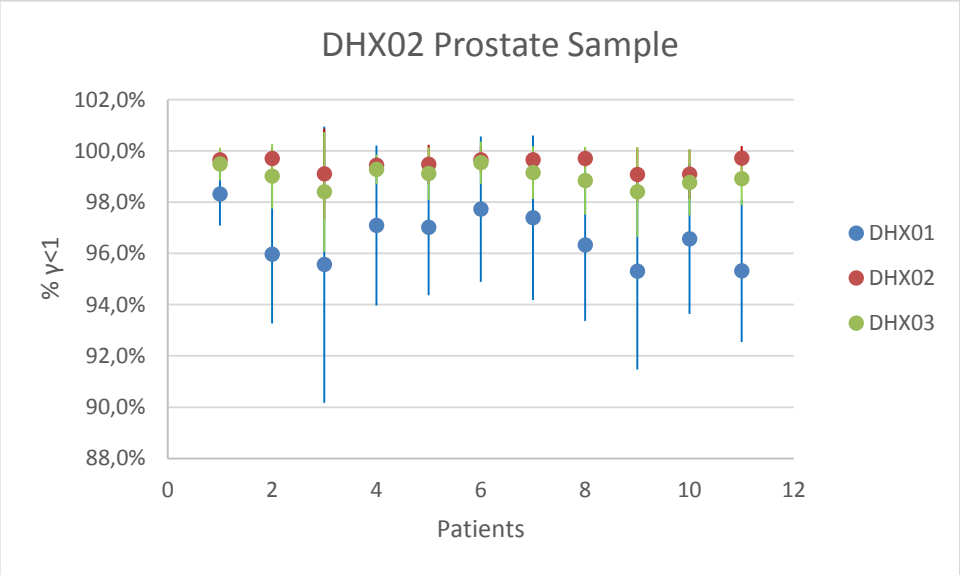

Figure 85 – Average gamma analysis agreement values for patient EPID verification of DHX02 prostate sample, using 3.0 %, 3.0 mm criterion.

The minimum, maximum, mean and standard deviation values relative to the DHX02 prostate sample are shown in Table 32.

DHX02 prostate Sample

Equipment	Minimum	Maximum	Mean	Std. Deviation
DHX01	95,30%	98,32%	96,60%	1,01%
DHX02	99,07%	99,71%	99,48%	0,26%
DHX03	98,40%	99,54%	98,99%	0,38%

Table 32 – Descriptive statistics for DHX02 prostate sample EPID verifications.

From the analysis of the original verification with DHX02 an average gamma agreement value of 99.48% was obtained, with minimum and maximum agreement values of 99.07% and 99.71%, respectively, indicating a strong concordance with the TPS prediction.

When the verification of this sample was performed using DHX03, similar results, although with slightly lower values, were obtained, with an average gamma agreement of 98.99% and minimum and maximum agreements of 98.40% and 99.54%, respectively, resulting in an average absolute deviation of 0.49% in relation to the original verification with DHX02. This deviation is clearly non-significant and the gamma agreement values obtained with DHX03 are in accordance with the recommended tolerance of 95.00% for all the patients, supporting the dosimetric equivalence between the two linear accelerators.

On the other hand, a slightly lower average gamma agreement, 96.60%, was obtained when the verification of this sample was performed with DHX01, with minimum and maximum agreements of 95.30% and 98.32%, respectively. This results in an average absolute deviation of 2.89% in relation to the original verification with DHX02, reflecting lower agreements for DHX01 in relation to TPS predictions. However, this deviation is not significant, since the agreement values obtained from the gamma analysis of DHX01 verification are above 95.00%.

Although it was not the main goal of the analysis of this sample, the average absolute deviation between DHX01 and DHX03 verifications was determined, having a value of 2.48%, which is similar to the obtained between DHX01 and DHX02 verifications and also non-significant.

The agreement values obtained were also lower for the DHX01 verification, but with a higher deviation than the observed for DHX01 prostate sample, which, as for H&N samples, can be explained by the higher TPS MLC transmission values in relation to the experimental values of this parameter, which leads to higher TPS predicted doses for all the linear accelerators and also by the higher experimental DLS values of DHX02 and DHX03 in relation to DHX01, which increases the measured doses, creating a higher concordance with the TPS predictions, while DHX01 doses remain slightly lower.

Another important observation, already mentioned for H&N samples, relates with DHX03 gamma agreement values, which are, in general, slightly lower than DHX02 values, although very similar. This observation supports the previous implication of MLC transmission and DLS values in the behavior of the three linear accelerators, since DHX02 and DHX03 are defined by the exactly same parameters and values in the TPS and, for this reason, the TPS predicted doses are

the same for both machines. However, as the experimental MLC transmission values are slightly lower than the implemented in the TPS, the agreement values obtained in the gamma analysis are, although significantly high, lower than 100.00%, since the experimental doses achieved are slightly lower than the predicted. On other hand, although with an inferior difference than the verified for DHX01, the experimental DLS values for DHX03 are slightly lower than the obtained with DHX02, leading to lower measured doses and, consequently, lower gamma agreement values for DHX02, even with minor differences.

Correlation coefficients were also determined for DHX02 prostate sample. The results are shown in Table 33.

		DHX01	**DHX02**	**DHX03**
DHX01	Pearson Correlation	1	0,394	0,860**
	Sig. (2-tailed)	----	0,231	0,001
DHX02	Pearson Correlation	0,394	1	0,693*
	Sig. (2-tailed)	0,231	----	0,018
DHX03	Pearson Correlation	0,860**	0,693*	1
	Sig. (2-tailed)	0,001	0,018	----

**. Correlation is significant at the 0.01 level (2-tailed).

*. Correlation is significant at the 0.05 level (2-tailed).

Table 33 - Correlation coefficients for DHX02 prostate sample EPID verifications.

As for DHX01 prostate sample, the correlation coefficients demonstrate that DHX02 and DHX03 verifications are correlated for a significance level of 0.05, with a coefficient of 0.693, supporting the dosimetric equivalence between both linear accelerators, since a high concordance was also obtained from the gamma analysis.

In relation to the comparison between DHX01 and DHX02, the two are non-correlated again, only demonstrating that the behavior patterns of both linear accelerators were not similar, but not compromising the change of equipment without recalculation for this sample, since the deviations obtained were not significant.

Finally, between DHX01 and DHX03 verifications for this sample a correlation coefficient of 0.860 was obtained for a significance level of 0.01, which indicates that the results from the two verifications describe identical behavior patterns, which is in accordance with the results of the gamma analysis. However, as mentioned for DHX01 prostate sample, due to the small size of the sample, the interpretation of the correlation coefficients is not absolute an do not influence significantly the conclusions of the analysis, having only the role of understanding if the agreement values obtained have or not a similar distribution between the different verifications, since the presence of an identical behavior, in addition to a high concordance in the gamma analysis, supports the existence of dosimetric equivalence.

DHX03 prostate sample results

The results from the verification of DHX03 prostate sample, originally verified using DHX03 linac and posteriorly verified using DHX01 and DHX02 linacs, can be observed in Figure 85.

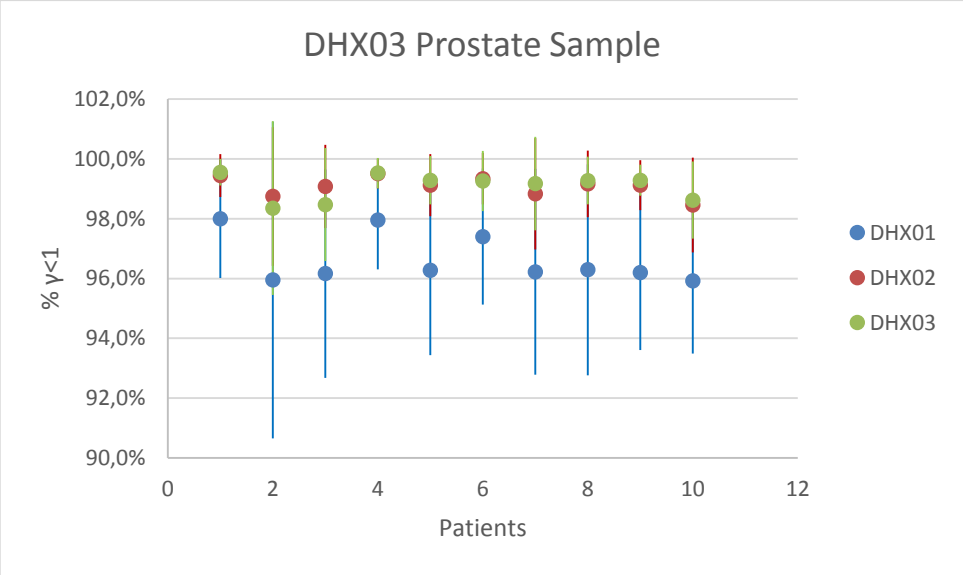

Figure 86 – Average gamma analysis agreement values for patient EPID verifications of DHX03 prostate sample, using 3.0%, 3.0 mm criterion.

The minimum, maximum, mean and standard deviation values relative to the DHX03 prostate sample are shown in Table 34.

DHX03 prostate Sample

Equipment	Minimum	Maximum	Mean	Std. Deviation
DHX01	95,92%	98,00%	96,64%	0,82%
DHX02	98,45%	99,51%	99,08%	0,33%
DHX03	98,36%	99,55%	99,08%	0,43%

Table 34 – Descriptive statistics for DHX03 prostate sample EPID verifications.

An average agreement value of 99.08% was obtained from the gamma analysis performed for the original verification, with DHX03, for DHX03 prostate sample, with minimum and maximum agreements of 98.36% and 99.55%, respectively, which are clearly concordant with the recommended tolerance for gamma analysis.

The verification of this sample with DHX02 resulted in very similar agreements, with an average of 99.08% and minimum and maximum agreements of 98.36% and 99.55%, which represent an almost negligible average absolute deviation of 0.22% in relation to the original verification.

When the sample was verified with DHX01, the gamma analysis results present slightly larger deviations, with an average agreement of 96.64% and minimum and maximum agreements of

95.92% and 98.00%, respectively, resulting in an average absolute deviation of 2.53% in relation to the original verification with DHX03.

For this sample, lower agreement values were also observed for DHX01, which results from the same cause as for the previous samples.

On other hand, for this sample the tendency for slightly lower agreements for DHX03 than for DHX02 was not verified, which could be due to the performing of the different verifications in distinct time periods and an sporadic variation of the DLS experimental values could have occurred due to the presence of dirt in the collimator leaves, for instance . However, this possibility cannot be confirmed, since the last trimestral quality assurances were performed more than one month before the verifications. Besides, although the tendency was verified for all the previous analyzes samples, the deviations were really low, as already mentioned, and, consequently, this subtle tendency can easily be influenced by small uncertainty sources.

Correlation coefficients were also determined for DHX03 prostate sample. The results are shown in Table 35.

		DHX01	**DHX02**	**DHX03**
DHX01	Pearson Correlation	1	0,824**	0,691*
	Sig. (2-tailed)	----	0,003	0,027
DHX02	Pearson Correlation	0,824**	1	0,743*
	Sig. (2-tailed)	0,003	----	0,014
DHX03	Pearson Correlation	0,691*	0,743*	1
	Sig. (2-tailed)	0,027	0,014	----

**. Correlation is significant at the 0.01 level (2-tailed).

*. Correlation is significant at the 0.05 level (2-tailed).

Table 35 - Correlation coefficients for DHX03 prostate sample EPID verifications.

The correlation coefficients obtained indicates that the three verifications are correlated, for a significance level of 0.01 for the comparison between DHX01 and DHX03 and for a significance level of 0.05 for the comparisons between DHX01 and DHX02 and also between DHX02 and DHX03. The correlation existent between the verifications, in addition to the gamma analysis results, supports the viability of indistinct use of the three linear accelerators for prostate samples.

4.4. Ionization Chamber Verification for Head and Neck IMRT treatments

From the results of the verification of Head and Neck IMRT treatments using EPID, it was verified that deviations of approximately 4.00% occurred when treatments originally planned for DHX02 and DHX03 were verified using DHX01. For this reason, it was decided that a further study was required to determine if these deviations resulted from different dosimetric characteristics of DHX01 linac or if, on the other hand, these deviations were caused by differences in the EPID device, which would not compromise the dosimetric equivalence of DHX01 in relation to the other linacs. For this purpose, a verification using an ionization chamber was performed for Head and Neck treatment plans originally planned only for DHX01 and DHX02 linacs, since the results obtained with DHX03 linac were very similar to the obtained with DHX02. All the treatment plans selected for this test were verified with DHX01 and DHX02. The results were divided by two categories:

- DHX01 sample, in which the treatments were originally planned for DHX01 and a comparison between the experimental results obtained using DHX01 and DHX02 and the TPS calculations for DHX01 linac was performed;
- DHX02 sample, in which the treatments were originally planned for DHX02 and a comparison between the experimental results obtained using DHX01 and DHX02 and the TPS calculation for DHX02 linac was performed.

The results of ionization chamber verifications for DHX01 and DHX02 H&N samples are shown in Figures 86 and 87.

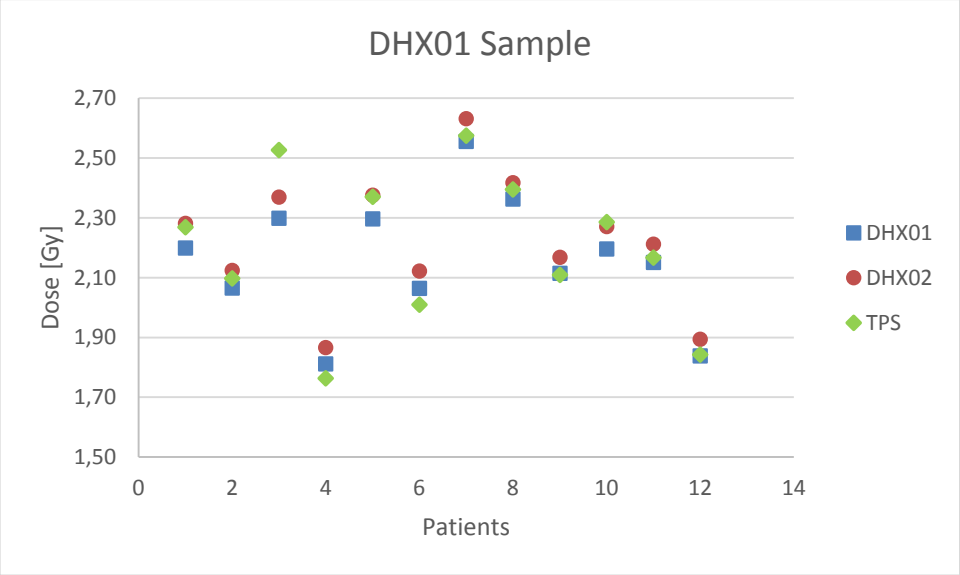

Figure 87 - TPS and experimental dose values obtained for DHX01 sample with the verifications with ionization chamber for DHX01 and DHX02 linacs.

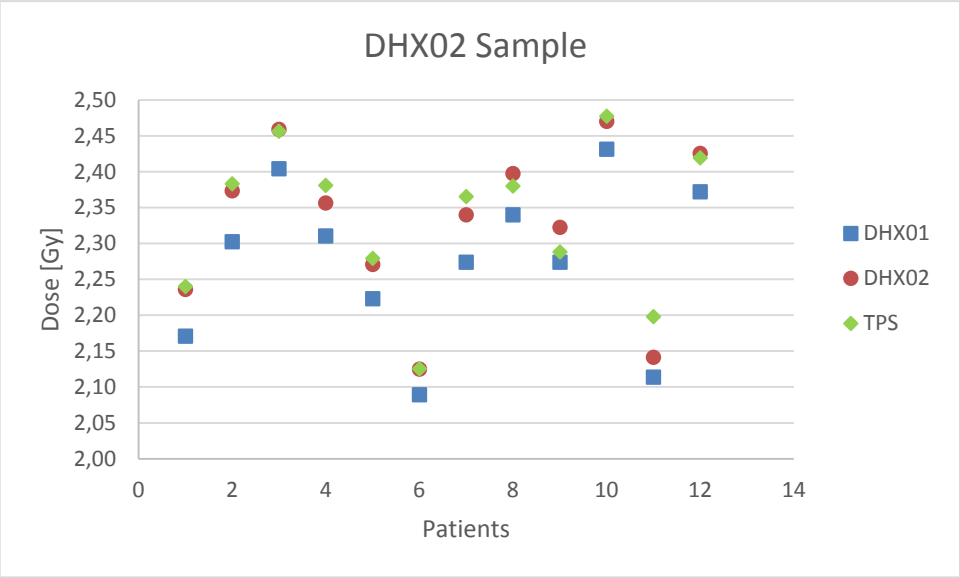

Figure 88 - TPS and experimental dose values obtained for DHX02 sample with the verifications with ionization chamber for DHX01 and DHX02 linacs.

The minimum, maximum, mean and standard deviation values of the absolute differences obtained from the comparisons between DHX01, DHX02 and TPS are summarized in Table 36 for the two samples in analysis.

Ionization Chamber Verification Absolute Deviations [%]

Sample	Comparison	Minimum	Maximum	Mean	Std. Deviation
DHX01 sample	DHX01/TPS	0,22%	4,08%	1,87%	1,34%
	DHX02/TPS	0,21%	5,46%	2,19%	1,79%
	DHX01/DHX02	2,25%	3,61%	2,91%	0,39%
DHX02 sample	DHX01/TPS	0,63%	4,01%	2,53%	1,03%
	DHX02/TPS	0,01%	2,66%	0,72%	0,76%
	DHX01/DHX02	1,30%	3,08%	2,24%	0,56%

Table 36 – Descriptive statistics for the absolute diferences obtained from the comparisons between DHX01, DHX02 and TPS.

First, it is important to state that, in both verifications for DHX01 sample, deviations slightly above the tolerance value of 3% were obtained for some patients, which do not exceed significantly this tolerance value and, for this reason, were considered acceptable. However, one of the patients was excluded from the sample since, for both the measures, the deviations in relation to the TPS dose were significantly high (> 6%) due to a very high dose gradient in the dose measure point and, although in accordance with the tolerance limit of 10% for high gradient, these results introduced significant changes in the average deviations for the sample, which did not represent correctly the sample behavior.

For DHX01 H&N sample, the mean absolute deviation between the experimental doses obtained with DHX01 and the TPS predicted doses for DHX01 is 1.87%, which is clearly in accordance with the tolerance of 3%. For the experimental doses obtained with DHX02 for this

sample, the mean absolute deviation in relation to the TPS prediction is slightly higher, with a value of 2.19%. From these results, it can be stated that the differences obtained in the experimental verifications in relation to the TPS predicted dose are not significant and the deviations obtained for both the experimental verifications are similar, although slightly higher for DHX02, as expected, since the predicted doses from TPS were obtained for DHX01, which is not beam-matched with DHX02. However, the average deviation between both the experimental verifications is 2.91% (near the tolerance limit of 3%) and it can be verified in Figure 50 that the doses obtained with DHX02 are higher than the obtained with DHX01 for all the patients, supporting the behavior observed in the verification with EPID.

In the verification DHX02 H&N sample, a similar behavior was observed. Comparing the experimental doses from DHX01 with the TPS predicted dose (the verification plans for this sample were obtained for DHX02) an average deviation of 2.53% was obtained, with deviation values higher than the tolerance of 3.0% for some of the patients. However, as the maximal deviation value observed is 4.01%, it was not considered very significant, since this value is relatively close to the tolerance limit, if it is took into account that the verification was performed in a different equipment than the one used in the verification plan and which is distinctly defined in the TPS. It was also observed that the dose values measured for DHX01 are lower than the TPS predicted dose values for all the patients in this sample.

For the verification with DHX02, the average absolute deviation between the experimental and TPS predicted doses is 0.72%, with a maximum of 2.66% (below the 3.0% tolerance limit). It is important to state that, for this sample, the proximity between DHX02 experimental doses and TPS predicted doses for DHX02 (original equipment) is more evident than it was for DHX01 in the previous sample. On the other hand, when the verification is performed with a different equipment, the difference were slightly more accentuated for DHX02 sample.

When both the experimental verifications for this sample are compared, an average deviation of 2.24% is obtained, with doses measured in the verification with DHX02 higher that the DHX01 for all the patients in this sample.

These observations support the hypothesis that slightly lower doses are obtained with DHX01 (although not significantly lower), which result from the lower dosimetric leaf separation values observed for this equipment, leading to slightly lower experimental dose values.

Chapter 5

Conclusions

From the results obtained from this study, it can be concluded that, in general, the results obtained with the three linear accelerators were in accordance with the recommended tolerance limits.

In the particular case of DHX02 and DHX03 linear accelerators, which are beam-matched in the TPS, their dosimetric equivalence was confirmed experimentally with this study, since the results obtained with the two machines were very similar (with deviations below 2.00%). both for basic dosimetry and IMRT treatments analysis. For the proposed goal of this study, to verify if small deviations in basic dosimetry results could compromise the indistinct use of the linear accelerator for IMRT treatments, it was demonstrated that, between DHX02 and DHX03, high agreements of the Gamma Analysis using EPID dosimetry was obtained, above the established target limit of 95.00%, both for H&N and prostate treatments. These results assure that, maintaining the present conditions, the indistinct use of the two machines is viable, not compromising the treatment outcome, which means that interchange of patients between both linear accelerators can be performed without limitations.

In relation to DHX01, the average deviations obtained were below 5.00% when comparisons with the other two machines were performed and agreement values above the recommended acceptance tolerance limits of 90.00% were obtained for IMRT treatments. In the case of prostate treatments, although the deviation values were, in average, below 3.00%, the agreement values of the Gamma Analysis were above the target limit of 95.00% for all the patients. However, for H&N treatments, the average agreement values of the Gamma Analysis obtained with DHX01 were below 95.00% (although above 90.00%) and relatively higher deviation (approximately 4.00% average and 8.00% maximum) occurred when treatments from DHX02 and DHX03 samples were verified using DHX01. It is considered that these results does not limit the indistinct use of this linear accelerator for prostate and H&N treatments, in which patients are changed from DHX01 to DHX02 and DHX03 without replanning.

However, in relation to the indistinct change of Head and Neck treatments from DHX02 and DHX03 to DHX01, although the results does not limit the indistinct use of this accelerator, it is

recommended to be used only when the replanning or change to other linear accelerator is not possible, since the influence of the obtained differences in the treatment outcome is not well known.

In order to reduce the deviations between DHX01 and the other two linear accelerators, an adjustment of MLC transmission values in the TPS is recommended, since the measured values during 2014 tend to converge to a value lower than the defined in the TPS. Although the difference is not very large (approximately 0.20%, which is below the tolerance limit of 0.50%), the endurance of this difference in all the measurements analyzed may be sufficient to justify the pattern of deviation obtained in IMRT TPS doses and pre-treatment verifications analysis. It is also recommended that a similar study, even with a reduced number of patients per sample, is performed after MLC transmission adjustment in the TPS, in order to confirm if it is the only source leading to the obtained deviations.

Bibliography

[1] Hrbacek, J. *et al.*, 2007. Quantitative evaluation of a beam-matching procedure using one-dimensional gamma analysis. *Medical physics*, 34(7), pp.2917–2927.

[2] Sjöström, D. *et al.*, 2009. A beam-matching concept for medical linear accelerators. *Acta oncologica (Stockholm, Sweden)*, 48(2), pp.192–200.

[3] Bhangle, J.R. *et al.,* 2011. Dosimetric analysis of beam-matching procedure of two similar linear accelerators. *Journal of medical physics / Association of Medical Physicists of India*, 36(3), pp.176–180.

[4] Attala, E. M. *et al.*, 2014. Dosimetric evaluation of a beam matching procedure. *Chinese-German J Clin Oncol,* 13(2), pp.89-93.

[5] Podgorsak, E., 2005. *Radiation Oncology Physics: A Handbook for Teachers and Students.* Vienna: International Atomic Energy Agency. Available at: http://www-pub.iaea.org/mtcd/publications/pdf/pub1196_web.pdf

[6] Das, I. J., Njeh, C. F. & Orton, C.G., 2012. Vendor provided machine data should never be used as a substitute for fully commissioning a linear accelerator. *Medical Physics,* 39(2), pp.569-572.

[7] The International Commission on Radiation Units and Measurements, 2011. ICRU Report nº85: Fundamental Quantities and Units for Ionizing Radiation. *Journal of the ICRU* 11 (1).

[8] Thariat, J. et al., 2013. Past, present, and future of radiotherapy for the benefit of patients. *Nature reviews. Clinical oncology*, 10(1), pp.52–60.

[9] Lopes, M. C., 2007. Um século de terapia com radiação. *Gazeta de Física,* 30 (I), pp.14-29.

[10] Bernier, J., Hall, E.J. & Giaccia, A., 2004. Radiation oncology: a century of achievements. *Nature reviews. Cancer*, 4(9), pp.737–747.

[11] Coolidge, W. D., 1913. A powerful Röntgen ray tube with a pure electron discharge. *Phys. Rev* 2(6), pp.409-430

[12] Linton, O. W., 1995. Medical applications of x-rays. *SLAC Beam Line* 25(2), pp.25-34.

[13] Bucci, M. K., Bevan, A. & Roach, M., 2005. Advances in Radiation Therapy: Conventional to 3D, to IMRT, to 4D, and Beyond. *CA Cancer J Clin,* 55(2), pp. 117-134.

[14] The International Commission on Radiation Units and Measurements, 2010. ICRU Report nº83: Prescribing, Recording, and Reporting Photon-Beam Intensity-Modulated Intensity Radiation Therapy (IMRT). *Journal of the ICRU* 10 (I).

[15] Yu, C.X. & Tang, G., 2011. Intensity-modulated arc therapy: principles, technologies and clinical implementation. *Physics in medicine and biology*, 56(5), pp.R31–R54.

[16] Foote, M., 2012. The development of advanced radiotherapy treatment techniques. *CancerForum* **36 (2)**.

[17] Attix, F. H., 1986. *Introduction to radiological physics and radiation dosimetry.* Weinheim: Wiley-VCH Verlag GmbH.

[18] Martin, J. E., 2006. *Physics for Radiation Protection: A Handbook.* Weinheim: Wiley-VCH Verlag GmbH.

[19] Jayaraman, S. & Lanzl, L. H., 2004. Clinical Radiotherapy Physics, 189-190. Springer Berlin Heidelberg. Preview available at: http://link.springer.com/book/10.1007/978-3-642-18549-6#page-1

[20] Vitoria, A. H., 2012, Equipos de radioterapia. In: Serreta A. B. & Arroyo, M. C. L., *Fundamentos de Física Médica,* Vol.3, 23-101. Spain: Sociedad Española de Física Médica. Available at: http://www.sefm.es/fisica-medica/es/documentos/6/coleccion-fundamentos-fisica-medica/84

[21] Nath, R. *et al.,* 1994. AAPM code of practice for radiotherapy accelerators: Report of AAPM Radiation Therapy Task Group No. 45. *Medical Physics,* 21 (7), pp.1093-1121.

[22] Klein, E. E. *et al.,* 2009. Task Group 142 report: quality assurance of medical accelerators. *Medical Physics,* 36 (9), pp.4197-4212.

[23] International Atomic Energy Agency, 2000. Absorbed Dose Determination in External Beam Radiotherapy: An International Code of Practice for Dosimetry Based on Standards of Absorbed Dose to Water. *Technical Reports Series* No.398.

[24] Varian Medical Systems, 2011. Eclipse Algorithms Reference Guide.

[25] Instituto Português de Oncologia de Lisboa Francisco Gentil, EPE., 2013. Manual de Gestão dos Equipamentos e Controlo de Qualidade.

[26] Sarkar, B. *et al.*, 2013. A mathematical approach to beam matching. *British Journal of Radiology*, 86(1031).

[27] International Atomic Energy Agency, 2004. Commissioning and Quality Assurance of Computerized Planning Systems for Radiation Treatment of Cancer. *Technical Reports Series* No.430.

[28] Ono, K. *et al.*, 2010. Dosimetric verification of the anisotropic analytical algorithm in lung equivalent heterogeneities with and without bone equivalent heterogeneities. Medical physics, 37(8), pp.4456–4463.

[29] Van Esch, A. *et al.*, 2006. Testing of the analytical anisotropic algorithm for photon dose calculation. *Medical physics*, 33(11), pp.4130–4148.

[30] Peralta, L., 2010. Introdução aos Métodos de Simulação Monte Carlo no transporte de radiação. Faculdade de Ciências da Universidade de Lisboa. Notes available for Dosimetry and Radiological Protection classes.

[31] The International Commission on Radiation Units and Measurements, 1993. ICRU Report nº 50: Prescribing, Recording and Reporting Photon Beam Therapy.

[32] Van Zijtveld, M. *et al.*, 2006. Dosimetric pre-treatment verification of IMRT using an EPID; clinical experience. *Radiotherapy and Oncology*, 81(2), pp.168–175.

[33] Van Esch, A. *et al.*, 2002. Acceptance tests and quality control (QC) procedures for the clinical implementation of intensity modulated radiotherapy (IMRT) using inverse planning and the sliding window technique: experience from five radiotherapy departments. *Radiotherapy and Oncology,* 65, pp.53-70.

[34] Herman, M.G., Kruse, J.J. & Hagness, C.R., 2000. Guide to clinical use of electronic portal imaging. *Journal of applied clinical medical physics / American College of Medical Physics*, 1(2), pp.38–57.

[35] Greer, P.B. & Popescu, C.C., 2003. Dosimetric properties of an amorphous silicon electronic portal imaging device for verification of dynamic intensity modulated radiation therapy. *Medical physics*, 30(7), pp.1618–1627.

[36] Antonuk, L.E., 2002. Electronic portal imaging devices: a review and historical perspective of contemporary technologies and research. *Physics in medicine and biology*, 47, pp.R31–R65.

[37] Herman, M.G. et al., 2001. Clinical use of electronic portal imaging: report of AAPM Radiation Therapy Committee Task Group 58. *Medical physics*, 28(5), pp.712–737.

[38] Howell, R.M., Smith, I.P.N. & Jarrio, C.S., 2008. Establishing action levels for EPID-based QA for IMRT. *Journal of applied clinical medical physics / American College of Medical Physics*, 9(3), p.2721.

[39] Low, D.A. et al., 1998. A technique for the quantitative evaluation of dose distributions. *Medical physics*, 25(5), pp.656–661.

[40] Depuydt, T., Van Esch, A. & Huyskens, D.P., 2002. A quantitative evaluation of IMRT dose distributions: Refinement and clinical assessment of the gamma evaluation. *Radiotherapy and Oncology*, 62(3), pp.309–319.

[41] Van Dyk, J. et al., 1993. Commissioning and quality assurance of treatment planning computers. *International journal of radiation oncology, biology, physics*, 26(2), pp.261–273.

[42] Harms, W.B. et al., 1998. A software tool for the quantitative evaluation of 3D dose calculation algorithms (abstract). *Medical Physics*, 25(10), p.1830.

[43] Low, D.A. & Dempsey, J.F., 2003. Evaluation of the gamma dose distribution comparison method. *Medical physics*, 30(9), pp.2455–2464.

[44] Low, D.A., 2010. Gamma Dose Distribution Evaluation Tool. *Journal of Physics: Conference Series*, 250, p.012071.

[45] Varian Medical Systems, 2011. Portal Dosimetry Reference Guide.

[46] Both, S. et al., 2007. A study to establish reasonable action limits for patient-specific quality assurance in intensity-modulated radiation therapy. *Journal of Applied Clinical Medical Physics*, 8(2), pp.1–8.

[47] Alber, M. *et al.*, 2008. *Guidelines for the verification of IMRT*. Brussels: ESTRO.

[48] Ezzell, G.A. et al., 2009. IMRT commissioning: multiple institution planning and dosimetry comparisons, a report from AAPM Task Group 119. *Medical physics*, 36(11), pp.5359–5373.

[49] PTW Freiburg GmbH. PTW QUICKCHECK^{webline} User Manual

[50] Varian Medical Systems, 2012. Costume Technical Bulletin

[51] Van Esch, A. et al., 2013. Optimized Varian aSi portal dosimetry: development of datasets for collective use. *Journal of applied clinical medical physics / American College of Medical Physics*, 14(6), p.4286.

[52] Van Esch, A., Depuydt, T. & Huyskens, D.P., 2004. The use of an aSi-based EPID for routine absolute dosimetric pre-treatment verification of dynamic IMRT fields. *Radiotherapy and Oncology*, 71(2), pp.223–234.

[53] IPOLFG. Protocolo de Tolerâncias para Nasofaringe

[54] IPOLFG. Protocolo de Tolerâncias para Próstata

[55] Hossain, M., 2014. Output trends, characteristics, and measurements of three megavoltage radiotherapy linear accelerators. *Journal of Applied Clinical Medical Physics*, 15(4), pp.137–151.